

UNIVERSIDADE DE LISBOA
FACULDADE DE CIÊNCIAS
DEPARTAMENTO DE FÍSICA



Biometric Authentication and Identification through Electrocardiogram Signals

Teresa Margarida de Campos Pereira

Mestrado Integrado em Engenharia Biomédica e Biofísica
Perfil em Engenharia Clínica e Instrumentação Médica

Dissertação orientada por:
Raquel Sebastião
Raquel Conceição

Acknowledgments

I would like to thank my supervisor Dr. Raquel Sebastião for giving me the opportunity to develop this project under collaboration with the Institute of Electronics and Informatics Engineering of Aveiro (IEETA), providing guidance, insight and understanding, and for always valuing my work over this past year.

I would also like to thank Dr. Raquel Conceição, who also supervised this dissertation, for her comprehension and availability, not only as a supervisor of this project, but also as my professor for the last five years at Faculdade de Ciências da Universidade de Lisboa.

I wish to express my gratitude towards my colleagues from the course, especially Marta, Sara, Cláudia, Bia, Ema and Lua, for the support, help and friendship during the course years.

I also wish to express my sincere gratitude and appreciation towards special people who have supported me over many years of my life. To Ré, Andreia, Rita, Maria and Rei, for their unconditional support and friendships, for all the moments together throughout our lives and for always being there for me. To my brother-in-law, Tiago, for helping me with everything I need and for always being available for me. To Gil, for his love, for always believing in me and making me believe in myself, for the trust and for being always by my side.

Finally, and the most important, I would like to thank my family. For my grandparents, who inspire me every day with their strength to overcome all the difficulties that come along the way. For my mum, dad and sister, for all the support, motivation, help, kindness and love, and for being my safe haven. I hope I can give them back all the love they have been giving me all these years.

Resumo

O reconhecimento biométrico tem sido alvo de diversas investigações ao longo dos anos, sendo a impressão digital, a face e a iris, os traços biométricos mais explorados. Apesar do seu elevado potencial no que diz respeito a possíveis aplicações tecnológicas, alguns estudos apresentam limitações a estes traços biométricos, nomeadamente a falta de fiabilidade e praticidade num sistema biométrico. Recentemente, vários estudos exploraram o potencial do uso do electrocardiograma (ECG) como traço biométrico, por ser único e singular para cada indivíduo, e dificilmente roubado por outrem, por ser um sinal fisiológico.

Nesta dissertação, foi investigada a possibilidade de usar sinais ECG como traço biométrico para sistemas de identificação e autenticação biométrica. Para tal, recorreu-se a uma base de dados pública chamada Check Your Biosignals Here initiative (CYBHi), criada com o intuito de propiciar investigações biométricas. As sessões de aquisição contaram com 63 participantes e ocorreram em dois momentos distintos separados por três meses, numa modalidade “off-the-person”, com recurso a um elétrodo na palma da mão e eletrolícras nos dedos. Os sinais da primeira aquisição correspondem, num sistema biométrico, aos dados armazenados na base de dados, enquanto que os sinais da segunda aquisição correspondem aos dados que serão identificados ou autenticados pelo sistema.

Os sistemas de identificação e autenticação biométrica propostos nesta dissertação incluem diferentes fases: o pré-processamento, o processamento e a classificação. O pré-processamento consistiu na aplicação de um filtro passa-banda IIR de 4^a ordem, para eliminar ruídos e artefactos provenientes de atividade muscular e da impedância elétrica dos aparelhos de aquisição. A fase de processamento consistiu em extraer e gerar os *templates* biométricos, que serão os *inputs* dos algoritmos de classificação. Primeiramente, extraíram-se os ciclos cardíacos através do *Neurokit2* disponível no *Python*. Para tal, foram localizados os picos R dos sinais ECG e, posteriormente, estes foram segmentados em ciclos cardíacos, com 200 amostras antes e 400 amostras depois dos picos. Com o objetivo de remover os segmentos mais ruidosos, os ciclos cardíacos foram submetidos a um algoritmo de eliminação de segmentos que consistiu em encontrar, para cada sujeito, os 20 e 60 ciclos mais próximos entre si, designados de *Set 1* e *Set 2*, respetivamente. A partir desses dois conjuntos de ciclos, criaram-se dois tipos de *templates*: 1) os ciclos cardíacos, e 2) escalogramas gerados a partir dos ciclos, através da transformada de *wavelet* contínua, com dois tamanhos distintos: 56x56 e 224x224, denominados por *Size 56* e *Size 224*, respetivamente. Devido ao elevado tamanho dos escalogramas, foi utilizada a análise de componentes independentes para reduzir a dimensionalidade.

Assim, os sistemas biométricos propostos na presente investigação, foram testados com os conjuntos de 20 e 60 *templates*, quer para ciclos quer para escalogramas, de forma a avaliar o desempenho do sistema quando usados mais ou menos *templates* para os processos de identificação e autenticação. Os *templates* foram também testados com e sem normalização, para que pudessem ser analisados os benefícios deste processo. A classificação foi feita através de diferentes métodos, testados numa modalidade “entre-sessões”, isto é, os dados da 2^a aquisição, considerados os dados de teste, foram comparados com os dados da 1^a aquisição, denominados dados de treino, de forma a serem classificados. Quanto ao sistema de identificação com ciclos cardíacos, foram testados diferentes classificadores, nomeadamente LDA, kNN, DT e SVM. Para o kNN e SVM, foi feita uma otimização para encontrar o valor de “k” e os valores de γ e C , respetivamente, que permitem o sistema alcançar o melhor desempenho possível. A melhor *performance* foi obtida através do LDA, alcançando uma taxa de identificação de 79,37% para a melhor configuração, isto é, usando 60 ciclos normalizados. Os *templates* com base em escalogramas foram

testados como inputs para dois métodos distintos: 1) redes neurais e 2) algoritmo baseado em distâncias. A melhor *performance* foi uma taxa de identificação de 69,84%, obtida quando usados 60 escalogramas de tamanho 224, não normalizados. Deste modo, os resultados relativos à identificação provaram que utilizar mais *templates* (60) para identificar um indivíduo otimiza a *performance* do sistema biométrico, independentemente do tipo de *template* utilizado. Para além disto, a normalização mostrou-se um processo essencial para a identificação com ciclos cardíacos, contudo, tal não se verificou para escalogramas. Neste estudo, demonstrou-se que a utilização de ciclos tem mais potencial para tornar um sistema de identificação biométrica eficiente, do que a utilização de escalogramas.

No que diz respeito ao sistema de autenticação biométrica, foi utilizado um algoritmo baseado em distâncias, testado com os dois tipos de *templates* numa configuração concatenada, isto é, uma configuração na qual cada sujeito é representado por um sinal que contém uma sequência de todos os seus templates, seguidos uns dos outros. A avaliação da *performance* do sistema foi feita com base nos valores de taxa de autenticação e taxa de impostores, que indicam o número de indivíduos corretamente autenticados face ao número total de indivíduos, e o número de impostores autenticados face ao número total de indivíduos, respetivamente. Os ciclos cardíacos foram testados com e sem redução de dimensionalidade, sendo que a melhor *performance* foi obtida usando 60 ciclos não normalizados sem redução de dimensionalidade. Para esta configuração, obteve-se uma taxa de autenticação de 90,48% e uma taxa de impostores de 13,06%. Desta forma, concluiu-se que reduzir a dimensionalidade dos ciclos cardíacos prejudica o desempenho do sistema, uma vez que se perdem algumas características indispensáveis para a distinção entre sujeitos. Para os escalogramas, a melhor configuração, que corresponde ao uso de 60 escalogramas normalizados de tamanho 56, atingiu uma taxa de autenticação de 98,42% e uma taxa de impostores de 14,34%. Sendo que a dimensionalidade dos escalogramas foi reduzida com recurso a ICA, foi ainda avaliada a *performance* do sistema quando reduzido o número de componentes independentes. Os resultados mostraram que um número de componentes igual ao número de sujeitos optimiza o desempenho do sistema, uma vez que se verificou um decréscimo da taxa de autenticação quando reduzido o número de componentes. Assim, concluiu-se que são necessárias 63 componentes independentes para distinguir corretamente os 63 sujeitos. Para a autenticação através de ciclos cardíacos, a normalização e a redução de dimensionalidade são dois processos que degradam a *performance* do sistema, enquanto que, quando utilizados escalogramas, a normalização é vantajosa. Os resultados obtidos provaram ainda que, contrariamente ao que acontece para processos de identificação, a utilização de escalogramas é uma abordagem mais eficiente e eficaz para a autenticação de indivíduos, do que a utilização de ciclos.

Esta investigação comprovou o potencial do ECG enquanto traço biométrico para identificação e autenticação de indivíduos, fazendo uma análise comparativa entre diferentes *templates* extraídos dos sinais ECG e diferentes metodologias na fase de classificação, e avaliando o desempenho do sistema em cada uma das configurações testadas. Estudos anteriores apresentaram algumas limitações, nomeadamente, o uso de aquisições “on-the-person”, que apresentam pouco potencial para serem integradas em sistemas biométricos devido à baixa praticidade, e a classificação numa modalidade “intra-sessão”, na qual os dados classificados e os dados armazenados foram adquiridos numa só sessão. Este estudo preenche essas lacunas, visto que utilizou dados adquiridos “off-the-person”, dados esses que foram testados numa modalidade “entre-sessões”. Apesar das aquisições “off-the-person” estarem sujeitas a mais ruídos e, consequentemente, dificultarem processos de identificação ou autenticação, estas abordagens são as mais adequadas para sistemas biométricos, dada a sua possível integração nas mais diversas aplicações tecnológicas. A modalidade “entre-sessões” resulta também numa pior *performance* relativamente à utilização de sinais de uma só sessão. No entanto, permite comprovar a estabilidade do ECG ao longo do tempo, o que é um fator indispensável para o funcionamento adequado de um sistema biométrico, uma vez que o mesmo terá que comparar diversas vezes o ECG apresentado no momento de identificação ou autenticação, com o ECG armazenado uma única vez na base de dados. Apesar dos bons resultados apresentados nesta dissertação, no futuro devem ser exploradas bases de dados que contenham mais participantes, com uma faixa etária mais alargada, incluindo participantes com diversas condições de saúde, com aquisições separadas

por um período de tempo mais longo, de forma a simular o melhor possível a realidade de um sistema biométrico.

Palavras-chave: Biometria, Eletrocardiograma, Extração de características, Algoritmos de classificação, Análise comparativa.

Abstract

Biometrics is a rapidly growing field with applications in personal identification and authentication. Over the recent years, several studies have demonstrated the potential of Electrocardiogram (ECG) to be used as a physiological signature for biometric systems. In this dissertation, the possibility of using the ECG signal as an unequivocal biometric trait for identification and authentication purposes has been presented. The ECG data used was from a publicly available database, the Check Your Biosignals Here initiative (CHBYi) database, developed for biometric purposes, containing records of 63 participants. Data was collected through an off-the-person approach, in two different moments, separated by three months, resulting in two acquisitions per subject. Signals from the first acquisition represent, in a biometric system, the data stored in the database, whereas signals from the second acquisition represent the data to be authenticated or identified.

The proposed identification and authentication systems included several steps: signal pre-processing, signal processing, and classification. In the pre-processing phase, signals were filtered in order to remove noises, while the signal processing consisted of extracting and generating the biometric templates. For that, firstly, the cardiac cycles were extracted from the ECG signals, and segment elimination was performed to find the segments more similar to one another, resulting in two sets of templates, with 20 and 60 templates per participant, respectively. After that, two types of templates were generated: 1) templates based on cardiac cycles, and 2) templates based on scalograms generated from the cardiac cycles, with two different sizes, 56x56 and 224x224. Due to the large size of the scalograms, ICA was applied to reduce their dimensionality. Thus, the biometric systems were evaluated with two sets of each type of template in order to analyze the advantages of using more or fewer templates per subject, and the templates were also tested with and without normalization. For the identification system using cardiac cycles, LDA, kNN, DT, and SVM were tested as classifiers in an “across-session” modality, reaching an accuracy of 79.37% for the best model (LDA) in the best configuration (60 normalized cardiac cycles). When using scalograms, two different methodologies were tested: 1) neural network, and 2) a distance-based algorithm. The best accuracy was 69.84% for 60 not-normalized scalograms of *Size 224*, using NN. Thus, results suggested that the templates based on cardiac cycles are a more promising approach for identification tasks. For the authentication, a distance-based algorithm was used for both templates. Cardiac cycles were tested with and without dimensionality reduction, and the best configuration (60 not-normalized cardiac cycles without dimensionality reduction) reached an accuracy of 90.48% and an impostor score of 13.06%. For the scalograms, the best configuration (60 normalized scalograms of *Size 56*) reached an accuracy of 98.42% and an impostor score of 14.34%. Therefore, using scalograms for the authentication task proved to be a more efficient and accurate approach.

The results from this work support the claim that ECG-based biometrics can be successfully used for personal identification and authentication. This study brings novelty by exploring different templates and methodologies in order to perform a comparative analysis and find the approaches that optimize the performance of the biometric system. Moreover, this represents a step forward towards a real-world application of an ECG-based biometric system, mainly due to the use of data from off-the-person acquisitions in an across-session modality.

Keywords: Biometrics, Electrocardiogram, feature extraction, classification algorithms, comparative analysis.

Index

Acknowledgments	i
Resumo	ii
Abstract	v
List of Figures	ix
List of Tables	xi
List of Acronyms	xii
1 Introduction	2
1.1 Objectives and Contributions	2
1.2 Document Organization	3
2 Background	4
2.1 Biometrics	4
2.1.1 Biometric Applications	5
2.1.2 Biometric Systems	6
2.2 Electrical Activity of the Heart	6
2.2.1 ECG Waves and Time Intervals	7
2.2.2 Noise and Artifacts	8
2.3 Electrocardiogram for Biometric Recognition	8
2.3.1 Uniqueness	9
2.3.2 Stability	9
2.3.3 Collectability	9
2.3.4 Performance	9
2.3.5 Acceptability	9
2.3.6 Circumvention	10
2.4 Wavelet Transform	10
2.4.1 Continuous Wavelet Transform	10
2.4.2 Mother Wavelet	11
2.5 Independent Component Analysis	11
2.5.1 FastICA Algorithm	12
2.6 Classifiers	13
2.6.1 Linear Discriminant Analysis	13
2.6.2 K-Nearest Neighbours	14
2.6.3 Decision Trees	14
2.6.4 Support Vector Machines	15

2.6.5 Neural Networks	16
3 Literature Review	18
3.1 Data Acquisition	18
3.1.1 ECG Recording Techniques	18
3.1.2 Acquisition Conditions	21
3.2 Feature Selection	21
3.3 Template Matching	22
3.3.1 Classifiers	22
3.3.2 Metric-based Matching	23
3.3.3 System Evaluation	23
3.4 Related Works	25
4 Biometric Data and Systems	26
4.1 Data Collection	26
4.1.1 Experimental Setup	28
4.1.2 Participants	29
4.1.3 Experimental Procedure	29
4.2 Data Pre-processing	29
4.2.1 Signal Filtering	29
4.2.2 Templates Generation	30
4.2.3 Templates Concatenation	32
4.2.4 Dimensionality Reduction	33
4.3 Identification Algorithm	34
4.3.1 Identification based on Cardiac Cycles	34
4.3.2 Identification based on Scalograms	35
4.4 Authentication Algorithm	37
4.4.1 Distance-based Authentication Algorithm	37
4.4.2 Leave-one-out Cross-Validation	37
5 Identification Results	39
5.1 Identification based on Cardiac Cycles	39
5.1.1 Optimization of the Classifiers	39
5.1.2 Not Normalized vs Normalized Cardiac Cycles	43
5.2 Identification based on Scalograms	45
5.2.1 Identification based on Neural Networks	45
5.2.2 Identification based on Distance Metrics	46
6 Authentication Results	49
6.1 Authentication based on Cardiac Cycles	49
6.1.1 Discussion	52
6.2 Authentication based on Scalograms	53
6.2.1 ICA Dimensionality for Normalized Scalograms	54
6.2.2 Discussion	55
7 Conclusion	56
Bibliography	57

A	Related work	66
B	Optimizations of SVM	70
B.0.1	SVM Optimization for Normalized Cardiac Cycles in <i>Configuration 60/60</i>	70
B.0.2	SVM Optimization for Not Normalized Cardiac Cycles in <i>Configuration 20/20</i>	72
B.0.3	SVM Optimization for Not Normalized Cardiac Cycles in <i>Configuration 60/60</i>	73

List of Figures

2.1	The sequence of depolarization and repolarization events in the heart, and their relationship with the different heartbeat waveforms in an ECG signal.	8
2.2	Representation of the functioning of an LDA classifier.	13
2.3	Representation of the kNN classifier.	14
2.4	Classification of various objects using a Decision Tree Classifier.	15
2.5	Representation of the SVM classifier.	15
2.6	Representation of a Neural Network classifier with one input layer, two hidden layers and one output layer.	16
2.7	Representation of a Convolutional Neural Network.	17
3.1	Medical acquisition configurations: electrode placements and leads on the standard 12-lead configuration and orthogonal configuration.	19
3.2	Acquisition settings with movement, fewer electrodes, and longer duration: example of a five-electrode Holter System.	19
3.3	Examples of off-the-person ECG acquisition settings.	20
3.4	Wearable and seamless acquisitions: examples of investigated configurations.	21
3.5	Confusion Matrix Schematic.	24
4.1	Flow diagram of the proposed systems.	27
4.2	Electrocardiography sensors and electrodes arrangement.	28
4.3	Full experimental setup comprising the hardware configuration used in Silva et al. experiments for biosignal acquisition [2].	28
4.4	Representation of the raw ECG, in blue, and the filtered ECG, in red, for a randomly selected subject, using a 4th-order bandpass Butterworth IIR filter, with cutoff frequencies of 0.5 Hz to 30Hz. .	30
4.5	Individual heartbeat waveforms for a single subject (138 waveforms).	31
4.6	ECG variation within a single subject, after performing the segment elimination (60 waveforms). .	32
4.7	Scalogram representations of a randomly selected electrocardiogram.	33
4.8	Representation of the training and testing templates in each iteration for the leave-one-out cross-validation method.	38
5.1	Optimization of the kNN Classifier for <i>Configuration 20/20</i> on the left and <i>Configuration 60/60</i> on the right, with not normalized and normalized cardiac cycles.	40
5.2	Optimization of the parameters for RBF Kernel for normalized cardiac cycles in <i>Configuration 20/20</i>	41
5.3	Optimization of the parameters for Linear kernel for normalized cardiac cycles in <i>Configuration 20/20</i>	41
5.4	Optimization of the parameters for Polynomial kernel for normalized cardiac cycles in <i>Configuration 20/20</i>	42

5.5	Representation of the accuracy obtained by the biometric identification algorithm based on distance metrics, when using different number of IC.	47
6.1	Distance Matrix between training and testing templates.	50
6.2	Number of authenticated imposters when using scalograms from not normalized cardiac cycles. .	51
6.3	Representation of the accuracy obtained by the biometric authentication system when using different number of ICs for normalized scalograms.	54
B.1.1	Optimization of the parameters for RBF Kernel for normalized cardiac cycles in <i>Configuration 60/60</i>	70
B.1.2	Optimization of the parameters for Linear Kernel for normalized cardiac cycles in <i>Configuration 60/60</i>	71
B.1.3	Optimization of the parameters for Polynomial Kernel for normalized cardiac cycles in <i>Configuration 60/60</i>	71
B.2.1	Optimization of the parameters for RBF Kernel for not normalized cardiac cycles in <i>Configuration 20/20</i>	72
B.2.2	Optimization of the parameters for Linear Kernel for not normalized cardiac cycles in <i>Configuration 20/20</i>	72
B.2.3	Optimization of the parameters for Polynomial Kernel for not normalized cardiac cycles in <i>Configuration 20/20</i>	73
B.3.1	Optimization of the parameters for RBF Kernel for not normalized cardiac cycles in <i>Configuration 60/60</i>	73
B.3.2	Optimization of the parameters for Linear Kernel for not normalized cardiac cycles in <i>Configuration 60/60</i>	74
B.3.3	Optimization of the parameters for Polynomial Kernel for not normalized cardiac cycles in <i>Configuration 60/60</i>	74

List of Tables

2.1	A comparison of several biometric traits.	5
5.1	Comparison of the performance of the identification task based on classifiers for not normalized cardiac cycles.	43
5.2	Comparison of the performance of the identification task based on classifiers for normalized cardiac cycles.	43
5.3	Comparison of the performance of the identification algorithm based on 15-layers NN between not normalized and normalized scalograms of <i>Size 56</i> and <i>Size 224</i>	45
5.4	Comparison of the performance of the identification algorithm based on distance metrics between not normalized and normalized scalograms <i>Size 56</i> and <i>Size 224</i>	46
6.1	Comparison of the accuracy of the authentication algorithm between not normalized and normalized segments with and without DR.	51
6.2	Comparison of the impostor score of the authentication algorithm between not normalized and normalized segments with and without DR.	52
6.3	Comparison of the accuracy of the authentication algorithm between not normalized and normalized scalograms <i>Size 56</i> and <i>Size 224</i>	53
6.4	Comparison of the Impostor Score of the authentication algorithm between not normalized and normalized scalograms <i>Size 56</i> and <i>Size 224</i>	54
A.1	Related Work on ECG-based biometrics - Part I.	66
A.2	Related Work on ECG-based biometrics - Part II.	67
A.3	Related Work on ECG-based biometrics - Part III.	68
A.4	Related Work on ECG-based biometrics - Part IV.	69
A.5	Techniques and performances comparison for previous studies using CYBHi database.	69

List of Acronyms

AC Autocorrelation coefficients.

ANN Artificial neural network.

AUROC Area under the ROC curve.

BS Biometric system.

CM Confusion Matrix.

CNN Convolutional neural network.

CWT Continuous wavelet transform.

CYBHi Check your biosignals here initiative.

DBNN Decision-based neural network.

DCT Discrete cosine transform.

DR Dimensionality Reduction.

DT Decision Trees.

DWT Discrete wavelet transform.

ECG Electrocardiogram.

EEG Electroencephalogram.

EER Equal error rate.

FAR False acceptance rate.

FN False negative.

FP False positive.

FRR False rejection rate.

IC Independent component.

ICA Independent component analysis.

IDR Identification rate.

ISO International Organization for Standardization.

kNN k-Nearest Neighbors.

LDA Linear Discriminant Analysis.

MLP Multilayer perceptron.

NN Neural Network.

PCA Principal component analysis.

PNN Probabilistic neural network.

PSD Power spectral density.

RBF Radial basis function.

RBFNN Radial basis function neural network.

RMSE Root mean square error.

ROC Receiver operating characteristics.

SIMCA Soft independent modelling if class analogy.

SVM Suport vector machines.

TN True negative.

TP True positive.

WDIST Wavelet distance.

WT Wavelet transform.

Chapter 1

Introduction

In today's world, electrocardiogram (ECG) is increasingly used in the most varied areas and applications. Websites, smartphones, safes, cars, houses, buildings, banks, and airports are just a few of our society's facilities that rely on recognition systems to protect and guard ourselves, our information, or our belongings. Several still depend on traditional systems based on extrinsic entities or knowledge, like cards, keys, or passwords. Traditional passwords are the most common mechanism for the authentication of users, despite numerous usability and security problems. Passwords create a burden for users, as they must be memorized and, ideally, should be long and unique. Therefore, it should not come as surprise, that many users opt to use easy-to-guess passwords that are reused across different services, leading to account takeovers and personal data compromise. Research has shown, for instance, that over 50% of users have the same passwords for different services¹ and 81% of data breaches occur due to poor password handling². Hence, surrogate representations of identity, such as passwords, no longer suffice.

There has been a recent shift of interest towards the field of biometric recognition, which refers to the automatic identification of people based on their distinctive physiological (e.g., face, fingerprint, iris, hand geometry) and behavioral (e.g., voice, gait) characteristics. The most common biometric trait involves using a fingerprint scanner, as seen in modern smartphones and laptops. While this is a big step forward, there are still problems related to fingerprint usability and reliability.

As the ECG is a signal originated internally and unique to each person, it has the potential to turn into a reliable source for biometrics [1]. Nevertheless, current challenges include extracting relevant and reliable features from ECG signals and designing accurate models for template matching, protecting against identity attacks. In this project, the potential of using ECG as a biometric trait for identification and authentication of individuals was investigated.

1.1 Objectives and Contributions

This work aims to address some of the limitations of existing research regarding the use of ECG signals for biometric identification and authentication. The first step was to perform an extensive literature review on this area. The first limitation found in literature is that most of the studies rely on existing datasets, and only a few investigate the stability and usability of ECG as a biometric.

The world has been facing a severe pandemic for the last two years, and so, COVID-19 is withholding scientific research, especially those that involve data collection from many people. For this reason, this research had to rely on public datasets. However, the ECG data used for this experiment was taken from Check Your Biosignals Here initiative (CYBHi) database [2], which allowed overcoming some of the limitations of the data collection process. Firstly, an off-the-person approach was used to collect ECG signals, which is less intrusive than the medical

¹<https://www.pandasecurity.com/en/mediacenter/security/password-reuse/> (Accessed on 28/11/2021)

²<https://bnd.nd.gov/81-of-company-data-breaches-due-to-poor-passwords/> (Accessed on 28/11/2021)

acquisition configuration, allowing many potential applications since this configuration can be easily integrated into real-world scenarios. Secondly, data was collected from the same participants over two sessions, separated in time by three months, which allowed to examine the usability and uniqueness, and also the stability of human ECG.

Another challenge of using ECG data for biometric authentication and identification is to extract distinct features from the signal that can be used to match users with their records. Most existing work focuses on locating reference points within the ECG trace used to create the input features. However, correctly identifying the reference points is a non-trivial task in itself and may constitute a single point of failure if performed incorrectly [3]. The approach used in this project relies on locating the R-wave peaks, which is the most prominent feature of the trace. These peaks were used to segment the signal into smaller heartbeat waveforms, forming the base for the biometric templates. The present work used two biometric templates: one corresponding to the exact cardiac cycles and the other corresponding to the scalograms of the cardiac cycles.

In order to perform authentication and identification, the algorithm has to match the biometrics recorded during the authentication or identification moment with the stored templates of the user. For this research, in what concerns the identification process, two different approaches were developed to perform template matching: the first one concerns the use of several classifiers, including Linear Discriminant Analysis, k-Nearest Neighbors, Decision Trees, Support Vector Machines, and Convolutional Neural Networks; the second approach corresponds to a distance-based algorithm. For authentication, a distance-based algorithm along with cross-validation was used.

Although researchers have proposed various types of features for ECG analysis, and different feature selection and classification methods, stating the best methods directly is not possible at all. Unlike what happens for the vast majority of the existing studies, this project brings novelty by comparing different ECG-based biometric templates and classification algorithms, to find the optimal solution for biometrics identification and authentication. Since there must be a trade-off between the optimality of the result and the entire processing time of the employed method, one should choose the method that best fits the expectations for the processing time and accuracy of the analysis.

1.2 Document Organization

In Chapter 2, a brief overview of biometrics, their characteristics, and applications are presented. Some theoretical concepts related to the methodology used in the present study are also presented in this chapter, namely, a review on Wavelet Transforms, a delineation of the Independent Component Analysis process, and the description of some classifiers. Chapter 3 consists of a review of the most relevant work in ECG biometrics. In Chapter 4, a description of the proposed biometric authentication and identification systems based on ECG signals is presented. Chapters 5 and 6 show the results obtained for the identification and authentication systems, along with the respective discussion. The dissertation concludes with a summary and future work directions in Chapter 7, followed by Appendix A and Appendix B.

Chapter 2

Background

2.1 Biometrics

Biometrics is an increasingly growing multibillion-dollar market expected to grow between \$36.6 billion in 2020 to around \$68.6 billion by 2025³.

Biometrics is defined by the International Organization for Standardization (ISO) as “the automated recognition of individuals based on their behavioral and biological characteristics”⁴. They are present in our daily life either for personal identification or authentication. In biometric authentication, the system validates the claimed identity of a particular person, whereas, in biometric identification, the system finds out who the person is without any previously claimed identity.

Distinctive features evaluated by biometrics, which are referred to as biometric traits, must have the following characteristics [3]:

- **Universality:** Every person should possess the characteristic.
- **Uniqueness:** Two persons should not have the same characteristic, or the probability of this event should be negligible. The differences between characteristics of different individuals should also be sufficient to discriminate their identities.
- **Stability:** The characteristic should be sufficiently invariant over the person’s lifetime.
- **Collectability:** The characteristic should be quantitatively measurable.
- **Performance:** The biometric trait must be robust, reliable, and easily analyzed when used for personal identification.
- **Acceptability:** Biometric collection and usage should be socially accepted.
- **Circumvention:** The biometric trait should not be easily imitated nor “spoofed” by a substitute.

Biometric traits are often divided into two categories: physiological and behavioral. Physiological biometrics relate to human physiology, whereas behavioral biometrics are based on human behavior. Examples of these traits include:

- **Physiological:** fingerprint, face, iris, hand geometry, voice, vein pattern, ear shape, or ECG;
- **Behavioral:** signature, keystroke, or gait.

Each biometric trait has different characteristics from one another, and so, deciding which one to use depends on the specific problem at hand. Table 2.1 presents a comparison of the most commonly used biometrics.

³<https://www.marketsandmarkets.com/PressReleases/biometric-technologies.asp> (Accessed on 30/12/2020)

⁴<https://www.iso.org/standard/55194.html> (Accessed on 29/12/2020)

Table 2.1: A comparison of several biometric traits (adapted from [4]).

Trait	Benefits	Drawbacks
Face	Easily measurable	Easy circumvention
	Affordable equipment	Depends on face visibility and lighting
Fingerprint	High performance Permanent over time	Requires contact
Iris	High performance	Expensive equipment
Palmprint	High measurability Permanent over time	Requires contact
Voice	Affordable equipment	Low performance
Gait	Easy to measure Affordable equipment	Low performance Variability over time
Electroencephalogram (EEG)	Universality Hidden nature	Extensive equipment Vulnerability to noise Variability over time
Electrocardiogram (ECG)	Universality Hidden Nature Simple Acquisition	Requires contact Variability over time

Biometrics provides many advantages over traditional means of access control, such as cards, passwords, and pins (among others). However, there are still serious concerns over the security and privacy of stored biometrics. For instance, facial features can be easily collected from photos available on social media websites, and voice can be obtained by recording phone calls or voice messages. Thereby, the goal of a biometric recognition system is to implement an efficient anti-attacks algorithm, which would mitigate the consequences of compromised biometrics.

2.1.1 Biometric Applications

Biometric applications can be generalized into four categories. The first application category controls access to data, such as logging into a device, PC, or network. The second category is controlling access to tangible materials or areas, such as physical access control. The third is to validate a claimed identity against an existing credential, such as in a border control environment. The fourth application registers or identifies individuals whose identities need to be established biometrically, most often using centralized or distributed databases.

Beyond this decomposition in categories, some specific biometric applications can be:

- **Law Enforcement:** Biometric technologies have long been utilized as a secure means to identify alleged criminals. The FBI currently possesses one of the largest biometric databases, comprised of tens of millions of civil and criminal fingerprint records.
- **Border Control:** The ever-increasing volume of international travel needs the implementation of technologies that can automate, streamline, and expedite border crossing. Driven by international standards for biometric-enabled passports, countries use fingerprints, iris, and face recognition technologies in border control applications.
- **Physical Access Control:** Physical access control uses biometrics to identify or verify the identity of individuals before permitting access to an area. Companies and government agencies deploy technologies, such as fingerprint, hand geometry, and iris recognition to control key entry and exit points.
- **Time and Attendance:** Biometrics can serve as a commercial application to assist in employee management. In this particular application, devices are used to track employee attendance. Hundreds of commercial deployments use hand geometry and fingerprint recognition to ensure the integrity of work hours and payroll.

2. BACKGROUND

- **Consumer Recognition:** This application refers to the confirmation of one's identity to execute a commercial transaction. Conventional authentication methods have utilized keycards, PINs, and signatures to ensure the validity of a given transaction.
- **Logical Access Control:** Biometrics are used to control access to systems and/or devices based on physical characteristics. It is commonly used to control access to centralized databases, healthcare information, or financial records. Many deployments have used fingerprint recognition due to its proven reliability, ease-of-use, and accuracy.

As seen by the application descriptions mentioned above, biometric technology is typically used in applications to improve security, increase efficiency, or enhance convenience. Additionally, biometrics allows users to forego the responsibility of creating passwords and carrying keycards while maintaining a level of security that meets, and in some cases surpasses, that of conventional authentication methods.

2.1.2 Biometric Systems

A biometric system (BS) is a system that has the objective of performing a biometric task based on three main stages: data acquisition, data processing, and pattern matching.

Regarding data acquisition, BSs require two types of templates: 1) enrollment template and 2) presentation template. The enrollment template is generated when a user registers for the first time. The presentation template is generated every time a user tries to gain access [5].

Once the biometric signals are captured, they are transformed, using signal processing techniques as reference templates used to distinguish the individual. This may involve several steps, such as signal filtering, signal segmentation, amplitude and time normalization, outlier detection, and features extraction. The filtering process consists of eliminating noises and artifacts. Signal segmentation is the most commonly used signal processing technique among the surveyed approaches. It is used to limit the signal span for feature extraction or to set a fixed size to ease template matching when the feature is the signal itself. Normalization is usually performed to minimize differences caused by external factors, allowing the comparison between signals to be more accurate. Outlier detection is generally applied to discard deflected signals. To avoid harming the recognition process, this process should be applied equally for both enrollment and presentation templates.

Regarding features extraction, BSs can be fiducial, non-fiducial, or partially-fiducial, depending on the nature of the used features. Fiducial approaches exclusively use the measurements of fiducial landmarks of the signal in the time domain as features. Non-fiducial approaches are those that use the entire signal (or segments of it) holistically to extract features related to the waveform morphology. The partially-fiducial or hybrid approaches are those that use features from both fiducial and non-fiducial origins.

Concerning pattern matching, a biometric algorithm takes the features from the stored reference template, along with the features extracted from the presentation sample, and compares them to generate a score that indicates the likelihood that both are from the same person. The algorithm can support one or two crucial functions: authentication and identification. Authentication involves confirming or denying a person's claimed identity. The system performs a one-to-one comparison of the acquired biometric data with the stored information associated with the claimed identity. In identification, the biometric system must establish a person's identity by performing a one-to-many comparison of the acquired biometric data with the information of a set of individuals. The identification mode does not require the user to claim an identity.

2.2 Electrical Activity of the Heart

Before discussing the potential of an ECG as a biometric, this dissertation presents an overview of the physiology of the heart, its electrical conduction system, and how it relates to electrocardiograms.

The heart is a muscular organ whose primary function is to pump oxygen-rich blood through the blood vessels to the body tissues. Its anatomy is divided into four chambers: the upper two are the left and right atria, while the lower two chambers are the left and right ventricles.

The wall of the heart is called the myocardium, being primarily composed of muscle cells that produce mechanical force during the contraction of the heart. The contractions are initiated by an impulse generated in the sinus node, located in the right atrium. The myocardium also contains specialized muscle cells, which are connected to a network that allows that electrical impulse to spread throughout the heart rapidly. A cardiac cycle is created when such impulse propagates through the conduction system [6].

The sequence of mechanical events that defines a cardiac cycle can be assumed to start in the right atrium, where oxygen-poor blood collected from all the veins in the body, except those of the lungs, enters the heart through two large veins, the inferior and superior vena cava. When the right atrium is triggered to contract, it forces blood into the right ventricle. When the right ventricle has been filled, it contracts and forces blood into the lungs. Inside the lungs, a process called “gas exchange” occurs, and the blood replenishes the oxygen supply. The pulmonary veins return the oxygenated blood to the left atrium, which, in turn, empties into the left ventricle. Finally, it is the left ventricle that forces blood to all of the body organs and tissues, except the lungs, through the arterial vessels, which evolve into capillaries and, then, return into the heart through the venous system [7].

Each cardiac cycle comprises two phases, depolarization and repolarization, referred to in mechanical terms as contraction and relaxation. Depolarization is manifested by a rapid change in the membrane potential of the cell and constitutes the initial phase of the cardiac action potential. The rapid change in voltage causes neighboring cells to depolarize, and, as a result, an electrical impulse spreads from cell to cell throughout the myocardium. Depolarization is immediately followed by repolarization, during which the potential of the membrane gradually returns to its resting state [6].

2.2.1 ECG Waves and Time Intervals

A typical ECG wave of a normal heartbeat, like the one presented in Fig.2.1, consists of a P wave, a QRS complex, and a T wave.

The **P wave** is generated when the right and left atria are depolarized. Its amplitude usually is less than 300 μ V, and its duration is less than 120 ms. The spectral characteristic of a normal P wave is usually considered to be low-frequency, below 10-15 Hz.

The **QRS complex** reflects the depolarization of the right and left ventricles. The first negative deflection of the QRS complex is denoted the Q wave, the first positive is denoted the R wave, while the subsequent negative deflection is denoted the S wave. Its duration may extend up to 250 ms, and its frequency content is considerably higher than that of the other ECG waves and is mainly concentrated in the interval 10-50Hz. Since the QRS complex has the largest amplitude of the entire ECG waveform, sometimes reaching 2-3 mV, it is the first to be identified in any computer-based analysis [6].

Finally, the **T wave** occurs during ventricular repolarization and extends about 300 ms after the QRS complex. Atrial repolarization cannot usually be discerned from the ECG since it coincides with the much larger QRS complex.

Some other important characteristics of the ECG waveform are the intervals between waves:

The **ST segment** represents the interval during which the ventricles remain in an active, depolarized state.

The **RR interval** represents the length of a ventricular cardiac cycle, measured between two successive R waves, and serves as an indicator of ventricular rate.

The **PQ interval** is the time interval from the onset of atrial depolarization to the onset of ventricular depolarization.

The **QT interval** represents the time from the onset of ventricular depolarization to the completion of ventricular repolarization.

2. BACKGROUND

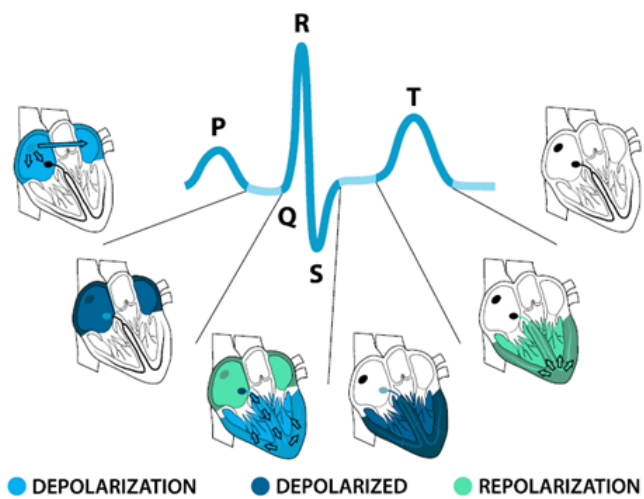


Figure 2.1: The sequence of depolarization and repolarization events in the heart, and their relationship with the different heartbeat waveforms in an ECG signal (extracted from [4]).

2.2.2 Noise and Artifacts

An important reason behind the success of computer-based ECG analysis is the capability to improve poor signal quality using signal processing algorithms. These results have been achieved thanks to good knowledge of signal properties and noise properties. Therefore, it is important to become familiarized with the most common types of noise and artifacts in the ECG before addressing methods in the following chapter, which compensate for their presence. A list of common non-cardiac noise sources follows:

- **Powerline interference** is caused by improper grounding of the ECG equipment and interference from nearby equipment. It affects the acquired signal as a high-frequency noise: 60 Hz in the United States and other American countries, and 50 Hz in Europe, Asia, and most other countries [4, 6].
- **Baseline wander** is a low-frequency activity in the ECG, which may interfere with signal analysis, rendering the clinical interpretation inaccurate and misleading. It may be caused by respiration, body movement, or poor electrode contact. Its frequency is usually below 1 Hz.
- **Electromyographic interference**, caused by the electrical activity of skeletal muscles during periods of contraction, can interfere with the signal while capturing ECG, resulting in high-frequency, high-amplitude, short-term bursts.
- **Electrode motion artifacts** are mainly caused by skin stretching, which alters the impedance of the skin around the electrodes. They occur mainly in the range of 1 to 10 Hz. In the ECG, these artifacts are manifested as large-amplitude waveforms, which are sometimes mistaken for QRS complexes [6].

2.3 Electrocardiogram for Biometric Recognition

Having discussed the heart's electrical activity and its relation with the ECG waves and time intervals, we can now consider whether ECG could be used as a viable biometric.

The ECG, compared to other biometric traits in Table 2.1, has proven to be the most promising of them, excelling in most of the characteristics that define the quality of a biometric trait. Its hidden nature and inherent liveness information make it not easily hacked without the consent of the user. Moreover, the ECG is believed to be unique and different from one person to another, making the ECG an accurate tool to distinguish between different individuals. Most existing literature focuses on proving the viability of an electrocardiogram as a biometric.

2.3.1 Uniqueness

Biometric recognition based on ECG was firstly investigated by Biel et al. [8], Irvine et al. [9], and Kyoso et al. [10]. The main hypothesis shared by these pioneer studies is that ECG contains sufficiently detailed information regarding the electrical operation of the heart and that its nature is sufficiently personal to be used in high-performance identity recognition systems. Most of the studies investigating this property of ECG do not evaluate the performance of their biometric system on huge datasets, as was done for other biometric traits. An exception is a study by Carreiras et al. [11], who assessed the performance of their biometric system on a database with ECG recordings collected from 618 subjects using a 12-lead ECG and obtained high recognition rates. The results from this work provided a positive perspective on the issue of ECG uniqueness. However, these promising results can fall apart when using an ECG with fewer details (for example, ECG acquired with one lead or even ECG collected at the hand palms or fingers).

2.3.2 Stability

While proving uniqueness can be achieved using data from a single point of time, proving stability requires data to be collected from the same individual over a sufficiently long period of time. Thereby, fewer studies investigated the stability of ECG signals. A study by Silva et al. [12] collected ECG data from 63 subjects, with two data acquisition sessions separated by a 3-month interval. Their results indicate that biometric authentication performs worse for longitudinal ECG data but is still viable for real-world applications.

2.3.3 Collectability

Traditional and clinical 12-lead ECG machines require ten self-adhesive electrodes to be placed on the subjects' chest and limbs. This makes the traditional ECG recording procedure not compatible with a biometric system since a biometric trait must be recorded easily and relatively fast. Moreover, the used machines are often non-portable, expensive, and take time to set up. However, nowadays, several minimally invasive devices can record ECG requiring electrodes to be placed only on the chest. These devices are portable and can also be used to record a single-lead ECG trace using electrodes when in contact with wrists or fingers. Although these consumer-grade ECG devices provide less information than the 12-lead clinical ECG machines, they can be used to record ECG in a non-invasive manner, which makes them appropriate and applicable for biometric systems [3].

2.3.4 Performance

The performance of a biometric system depends on several aspects, such as the signal acquisition process, the quality of the signal, the pre-processing procedures, the selected features, the template used, and the matching algorithm [3]. Some biometrics have established methods for transforming the raw signal into features used to recognize individuals. Fingerprint scanners, for instance, detect very specific fingerprint features called minutiae. Concerning ECG as a biometric, currently, there is no consensus over which features should be used. Thus, the performance of ECG biometric systems varies significantly across studies.

2.3.5 Acceptability

With the introduction of reliable consumer-grade ECG devices, there have been more opportunities to create ECG-based biometric systems that are minimally invasive and, consequently, more socially accepted. The “off-the-person” approaches for signal acquisition are particularly appealing for biometric applications, once the biometric sensors are usually embedded into existing systems, such as keyboards and vehicle steering wheels [11]. Nevertheless, to the best of our knowledge, there have been no studies investigating users' opinion of using ECG as a biometric.

2. BACKGROUND

2.3.6 Circumvention

All biometric systems are subject to attacks, which try to corrupt the system with an artifact or contraption. In order to compromise an ECG recording, the intruder has to steal the records from a medical institution or perform a social attack to manipulate the victim into giving his/her ECG. Once that is achieved, the intruder has to digitize the recording, in case it is on paper, and forge the voltage levels at the electrodes of an ECG sensor using a device that outputs electrical waveforms. Even though it was expected to be a very complex procedure, a study by Eberz et al. shows that technological barriers for the attacker are extremely low [13]. Thereby, more work in this area is required to establish a viable defense against ECG data compromise.

To summarize, ECG is proven to be a strong candidate to be used as a biometric trait for personal recognition. Several studies have demonstrated the uniqueness and stability of ECG over the last few years. The introduction of those low-cost consumer-grade ECG devices, which record ECG in a non-invasive manner, also provides the opportunity for systems to include these sensors into existing access control systems. However, there is still insufficient research on which features to extract from ECG signals to achieve the optimal performance of the system and prevent intruder attacks and guarantee that ECG-based biometric systems are socially accepted.

2.4 Wavelet Transform

A fundamental goal of signal processing is to extract specific information from a given signal. For that, signals are often transformed to different domains, expecting that the desired information can be highlighted easier.

The time-domain signals are noisy and complex, causing ECG signals not to be easily distinguishable due to the lack of discriminatory features. In order to overcome this limitation, studies have been conducted by converting signals into the frequency domains since frequency-time analysis enables hidden characteristics to be displayed and measured.

The wavelet transform (WT) is a powerful method for time-frequency transforms. Its tools can be categorized into continuous wavelet tools and discrete wavelet tools, used for signal analysis and signal processing, such as noise reduction, data compression, peak detection, among others. Since wavelets are localized in both time and frequency domains, wavelet signal processing is suitable for nonstationary signals, whose spectral content changes over time [14].

Morlet introduced a wavelet as a family of translations and dilatations from a single function called the mother wavelet. This new signal processing has been improved more efficiently by Mallat, Meyer, Daubechies, and Grossman, and has become a popular technique in biosignal analysis [15].

2.4.1 Continuous Wavelet Transform

Based on the recent works, ECG features are extracted using a continuous wavelet transform (CWT), since the discrete wavelet transform (DWT) has many defects, such as the indelicacy of the transform characterization and instability [16].

The CWT for the signal $f(t)$ is defined as the integration of the $f(t)$ with the shifted or scaled shapes from a mother wavelet $\Psi_{a,b}(t)$:

$$CWT(a,b) = \frac{1}{\sqrt{a}} \int_{-\infty}^{\infty} f(t) * \Psi\left(\frac{t-b}{a}\right) dt \quad (2.1)$$

$$a \in \mathbb{R}^+ \setminus \{0\}, b \in \mathbb{R}$$

In other words, the CWT is the sum of the signal multiplied by the shifted and scaled shapes from a mother

wavelet Ψ :

$$CWT(scale, position) = \int_{-\infty}^{\infty} f(t) * \Psi(scale, position, t) dt \quad (2.2)$$

2.4.2 Mother Wavelet

The original basic wavelet $\Psi(t)$ is called the mother wavelet, and its variations $\Psi_{a,b}(t)$ are called daughter wavelets. The daughter wavelets are the shifted or scaled shapes from a mother wavelet. The a is a scale factor for scaling the function $\Psi(t)$, while the b is a shift factor for translating the function $\Psi(t)$. The result of the CWT is a matrix filled with wavelet coefficients located by scale and position. Determining the scale parameters and mother wavelet in CWT is very important for analyzing ECG since When the wavelet most similar with the signal to be decomposed is used, better noise cancellation without distortion can be performed [15].

One of the most commonly used mother wavelets is the Morse wavelet, which is useful for analyzing signals with varying amplitude and frequency over time and localized discontinuities. There have been many studies on Morse wavelet theory and its application to signal analysis, resulting in an efficient algorithm for calculating the Morse wavelet. The Fourier transform of the generalized Morse wavelet is:

$$\Psi_{P,\gamma}(\omega) = U(\omega) a_{P,\gamma} \omega^{\frac{P^2}{\gamma}} e^{-\omega^\gamma} \quad (2.3)$$

where $U(\omega)$ is the function of unit step, P^2 is the time-bandwidth product, $a_{P,\gamma}$ is a constant for normalization, and γ is a parameter for determining the symmetry of the Morse wavelet. In many applications of the Morse wavelet, β is used as a decay or compactness parameter, rather than the time-bandwidth product, $P^2 = \beta\gamma$. The equation for the Morse wavelet using β and γ as parameters is:

$$\Psi_{\beta,\gamma} = U(\omega) a_{\beta,\gamma} \omega^\beta e^{-\omega^\gamma} \quad (2.4)$$

Various analytic wavelets could be obtained by varying the time-bandwidth product and symmetry parameters of a Morse wavelet. The wavelet duration in time is proportional to the square root of P , which is the time-bandwidth product. The duration affects the number of oscillations of the center window at its peak frequency, $(\frac{P^2}{\gamma})^{\frac{1}{\gamma}}$. The skewness of the Morse wavelet by demodulation is 0 when γ is 3 as the minimum Heisenberg area [14, 15].

2.5 Independent Component Analysis

Independent component analysis (ICA) is a generative model, which aims to decompose a data matrix into two more informative matrices, one with the individuals (rows) and the other with the variables (columns), by calculating linear combinations of the original variables. In ICA, a data matrix \mathbf{X} is regarded as a set of observed signals, which are linear mixtures of source signals. The objective of this model is to extract the source signals, the independent components (IC), and the proportions in which they are mixed together in the observed signals (also called signal mixtures).

In the context of ICA, a signal can be represented by the row vector \mathbf{x} , written as the weighted sum of q pure source signals \mathbf{s}_j , ($j = 1$ to q) by the weights, a_j :

$$\mathbf{x} = \sum_{j=1}^q a_j \mathbf{s}_j \quad (2.5)$$

So, for a set of n signals, each observed signal \mathbf{x}_i ($i=1$ to n) can be given by:

$$\mathbf{x}_i = \sum_{j=1}^q a_{ij} \mathbf{s}_j \quad (2.6)$$

2. BACKGROUND

Eq. 2.6 implies that, although the source signals, s_j , are independent, the mixture signals, which are linear combinations of the same source signals, are not.

If the n signals are in the rows of an \mathbf{X} matrix, Eq. 2.6 can be written in matrix form:

$$\mathbf{X} = \mathbf{A} \cdot \mathbf{S} \quad (2.7)$$

where \mathbf{X} is the original data matrix of mixed sources, \mathbf{A} is the mixing matrix, whose element a_{ij} describes the weight of source signal j in the mixed signal \mathbf{x}_i ; and \mathbf{S} is the matrix of pure source signals.

The objective of ICA is to determine \mathbf{A} and \mathbf{S} , knowing only \mathbf{X} . In order to find \mathbf{A} , a demixing matrix \mathbf{W} is calculated such that:

$$\mathbf{S} = \mathbf{W} \cdot \mathbf{X} \quad (2.8)$$

which implies that \mathbf{W} is the inverse of \mathbf{A} . After calculating \mathbf{W} , Eq. 2.8 enables the calculation of the independent source signals, \mathbf{S} , i.e., the ICs. \mathbf{A} is then obtained from Eq. 2.9 :

$$\mathbf{A} = \mathbf{X} \cdot \mathbf{S}^T \cdot (\mathbf{S} \cdot \mathbf{S}^T)^{-1} \quad (2.9)$$

Different algorithms exist to compute an ICA model. In the present work, ICA was computed based on the FastICA algorithm⁵.

2.5.1 FastICA Algorithm

This fixed-point algorithm was developed by Hyvärinen et al., and has been presented in several books and articles [8, 28]. This algorithm aims at maximizing an approximation of negentropy. Since Eq. 2.10 represents the approximation of negentropy, in order to find an IC, one should maximize the negentropy of the searched source signals \mathbf{s} (which according to Eq. 2.8 would be equal to $\mathbf{W}^T \mathbf{x}$), defined as:

$$J(\mathbf{w}^T \mathbf{x}) = [E\{G(\mathbf{w}^T \mathbf{X})\} - E\{G(v)\}]^2 \quad (2.10)$$

where \mathbf{w} is such that $E\{(\mathbf{w}^T \mathbf{x})^2\} = 1$.

The different steps of FastICA can be then summarized as follows:

- Choose an initial random “demixing” vector \mathbf{w} .
- Maximize the non-Gaussianity of $\mathbf{w}^T \mathbf{x}$.
 1. Define $\mathbf{w}^+ = E\{\mathbf{x}g(\mathbf{w}^T \mathbf{x})\} - E\{g'(\mathbf{w}^T \mathbf{x})\}\mathbf{w}$.
 2. Set $\mathbf{w} = \mathbf{w}^+ / ||\mathbf{w}^+||$.
 3. Check the convergence of \mathbf{w} . If it has not converged, go back to 1.
- After convergence, the data are deflated by $\mathbf{w}^T \mathbf{x}$ (i.e., decorrelation with respect to the previously estimated ICs) and the whole procedure is repeated to find the next demixing vector \mathbf{w} .
- When all the \mathbf{w} ’s have been computed, Eqs. 2.8 and 2.9 give \mathbf{S} and \mathbf{A} , respectively.

The first step of this algorithm is a random initiation of the \mathbf{w} vector. This has consequences on the results obtained at each iteration of the algorithm, as in two successive runs of FastICA applied to the same data, different first estimates of \mathbf{w} may lead to a different final solution. Another risk of random initialization is the possibility for the algorithm to converge to a local optimum rather than the global optimum. The approximation of the negentropy and the chosen G function are also critical parameters that can influence the output of FastICA.

⁵<https://github.com/aludnam/MATLAB> (Accessed on 15/11/2021)

2.6 Classifiers

2.6.1 Linear Discriminant Analysis

Linear Discriminant Analysis (LDA) may be used to reduce the dimensionality of data and for classification purposes. LDA assumes that all classes are linearly separable and tries to find the hyperplanes that allow to distinguish the classes.

If there are two classes, the LDA draws one hyperplane and projects the data onto this hyperplane in such a way that the within-class distance is minimized and, contrary, the between-class distance is maximized. This results in a maximum class separability [17]. This can be achieved in three steps [18]:

- Firstly, the algorithm calculates the separability between classes which is the distance between the mean of different classes. This is called the between-class variance:

$$S_b = \sum_{i=1}^g N_i (\bar{x}_i - \bar{x})(\bar{x}_i - \bar{x})^T \quad (2.11)$$

- The second step is to compute the distance among the mean and sample of each class, that is known as the within class variance.

$$S_w = \sum_{i=1}^g (N_i - 1) S_i = \sum_{i=1}^g \sum_{j=1}^{N_i} (x_{i,j} - \bar{x}_i)(x_{i,j} - \bar{x}_i)^T \quad (2.12)$$

- The last step is to create the dimensional space that minimizes the within-class variance and maximizes the between-class variance. Assuming P as the dimensional space projection, that is known as Fisher's criterion:

$$P_{LDA} = \text{argmax} \frac{P^T S_b P}{P^T S_w P} \quad (2.13)$$

The algorithm makes predictions based upon the probability of a new input dataset belonging to a certain class. The class which has the highest probability is considered the output class, and, then, the prediction is made. Fig. 2.2 shows a representation of the functioning of an LDA classifier.

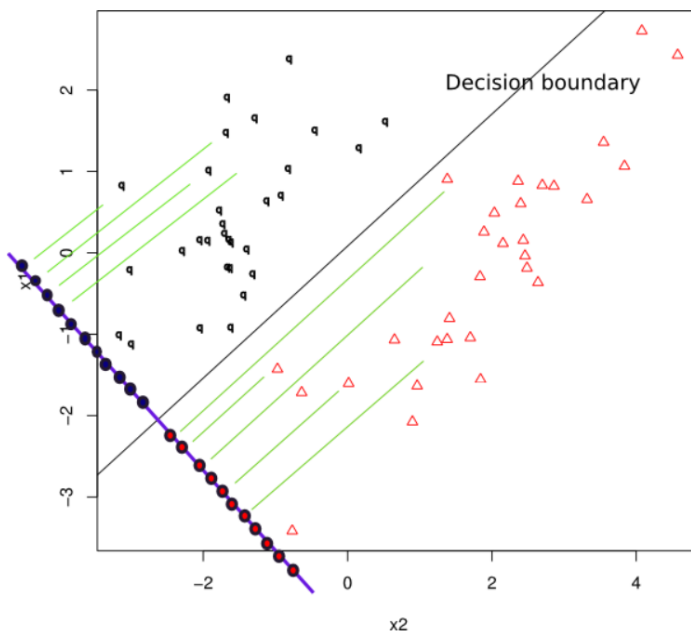


Figure 2.2: Representation of the functioning of an LDA classifier (adapted from ⁶).

2. BACKGROUND

2.6.2 K-Nearest Neighbours

The k-Nearest Neighbours (kNN) is a classification method used to solve both classification and regression problems. The algorithm is based on a simple principle: the distances between each training point and the new observation are computed during the prediction phase. The algorithm then assigns a label to the new observation by choosing the class shared by the majority of the k nearest data points from the training set. In this model, there is no explicit “training” phase, which simplifies the design of the algorithm. Conversely, to predict a new label, kNN has to loop over the entire training set, which makes it impractical for large datasets.

In kNN, k is a parameter that refers to the number of nearest neighbors of a particular data point that will be included in the decision-making process. This is a crucial decisive factor as the classifier output depends on the class to which the majority of these neighboring points belongs. Smaller values of k make the model prone to overfitting, as the prediction is made based only on a few neighbors, which is sensitive to distortions (e.g., noise and outliers) specific to the chosen training set. Conversely, higher values of k put less emphasis on the location of the new observation and more on the general frequency of the samples. In binary problems, the value of k is generally taken as an odd number to avoid ties during decision making [17].

Another factor that affects predictions is the metric used to compute the distance between pairs of points. Euclidean distance is the most common choice, which calculates the ordinary straight line distance between two points in the Euclidean space. Another option can be the Manhattan distance, often referred to as the city block metric, in which the distance between two points is the absolute difference of their Cartesian coordinates, which are common in the case of high dimensionality [3]. Fig. 2.3 shows a representation of a kNN classifier.

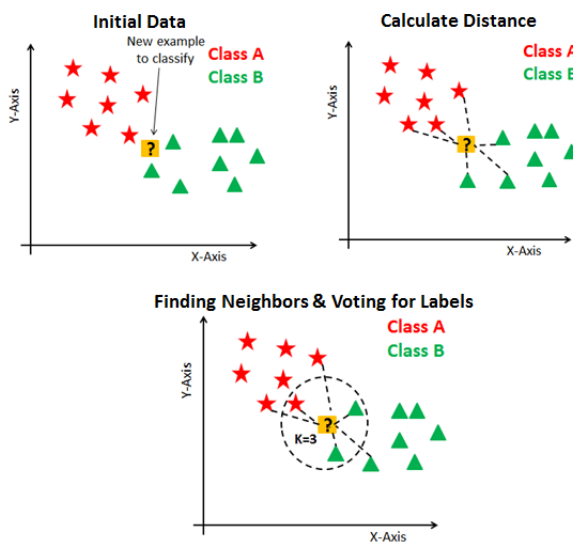


Figure 2.3: Representation of the kNN classifier applied to a two-class problem, considering three neighbors ($k = 3$) (extracted from ⁷).

2.6.3 Decision Trees

Decision Trees (DT) are predictive models used in machine learning, which aim to map observations and predict their target class label or their target value. Depending on their aim, DT structures can be used for classification or regression trees. While the leaves of classification trees represent class labels, the leaves of regression trees represent continuous values [19].

Even though DTs are inexpensive to construct and extremely fast at classifying, they may not provide the same level of accuracy as other classification and regression algorithms since they are prone to overfitting. One way to avoid overfitting is to use Random Forests, a type of ensemble classifier that uses many decision trees. In this

⁶<https://nirpyresearch.com/classification-nir-spectra-linear-discriminant-analysis-python/> (Accessed on 16/11/2021)

⁷<https://www.datacamp.com/community/tutorials/k-nearest-neighbor-classification-scikit-learn> (Accessed on 16/11/2021)

approach, multiple decision trees are trained with subsets of training data. This approach uses a type of majority voting in which the output class label is assigned according to the number of votes from all the individual trees. Fig. 2.4 shows an example of how the classification of objects is performed using a DT.

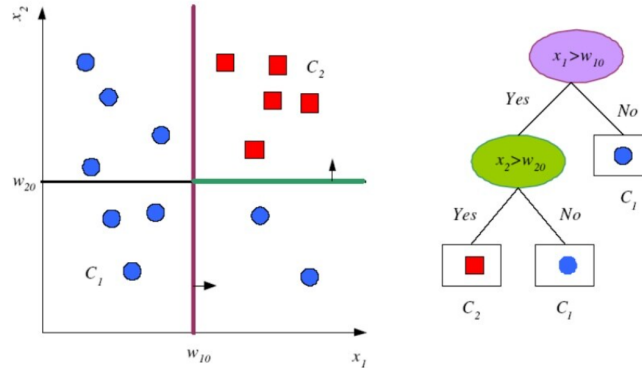


Figure 2.4: Classification of various objects using a Decision Tree Classifier (extracted from ⁸).

2.6.4 Support Vector Machines

Support Vector Machines (SVM) are a classification algorithm highly preferred by many as it produces significant accuracy with less computation power. The objective of the SVM is to find a hyperplane in an N-dimensional space (N = dimension of the feature space) that distinctly classifies the data points.

During the training of SVM, the distance from data points to the class separating hyper-plane is maximized. Generally, the data are not linearly separable. Therefore non-linear kernel transformation is performed. The application of a kernel will transform our data to a higher feature space, where data are linearly separable. There are various kernels that can be used during SVM training. These include Gaussian (Radial Basis) function, Polynomial, and linear kernels. The SVMs also have two other training parameters: the cost parameter (C), which controls the trade-off between smooth decision boundaries and classifying the training points correctly, and the gamma parameter (γ), which controls the degree of non-linearity of the model.

There are potentially many hyperplanes that could be chosen. Thereby, the parameters of the hyperplanes must be optimized to find a plane that has the maximum margin, i.e., the maximum distance between data points and the decision hyperplane. The resulting hyperplane is then used to perform classification of new data points [3]. Fig. 2.5 presents a representation of the SVM classifier.

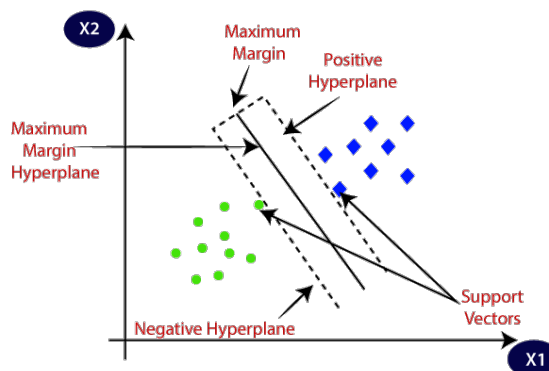


Figure 2.5: Representation of the SVM classifier (extracted from ⁹).

⁸<https://www.slideshare.net/marinasantini1/lecture02-machine-learning> (Accessed on 26/08/2021).

⁹<https://www.javatpoint.com/machine-learning-support-vector-machine-algorithm> (Accessed on 27/08/2021).

2. BACKGROUND

2.6.5 Neural Networks

Neural networks (NN), also known as artificial neural networks (ANN), are a subset of machine learning and are at the heart of deep learning algorithms. The concept of the artificial neural network was inspired by human biology and how neurons of the human brain function together to understand inputs from human senses.

NNs comprise node layers, containing one input layer followed by one or more hidden layers and one last layer called output layer. NNs produce a result by propagating the inputs through the layers, while each neuron performs a weighted sum of its inputs [1]. Fig. 2.6 shows a representation of a NN with multiple layers.

The layers are made of nodes. Computation happens at each node, loosely patterned on a neuron in the human brain, which fires when it encounters sufficient stimuli. A node combines input from data with a set of coefficients, or weights that either amplify or dampen that input, thereby assigning significance to inputs with regard to the data the algorithm is trying to learn. These input-weight products are summed, and then the sum is passed through a node's so-called activation function to determine whether and to what extent that signal should progress further through the network to affect the classification [20]. If the signal passes through, the neuron is "activated". A node layer is a row of those neuron-like switches that turn on or off as the input is fed through the net. Each layer's output is simultaneously the subsequent layer's input, starting from an initial input layer receiving the data [1].

Earlier versions of neural networks such as perceptrons were shallow, composed of one input and one output layer and one hidden layer in between. More than three layers (including input and output) qualify as "deep" learning. In deep-learning networks, each layer of nodes trains on a distinct set of features based on the previous layer's output. The larger the neural net, the more complex are the features that the nodes can recognize since they aggregate and recombine features from the previous layer. This is known as feature hierarchy, and it is a hierarchy of increasing complexity, and abstraction¹⁰.

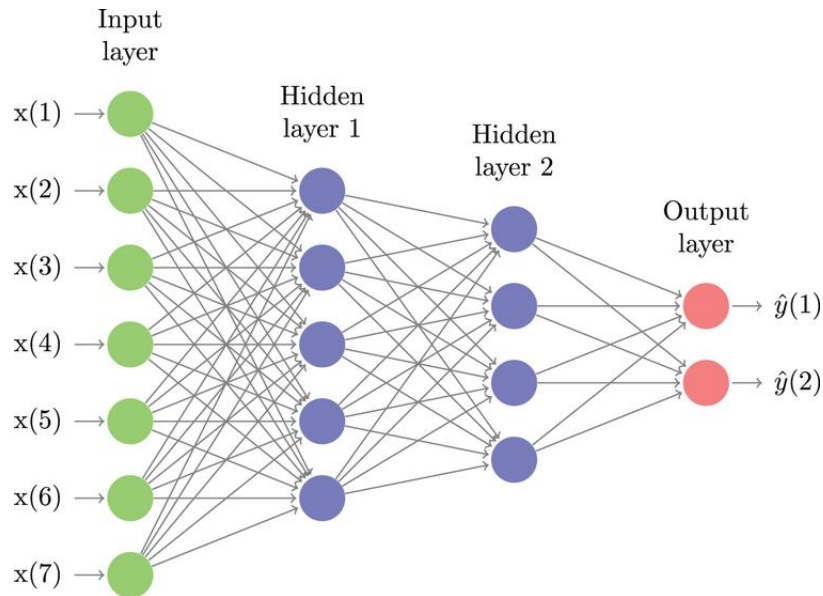


Figure 2.6: Representation of a Neural Network classifier with one input layer, two hidden layers and one output layer (extracted from ¹⁰).

2.6.5.1 Convolutional Neural Network

A convolutional neural network (CNN) is a class of deep neural networks most commonly applied to analyze images. The input for a CNN is an n-dimensional vector carrying the input information. It may be, for example, a 2D matrix representation of an image or a 3D sequence of images (video).

CNNs are composed of multiple layers of artificial neurons, which are mathematical functions that calculate the weighted sum of multiple inputs and output an activation value. Any layer in a network with this ability is

¹⁰<https://wiki.pathmind.com/neural-network> (Accessed on 27/08/2021).

called a convolutional layer, because it is based on the convolution operation. When an image is inputted in a CNN, each layer generates several activation functions that are passed on to the next layer. The first layer usually extracts basic features such as shapes, edges, and other patterns that may appear in an image. The output of these layers is passed on to the next layer, which detects more complex features such as corners or combinational edges. After a convolution, a pooling layer may be used to reduce the dimensions of the feature maps. As we move deeper into the network, it can identify even more complex features such as objects and faces. Based on the activation map of the final convolution layer, the classification layer outputs a set of confidence scores that specify how likely the image is to belong to a class [1]. Fig. 2.7 shows an example of a CNN.

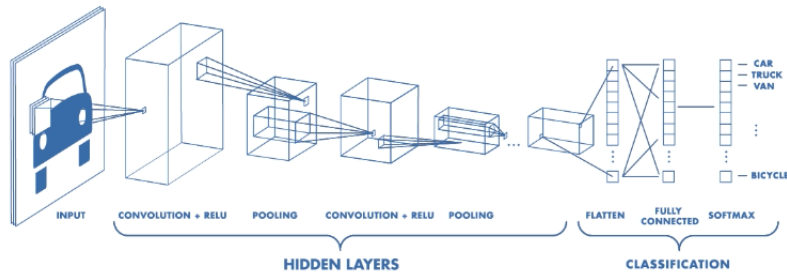


Figure 2.7: Representation of a Convolutional Neural Network, extracted from¹¹, with one input layer corresponding to an image, followed by a few hidden layers, namely a convolutional layer and a pooling layer, and finally some classification layers, such as a fully connected layer or a softmax layer.

¹¹<https://towardsdatascience.com/convolutional-neural-networks-explained-9cc5188c4939> (Accessed on 27/08/2021).

Chapter 3

Literature Review

This chapter includes a review of the most relevant works in ECG biometrics, presenting the data used, the methodology and approaches applied, and the results obtained. Previous studies on ECG-based biometric systems can be differentiated according to the design choices made with respect to data acquisition, feature selection, and template matching techniques.

3.1 Data Acquisition

3.1.1 ECG Recording Techniques

The configurations used for ECG acquisition in biometrics research have significantly evolved over the years, mainly intending to overcome the major disadvantages of ECG as a biometric trait: acquisition acceptability. There is a description below of the different stages of this evolution and examples of investigations that use them.

3.1.1.1 Medical Acquisitions

For medical purposes, there are a few standardized configurations of electrodes for measuring electrocardiogram signals that ease the diagnostic of cardiac conditions. The standard 12-Lead configuration is the most widely used in clinical routine, allowing the acquisition of an ECG signal in 12 leads (or channels): three bipolar limb leads - Lead I, II and III -, three augmented unipolar limb leads - aVF, aVL and aVR -, and six precordial leads - V1-V6 -, as represented in Fig. 3.1. The orthogonal configuration (Frank leads) reflects the electrical activity in the three perpendicular directions X, Y, and Z, requiring only seven electrodes. Although the information contained in this configuration has been found useful in specific applications, the 12-lead ECG continues to be the most used in medical acquisitions because of the existence of well-established criteria for its interpretation. In early ECG biometric research, recordings from standard 12-lead or Frank leads were commonly used for the development of biometric algorithms [21, 22, 23]. Over time, researchers started investigating the selective use of certain leads of these configurations, especially Lead I [24, 25, 26], because of its higher acceptability due to the possibility of placing the electrodes on the wrists, but also Lead II [10, 27, 28], or two chest leads [29, 30].

Nevertheless, there are several limitations associated with medical configurations, namely, the large number of electrodes and their uncomfortable placement, the limited movement, and the duration of the recording that hinder the development of robust biometric systems.

MEDICAL ACQUISITION SETTINGS

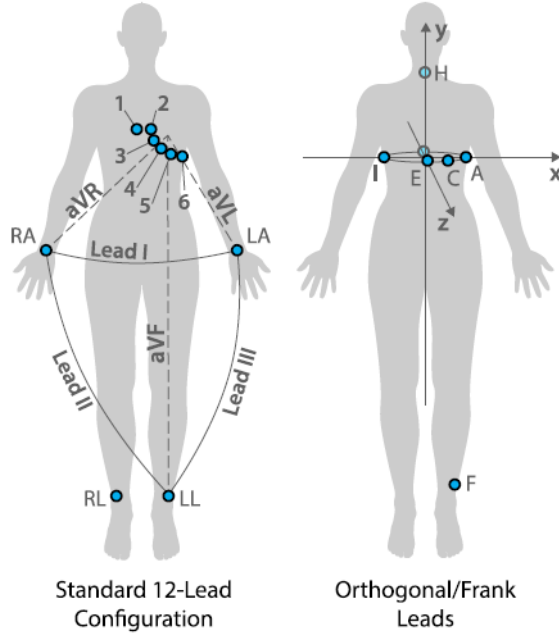


Figure 3.1: Medical acquisition configurations: electrode placements and leads on the standard 12-lead configuration and orthogonal configuration (extracted from [4]).

3.1.1.2 Movement Freedom and Holter Systems

In order to smooth the limitations associated with medical acquisitions, some researchers opted for acquisitions without movement restrictions, with fewer electrodes, and with longer duration. One of the most notable examples was the use of Holter systems, presented in Fig. 3.2, which are prepared to acquire ECG signals during several hours while the subjects are performing their daily basis activities. Labati et al. [31] used 24-hour-long Holter acquisitions to investigate the effect of ECG variability over time on identification performance. Similarly, Zhou et al. [32] used a mini-Holter system to record ECG signals continuously. Even though Holter systems allow longer acquisitions with movement and activity, they still require the placement of electrodes on the torso. This significantly reduces acquisition acceptability and comfort and damages the ECG strength as a biometric trait.

HOLTER ACQUISITION EQUIPMENT

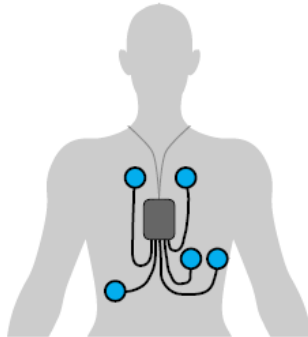


Figure 3.2: Acquisition settings with movement, fewer electrodes, and longer duration: example of a five-electrode Holter System (extracted from [4]).

3.1.1.3 Off-the-person Settings

Researchers took a number of actions regarding the acquisition of ECG signals to improve acceptability and acquisition comfort and be easily integrated into real-world scenarios. Dry metallic electrodes replaced wet elec-

3. LITERATURE REVIEW

trodes, their number was reduced to two or three, and their placement was confined to the upper limbs, especially on the wrists, hands, or fingers. These configurations are called off-the-person settings, unlike the on-the-person settings described in the two topics above. The first research work in ECG biometrics to use off-the-person signals were, to the best of our knowledge, Molina et al. [24] and Chan et al. [33], who used commercial metallic electrodes strapped to the wrists of the subjects and dry button electrodes held by the subjects in contact with their thumbs, respectively. Shen et al. [34] recorded signals from both palms from the subjects while they held two small metallic rod electrodes and, more recently, Matos et al. [35] used only two Ag-AgCl electrodes (with the virtual ground) to acquire ECG at the index fingers. Silva et al. proposed a setup for ECG data acquisition at the hand palms with dry Ag/AgCl electrodes and at the fingers with Electrolycras and created a database, publicly available for the biometric research purpose [2]. Fig. 3.3 shows some of the examples introduced above.

Nevertheless, off-the-person systems do not remove entirely, the disadvantage of ECG over other biometric traits that can be used for unconstrained recognition since they still require the user to hold the electrodes or place the finger or palms over them.

OFF-THE-PERSON CONFIGURATIONS

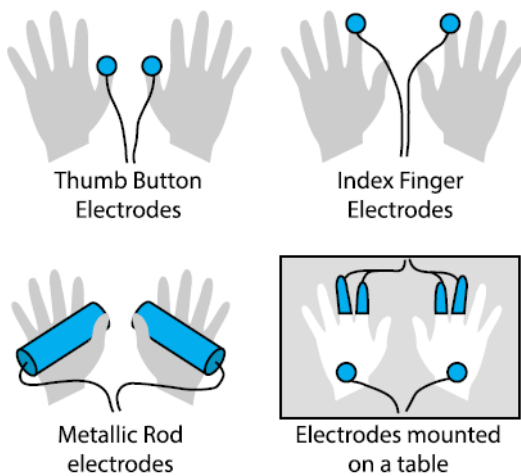


Figure 3.3: Examples of off-the-person ECG acquisition settings, using thumb electrodes [33], index finger electrodes [35], metallic rods grabbed by the subjects [34, 36, 37], or electrodes mounted on a table [35] (extracted from [4]).

3.1.1.4 Wearables and Seamlessly Integrated Acquisition

Recently, some researchers have been improving off-the-person configurations to convert them into unconstrained settings in ECG biometrics and, consequently, close the gap to real applications by developing wearable technologies for ECG acquisition or embedding the sensors into ordinary objects. In research, the first example of this type of configuration was proposed by Coutinho et al. [38, 39], who developed a sensor pad to be used alongside a computer keyboard. While the users use the keyboard, their palms rest on the sensor pad, which continuously acquires their ECG signal to be used for authentication. Silva et al [12] also used this configuration. More recently, Zhang et al. [40] have shown it is possible to acquire ECG signals from a single arm and successfully use them for biometric recognition. An example of a commercial application is the Nymi Band [13], a wearable wristband that acquires the ECG using two metallic electrodes on its inner and outer surface. For the authentication to be performed, the user needs to place a finger of the opposite hand on the outer electrode of the band. The CardioWheel [41] is an example of the incorporation of acquisition electrodes and hardware into common objects. It is a steering wheel cover using conductive leather. Besides seamless and continuous biometric recognition, it also performs health monitoring of drivers, aiming towards automatic personalization of driving settings and remote fleet supervision. Both the Nymi Band and the CardioWheel are represented in Fig.3.4.

These efforts have brought ECG biometrics closer to viable, unconstrained applications. However, there are still a few limitations regarding wearables and seamless acquisitions, such as the fact that the user needs to wear the

product for long periods of time or even touch the electrode to start the acquisition session. Concerning integrated acquisition settings like the CardioWheel, acquisitions are expected to present undesirable noise and frequent signal loss, as the user moves or takes their hands off the electrodes. Hence, these issues must be addressed and adequately solved to obtain viable commercial ECG biometric systems.

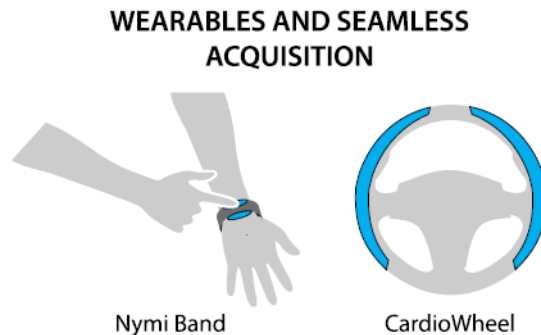


Figure 3.4: Wearable and seamless acquisitions: examples of investigated configurations (extracted from [4]).

3.1.2 Acquisition Conditions

The vast majority of the existing studies use data collected over a single acquisition, as observed in [8, 9, 10, 38, 42, 43, 44]. Although single-session datasets are easier to create, authors cannot use them to draw conclusions about the stability of the ECG as a biometric trait. While several authors used longitudinal ECG data in their studies, to the best of our knowledge, only one study explicitly provided a side-by-side comparison of results achieved using both single-session and multiple-sessions data collected over a period of four months [12]. Silva et al. concluded that ECG-based biometric exhibit promising recognition rates using short-term data collected at a single session and long-term data collected over multiple-sessions [2].

In terms of scale, most studies do not assess the performance of their ECG recognition systems on very large datasets, as it is seen with other biometric modalities. An exception is a research conducted by Carreiras et al., which evaluated the performance of a biometric system using a database of ECG recording collected from 618 subjects, collected over a single acquisition, and obtained high recognition rates [11].

Even though ECG signals obtained during normal resting conditions have been investigated in most studies, some researchers test the feasibility of ECG biometrics under different conditions. Israel et al. explored biometric recognition based on ECG during changes in emotional and mental states, concluding that it is invariable to the individual's state of anxiety [9]. Kim et al. evaluated the performance of their biometric system with ECG data recorded at rest and during physical exercise, proving that with a faster heart rate, the accuracy of human identification decreases [45]. Odinaka et al. tested their system with ECG data from individuals with cardiovascular disorders and also from individuals that used drugs or other substances that may affect ECG signals. Results showed that, even though the cases of misclassification appeared mostly among non-healthy subjects, ECG-based human identification in heartbeat disorder scenarios is quite feasible [46, 47].

3.2 Feature Selection

With respect to feature selection, existing approaches can be broadly classified as fiducial, partially-fiducial, and non-fiducial [3, 12].

- 1. Approaches based on Fiducial Features:** Algorithms based on fiducial features extract temporal, amplitude, area, angle, or dynamics (across heartbeats) measurements derived from the reference points within the signal (e.g., waves or QRS complexes), to create the feature vectors that form the biometric templates. Most of the research in the field of ECG based biometrics is carried out by obtaining fiducial based features

3. LITERATURE REVIEW

to develop identification and authentication systems [8, 9, 10, 25, 26, 28, 45, 48, 49, 50, 51, 52, 53, 54]. Therefore, fiducial features completely depend on the precise detection of points of interest, which is a challenging process due to the high variability of the signal [55].

2. **Approaches based on Non-Fiducial Features:** The most important advantage of approaches based on non-fiducial features, over the fiducial-based approaches, relies on computational costs, as they do not have to determine wave boundaries nor detect fiducial points. Indeed, non-fiducial-based techniques extract discriminative information within the ECG waveform without having any particular reference points in the heartbeat cycles as features. Different types of non-fiducial methodologies have been presented, such as methods based on Wavelet Transform, Discrete Cosine Transform (DCT), and Autocorrelation Coefficients (AC). Chan et al. used Wavelet Distance (WDIST) to measure a distance between wavelet coefficients [33], whereas Plataniotis et al. have suggested a new and robust approach that relies on a combination of AC and DCT of the overall morphology of ECG waveform [22, 56].
3. **Approaches based on Partially-Fiducial Features:** Partially-Fiducial approaches rely on fiducial information only for ECG segmentation. Following the state-of-the-art analysis, these proved to be significantly more uncommon than the other two types of approaches. Palaniappan et al. combined the common fiducial features with a non-fiducial QRS complex form factor, computed using the segment and its first and second derivatives [25]. Ergin et al. proposed the fusion of QRS fiducials, with several time domains, WT, and Power Spectral Density (PSD) features [57]. Dar et al. opted for the extraction of a total of 46 features from Haar transform, and heart-rate-variable RR intervals [58].

3.3 Template Matching

Based on the representation of the ECG acquisition, obtained through feature extraction and dimensionality reduction, the template matching aims to accurately attribute one of the enrolled identities to the user, in the case of identification tasks, or accept or reject an identity claim, for authentication tasks. In the case of identification, the template matching usually consists of a classification process, while, for authentication, the acceptance or rejection of the identity claim is generally based on a reference threshold T that is applied to the prediction score. Adequately assessing performance in both tasks is extremely important, and thus a few metrics have become common for the evaluation of biometric algorithms [58].

3.3.1 Classifiers

The template matching of the ECG biometric algorithms can consist of a classifier, trained with the stored templates from the subjects enrolled with the biometric system, which will discriminate between the subjects, to output an accurate decision when needed. Classifiers are more usual in identification tasks, and the most common are SVM, Nearest Neighbors classifiers, or neural networks.

SVM are classifiers that, based on a given set of training data, compute an optimal hyperplane that divides two classes, ensuring maximum margin between the boundary and the nearest samples [59]. Kernel functions allow mapping non-linearly separable datasets into alternative feature spaces, where an optimal hyperplane boundary can be found. SVM have been extensively used in ECG-based recognition [12, 30, 56, 59, 60, 61, 62]. In what concerns the kernel functions, Gaussian Radial Basis Function (RBF) and non-linear polynomial kernels have been the most used.

Nearest Neighbor Classifiers, commonly kNN, take the feature vector to be tested and those in the training group and, in the feature space, compute the distance between the test observation and each of the training observations. To the feature vector under test is, then, attributed the class corresponding to the majority vote among the k nearest vectors. Nearest Neighbor classifiers have been extensively used in ECG biometrics [11, 21, 23, 62, 63, 64] mainly because they offer the advantage of being easily updated when new samples become available by

just storing them on the database, while most of the other techniques would require the repetition of the training process [58].

As for neural networks, they mimic the function of their biological homonyms, which consist of webs of interconnected neurons that receive inputs, analyze and modify them, and pass them along until they reach a target organ or tissue [58]. These classifiers are composed of nodes (or neurons), arranged in various layers, and connected between them. The first layer receives the inputs (feature vectors), the nodes have activation functions, and their connections are weighted to guide the final classification, outputted by the last node layer [65]. Various types of these classifiers were used in the surveyed approaches, especially the Multilayer Perceptron (MLP) [21], but also Decision-based Neural Network (DBNN) [34], the Radial Basis Function Neural Network (RBFNN) [66], and the Probabilistic Neural Network (PNN) [21].

3.3.2 Metric-based Matching

Other methods are based on the comparison between the template of the currently acquired trait and the templates stored in the system database.

A substantial fraction of the research work that applies metric-based matching methods has opted to use distance metrics. The most popular distance metric was, by far, the Euclidean distance [12, 22, 27, 49, 67, 68, 69]. However, Euclidean distance is regarded by some researchers as unreliable in high dimensional spaces, leading to the use of other metrics, such as the cosine distance [12], the Mahalanobis distance [10, 48, 70], Root Mean Square Error (RMSE) or Wavelet Distance (WDIST) [58].

Besides proximity measures, other techniques can be found in the state-of-the-art. Examples include Gaussian log-likelihood [35, 71, 72] or Ziv-Merhav cross parsing algorithm [38, 39, 73]. In general, metric-based methods offer less accuracy than methods based on classifiers, but they have advantages since they do not have to be trained.

3.3.3 System Evaluation

Proper evaluation is an integral part of designing a viable biometric system. In general, a biometric system is evaluated by assessing the Identification rate (IDR) - the proportion between the correctly identified users and the total number of users in the stored database and can perform two types of errors: a *false acceptance*, which happens whenever a system incorrectly accepts an intruder, and a *false rejection*, which happens whenever a system incorrectly rejects a genuine user. The probability of occurrence of these errors is presented by two metrics: *false acceptance rate* (FAR) and *false rejection rate* (FRR).

In order to improve the overall biometric system performance, the system has to be designed to minimize both FAR and FRR. Eberz et al. define additional metrics that incorporate both FAR, and FRR [13]:

1. **Equal Error Rate (EER):** An error rate that is achieved by tuning the detection threshold of the system so that FAR and FRR are equal.
2. **Receiver Operating Characteristics (ROC) curve:** A graph showing the performance of a classification model at all classification thresholds. The ROC curve allows deriving a set of pairs (FAR, FRR) at which the system can be run by changing the threshold [3].
3. **Area Under the ROC Curve (AUROC):** A measure of the ability of a classifier to distinguish between classes and is used to quantify the ROC curve. The higher the AUROC, the better the performance of the model at distinguishing between the classes.
4. **Confusion Matrix (CM),** also known as an error matrix, is a specific table that allows the visualization of the performance of an algorithm. Each row of the matrix represents the instances in a predicted class, while each column represents the instances in an actual class (or vice versa).

3. LITERATURE REVIEW

		True Class	
		Positive	Negative
Predicted Class	Positive	TP	FP
	Negative	FN	TN

Figure 3.5: Confusion Matrix Schematic.

A confusion matrix, such as the one represented in Fig. 3.5, is composed of four measures - True Positive, True Negative, False Negative, and False Positive -, from which it is possible to calculate some metrics for evaluating the performance of the algorithm. The measures can be defined as:

- **True Positives (TP):** the number of correct predictions for positive samples.
- **True Negatives (TN):** the number of correct predictions for negative samples.
- **False Negative (FN):** the number of incorrect predictions for positive samples.
- **False Positive (FP):** the number of incorrect predictions for negative samples.

These measures are used to calculate some evaluation metrics such as accuracy, precision, recall, F1-Score and so forth:

1. **Accuracy:** can be defined as the ratio of correct classifications to the number of total samples. The accuracy can be formulated as follows:

$$Accuracy = \frac{TP + TN}{TP + TN + FP + FN} \quad (3.1)$$

2. **Precision:** identifies how accurately the model predicts the positive classes. It is the proportion of the correctly predicted as positive samples inside the total number of positively predicted samples. The precision can be formulated as follows:

$$Precision = \frac{TP}{TP + FP} \quad (3.2)$$

3. **Recall (or Sensitivity):** measures how many of the actual positive samples are predicted as positive. The recall can be formulated as follows:

$$Recall = \frac{TP}{TP + FN} \quad (3.3)$$

4. **F1-Score:** considers both precision and recall. It is the harmonic mean (average) of the precision and recall. F1-Score is better if there is a balance between precision and recall in the system. Conversely, F1-Score is not so high if one measure is improved at the expense of the other.

$$F1 - Score = \frac{2 \cdot (Recall \cdot Precision)}{(Recall + Precision)} \quad (3.4)$$

3.4 Related Works

Biel et al. [8] used features directly outputted by an ECG medical acquisition device, Lead I, and performed decisions using Principal Component Analysis (PCA) and Soft Independent Modelling of Class Analogy (SIMCA), obtaining an IDR of 100% with 20 subjects. Kyoso and Uchiyama [10] extracted 34 fiducial latency features, and attained 99.5% and 94.2% IDR (with three and nine subjects, respectively), using LDA for dimensionality reduction and Mahalanobis distance for classification. Palaniappan et al. [25], Chan et al. [33] and Singh et al. [49] have also used features from the time-domain, and achieved an accuracy of 97.6%, 90.8%, and 99% for identification, respectively. Several approaches to non-fiducial point based systems have been attempted, such as Fourier Transform [45, 74], discrete wavelet transform [75, 76], autocorrelation [22, 77] and Legendre polynomials [78] with a recognition from 77% to 100% for as many as 35 subjects.

Chan et al. were the first researchers to explore the off-the-person approach for biometrics, with metallic electrodes on the thumbs, obtaining 89% of IDR [33]. Coutinho et al. acquired signals from hand palms, using a conductive mat next to a computer keyboard, and reaching 99.5% IDR [38]. More recently, an off-the-person approach was developed by a group of researchers from the University of Toronto [79] and used by Louis [80] for authentication, rendering an EER of 7.89% with 1012 subjects.

ECG, being a continuously available physiological signal, opens possibilities for the development of continuous or real-time recognition systems, which is especially advantageous for security or surveillance purposes. Guennoun et al. were the first to explore such systems, for authentication, using fiducial features and Mahalanobis Distance, and made decisions according to the individual matching of 35 consecutive heartbeats, obtaining 0.01% FRR and 0% FAR [48], for 16 subjects. Matta et al. pioneered continuous identification of 10 subjects, assessing identity every five seconds with 75% IDR, using AC and LDA for feature extraction and Euclidean distances for classification[69].

Fang et al. [29] and Zhang et al. [75] have concluded, respectively, that using one lead renders significantly worse results than three leads, and using limb leads such as I or II decreases the performance compared to the use of chest leads V1 or V2. This proves the additional difficulty placed upon off-the-person signals. Agrafioti and Hatzinakos also showed that, despite what happens when using one-lead for ECG identification tasks, it is possible to achieve 100% subject recognition rate with a database of 249 subjects in a 12-lead ECG system [81].

Pinto et al. investigated the influence of the training data on the performance of the system [82]. This approach was tested for identification and authentication tasks in two settings: using 70% of each subject's data for training and 30% for testing; and the second, using solely the first 30 seconds of data of each subject for training. The results were worse with scarce train data for both tasks (IDR decreased from 94.6% to 70.9% and authentication EER increased from 2.66% to 11.8%, when using the second setting).

Other aspects that have been explored in ECG biometrics address the effects of heart rate variability, different leads used, and long-term acquisitions. Pathoumvanh et al. verified that the IDR of their system, based on CWT features and Euclidean distance, decreased from 97% to 80% when using signals acquired after exercise [27]. Ye et al. observed that the performance, using DWT and ICA features with SVM (with RBF), on long-term signals is consistently worse than short-term [30].

Tables A.1, A.2, A.3, and A.4 presented in Appendix A, show the reviewed methodologies proposed for ECG recognition, and the corresponding results, in chronological order of publication.

Chapter 4

Biometric Data and Systems

This chapter describes the design of the proposed biometric identification and authentication systems based on ECG signals. It starts with the data description followed by the delineation of the pre-processing. Then, the process of the templates generation is explained and a detailed description of the methods used for the identification and authentication tasks is presented.

The suggested systems use a database based on “off-the-person” approaches for signal acquisition. Two different templates were used, cardiac cycles and scalograms. For that, features were extracted from the ECG trace using a partially-fiducial approach, since the present work proposes the fusion of QRS fiducials, with a time-frequency domain feature, the wavelet transform. Finally, several classifiers and a distance-based approach were tested for template matching. Fig. 4.1 illustrates the overall system design. The experiments were performed in Python (using the *Neurokit2* package¹²) and Matlab (MATLAB R2020b & Simulink R2020b).

4.1 Data Collection

Electrocardiogram data is one of the novel biometric traits, in which a growing interest is evident within the reference literature. A particularly important aspect, that is transversal to all the work done to date, is the access to large datasets to evaluate the robustness of the devised methods across research teams.

Recognizing the need and usefulness of centralized datasets that can be used as a common reference for researchers worldwide, several initiatives have been contributing with resources to mitigate this. Physionet¹³ is currently one of the main forums of dissemination and exchange of biomedical signals in general. Most publicly available datasets are currently centralized on the PhysioBank repository, and contain multiple parameters from healthy and pathological conditions (cardiorespiratory, neural, and others). However, in what concerns ECG datasets, most of the public resources found to date only contain signals collected at the chest with clinical grade equipment.

A recent initiative by Silva et al [2] aimed to create a standardized database to promote research in ECG biometrics. As a result of the work by the CYBHi, two public datasets were released, for short-term and for long-term assessment, with ECG data collected at palms and fingers.

¹²<https://github.com/neuropsychology/NeuroKit> (Accessed on 16/11/2021).

¹³<https://physionet.org/content/ecgidb/1.0.0/> (Accessed on 29/12/2020).

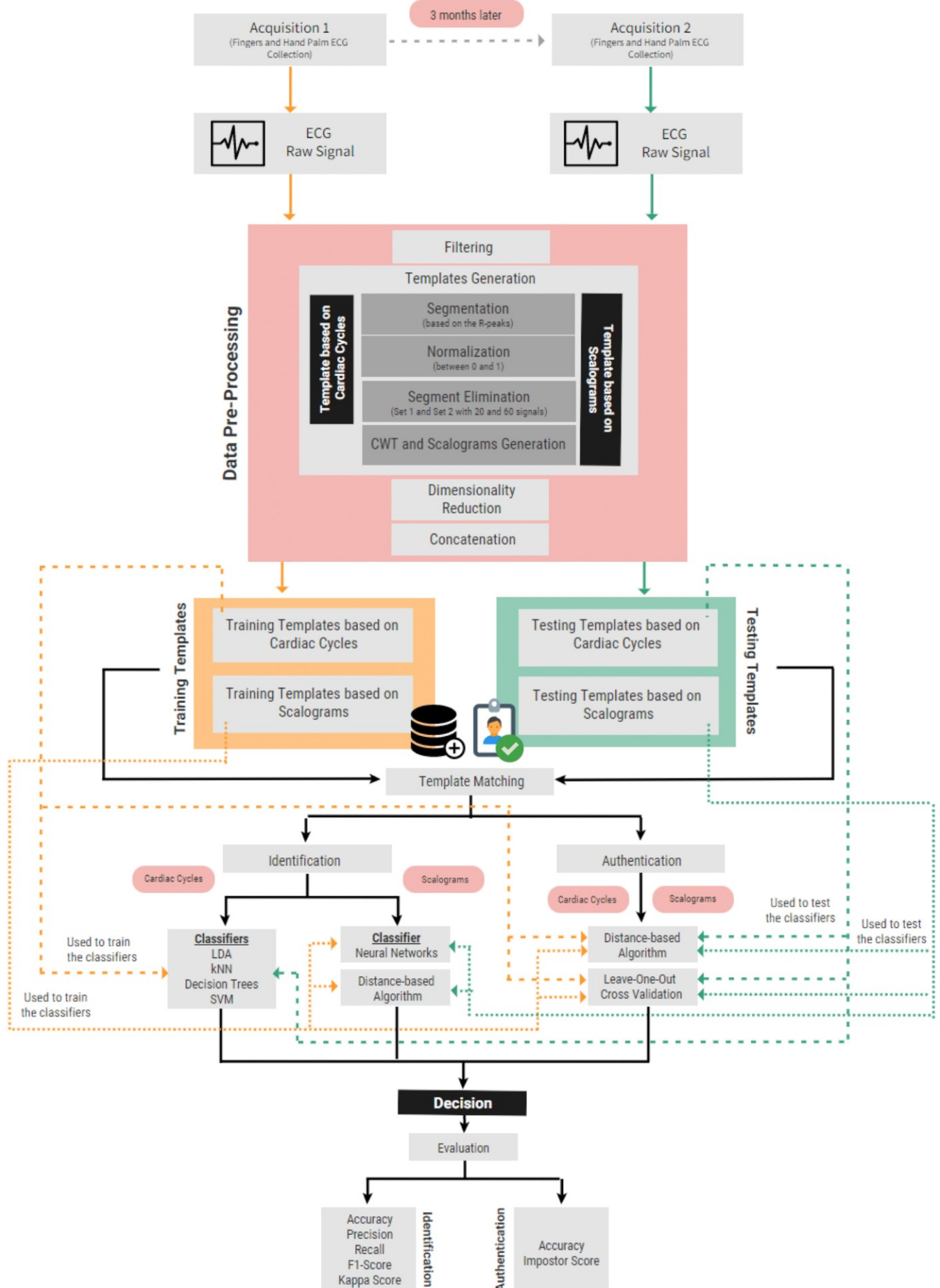


Figure 4.1: Flow diagram of the proposed systems.

4. BIOMETRIC DATA AND SYSTEMS

4.1.1 Experimental Setup

In the present research, a publicly available database, created for biometric purposes, was used: the CYBHi long-term dataset, which presents an adequate benchmark for evaluating ECG-based biometric systems. Using an off-the-person approach, Silva et al. [2] proposed a setup for ECG data acquisition at the hand palms with dry Ag/AgCl electrodes and at the fingers with Electrolycras, to assess the biometric potential of signals collected at these anatomic regions and compare the performance of both materials. ECG data acquisition was performed with a custom, two lead differential sensor design with virtual ground, proposed in [83]. Two ECG sensors were used in their experimental setup, one for signal acquisition at the hand palms with dry Ag/AgCl electrodes, and another for signal acquisition with Electrolycras at the index and middle fingers. For improved comfort and greater efficiency, the ECG sensors were fitted to a leather base, with the intended hand placement signaled in an unequivocal way. Fig. 4.2 depicts the devised sensor and electrodes arrangement. One of the ECG sensors was connected to the dry Ag/AgCl electrodes that were placed at the base of the hand palms, near the thenar eminence; the other ECG sensor was connected to the Electrolycra strips placed along the index and middle fingers. Fig. 4.3 presents the full experimental setup.

Raw biosignals were acquired with a bioPLUX research¹⁴, a bluetooth wireless biosignal acquisition unit; this device was used in a 12-bit resolution with 1 kHz sampling frequency configuration. To guarantee electrical isolation between both ECG sensors used in the experiments, two independent biosignal acquisition units were used.



Figure 4.2: Electrocardiography sensors and electrodes arrangement. At the top: the electrolycra strips; At the bottom: the dry Ag/AgCl electrodes [2].



Figure 4.3: Full experimental setup comprising the hardware configuration used in Silva et al. experiments for biosignal acquisition [2].

¹⁴<http://www.biosignalsplus.com/> (Accessed on 16/11/2021).

4.1.2 Participants

The experimental setup was prepared at the cardiopneumology laboratory located at the *Escola Superior de Saúde da Cruz Vermelha Portuguesa*, which was prepared to collect the participants.

The recruitment of volunteers was performed by advertising the days in which data acquisition sessions were held, and by providing an overview of the action during classes. A total of 63 subjects (nursing and health technologies students) were enrolled in the experiment and participated in the two acquisition sessions. The demographics showed 12 males and 49 females, with an average age of 20.68 ± 2.83 years old. None of the participants reported any health problems, reason for which the collected data is considered to be representative of normal population.

4.1.3 Experimental Procedure

Two data acquisition moments separated by a 3-month time-frame took place, and enabled data recollection from the set of volunteers enrolled in the experiment, with the purpose of studying the changes in the ECG morphology over time. Firstly, the coordinator of the experiment presented the informed consent to prospective participants, explaining the procedure in detail, goals of the study, and related background work. Once participants willingly showed interest in participating in the experiments, they were required to sign the document and were enrolled in the data collection program.

In both moments only ECG signals at the fingers were recorded, and in each of the sessions the subjects were asked to sit for 2 minutes in a resting position, with two fingers - one from the left and another from the right hand - placed in each of the dry Ag/AgCl electrodes. The recordings were stored in individual files for more efficient post-processing, and labeled with the date, identification of the system, and a code assigned to the subject. The fact that two sessions took place separated by several months apart makes this dataset particularly useful for benchmarking the performance of identity recognition systems taking into account potential variations in the heartbeat waveform over time.

4.2 Data Pre-processing

The pre-processing task performed in the present study, for both the identification and authentication algorithm, consists of the following stages:

1. Signal Filtering;
2. Templates Generation;
3. Templates Concatenation;
4. Dimensionality Reduction.

4.2.1 Signal Filtering

In general, every raw signal has a noise component, whose magnitude varies depending on the quality of the sensor and the measurement procedure. Often, a raw signal can suffer from a baseline wander, a low frequency noise caused by respiration, electrodes impedance, and movement. It is required to remove the baseline wander in order to minimize changes in beat morphology, which do not have cardiac origin. Another common source of noise is due to powerline interference, which has a frequency between 50 and 60 Hz [84]. Moreover, ECG signals collected at the hands and fingers, especially using dry electrodes, can also suffer from additional noise due to electrodermal and muscular activity. The removal of this type of noise represents an important filtering problem difficult to handle, because of the substantial spectral overlap between the ECG and muscle noise.

4. BIOMETRIC DATA AND SYSTEMS

In this work, a 4th-order Butterworth bandpass IIR filter, with cutoff frequencies of 0.5 Hz and 30 Hz was applied to the raw ECG data, using MATLAB, with the purpose of removing undesired frequencies and smoothing the signal. This type of filter is popular in signal processing due to having almost no ripple, i.e., oscillations in its pass band. It has been used for ECG denoising and, when compared to other filters, has a reported accuracy close to wavelet-based filters at a fraction of the computational cost [84].

The results of applying this filter on a raw ECG signal from a randomly selected subject is presented in Fig.4.4.

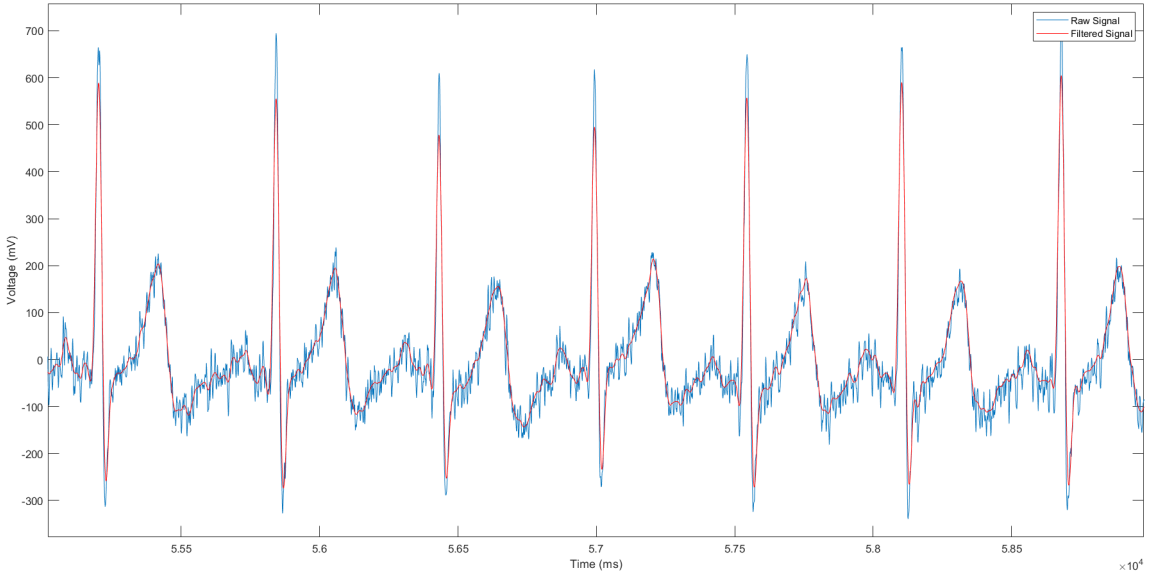


Figure 4.4: Representation of the raw ECG, in blue, and the filtered ECG, in red, for a randomly selected subject, using a 4th-order bandpass Butterworth IIR filter, with cutoff frequencies of 0.5 Hz to 30Hz.

4.2.2 Templates Generation

As previously reported, each subject was subjected to two ECG acquisition sessions. The signals from the first acquisition represent the training template and a label is associated with the corresponding user's identity. The second acquisition represents the testing template and will be compared to the training templates to authenticate or identify a subject. This section presents the feature extraction methods applied for both the training and testing templates. After filtering the ECG, two different types of featured-templates were generated to be tested by different template matching methods: 1) Template based on cardiac cycles, and 2) Template based on Scalograms of the cardiac cycles.

4.2.2.1 Template based on Cardiac Cycles

The template based on cardiac cycles is obtained through a three-step process: 1) Segmentation of the ECG signal using the Neurokit2 Package from Python [85]; 2) Normalization of the cardiac cycles to diminish differences in the same subjects in between acquisitions and to avoid potential differences between subjects due to acquisition equipment and external interactions; and 3) Segment elimination to drop corrupt cardiac cycles. After this process, two sets of templates, for both training and testing data, are assigned to each subject: one with 20 and other with 60 cardiac cycles.

1. Segmentation

After denoising the signal, the ECG trace can be used to extract features that comprise a biometric template of the subject. For this project, a partially-fiducial approach was used, involving extracting features from individual heartbeat waveforms. For this reason, an appropriate segmentation algorithm was required, which would locate the R peaks within the ECG trace and perform appropriate partitioning of the signal, based

on these peaks. For this segmentation, Neurokit2, which is an open-source Python package dedicated to neurophysiological signal processing, was used [85].

The delineate function of the Neurokit2 package [85] uses the location of the detected R-wave peaks to perform the signal partitioning into individual heartbeats with 600 samples, 200 before and 400 after the R-peak, in order to mitigate the fact that subjects have a variable heart rate during ECG data collection.

2. Normalization

As previously discussed, the electrocardiogram varies over time with several factors, such as differences in acquisition equipment or the interaction of the subject with it, which may cause differences in signal amplitude. Moreover, heart rate variability causes significant changes in the duration of the heartbeats and their waveforms. In order to ensure high performance regardless of this, some researchers include amplitude normalization techniques in the ECG biometric algorithms [4].

In the present work, each segment is scaled to lie between 0 and 1, according to the min-max normalization method proposed by Irvine et al. [86], i.e., by subtracting its minimum and dividing the result by the difference between its maximum and its minimum:

$$x' = \frac{x - \min(x)}{\max(x) - \min(x)} \quad (4.1)$$

where x denotes the cardiac cycle. The cardiac cycles were also tested without normalization to check whether normalization reduces the differentiability between acquisitions for the same subject, impairing, consequently, the capacity of the system to distinguish subjects.

Fig. 4.5 illustrates the normalized individual heartbeat waveforms obtained by the signal segmentation for a single subject.

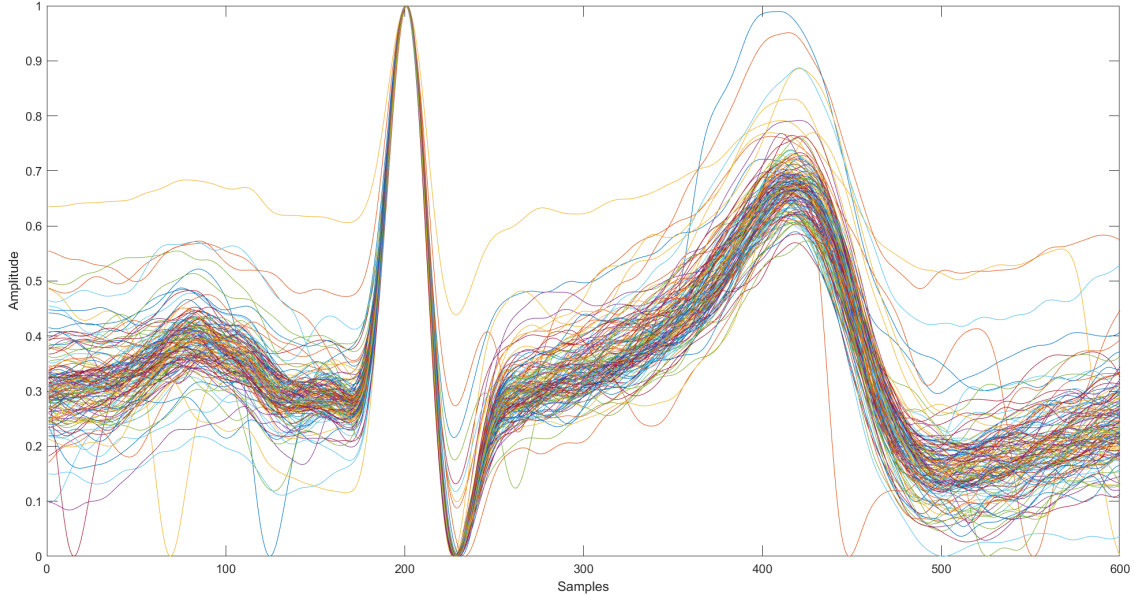


Figure 4.5: Individual heartbeat waveforms for a single subject (138 waveforms).

3. Segment Elimination

As the data were obtained through ECG measurements in suboptimal settings, namely hand palms and fingers, some segments may contain substantial amounts of noise and motion artifacts when compared to others. These unwanted events generally harm the performance of the model. Thus, in order to mitigate the effect of such interference, a simple outlier removal procedure was used to drop the corrupt segments.

4. BIOMETRIC DATA AND SYSTEMS

All the heartbeat waveforms for a particular subject were presented in the form of a matrix, where each row is a 600-dimensional vector representing a single heartbeat. As a first step, the algorithm computes the Euclidean distance between all the heartbeat waveforms. Then, it finds, for each subject, the 20 and the 60 cardiac cycles more similar to each other, corresponding to *Set 1* and *Set 2*, respectively. These two sets of segments correspond to the cardiac cycles-based templates.

In practice, this outlier removal procedure performed well even with the ECG signals severely corrupted by noise. Fig. 4.6 shows the *Set 2* of the training template of the subject presented in the previous figure, in which the more corrupted segments from Fig. 4.5 were eliminated.

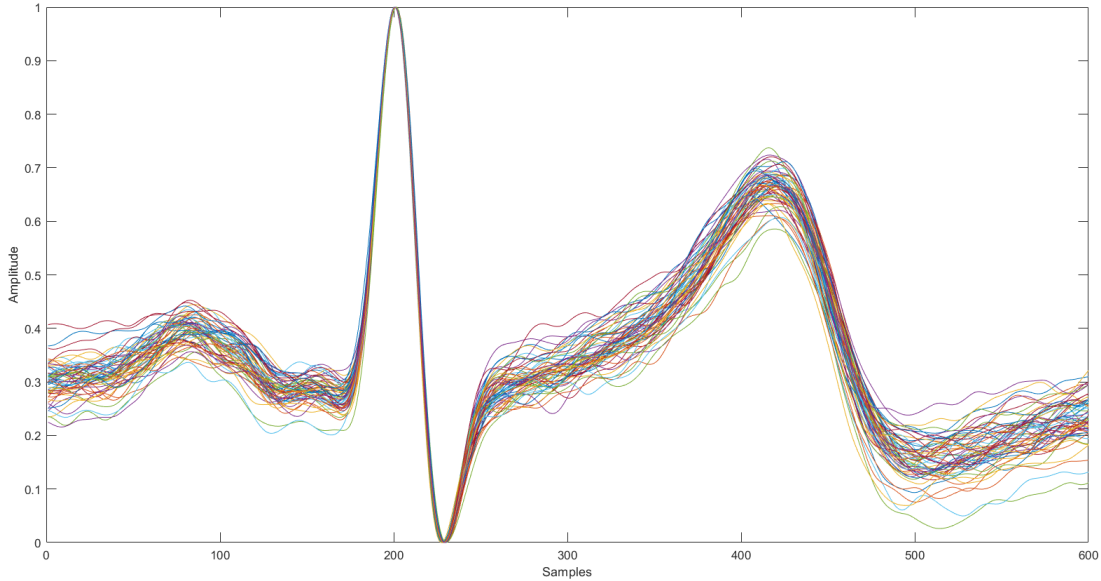


Figure 4.6: ECG variation within a single subject, after performing the segment elimination (60 waveforms).

4.2.2.2 Template based on Scalograms

As mentioned above, besides the templates based on cardiac cycles, the other type of template used in the present investigation were based on scalograms. A scalogram is the absolute value of the CWT coefficients of a signal. By transforming the signal from the time domain to the frequency and time domains, the 1-D signal becomes a 2-D matrix, and it could be analyzed on multiresolution.

In the present work, CWT based on the Morse wavelet with $\gamma = 3$ and $P^2 = 60$ were used to transform the cardiac cycles to a series of corresponding 2D time-frequency scalogram representations. The wavelet-transformed scalograms were resized to squared-scalogram with 56x56 and 224x224 - called, from now on, *Size 56* and *Size 224* -, corresponding to 9408 and 150528 pixels, respectively. Fig. 4.7 illustrates the time-frequency scalogram representation of a cardiac cycle from a randomly selected subject. As for the cardiac cycles, two sets of templates based on scalograms were generated for each subject - *Set 1* and *Set 2* -, with 20 and 60 scalograms each, respectively. Furthermore, for distance-based classification purposes, each scalogram, represented by a 56x56x3 or 224x224x3 matrices, was transformed to produce the columns into a vector, originating templates of scalograms vectors of sizes 9.408 and 150.528 (respectively).

4.2.3 Templates Concatenation

From the segment elimination process resulted the *Set 1* with 20 templates and the *Set 2* with 60 templates, for the training and testing sets of each participant, either for the cardiac cycles and for the scalograms vectors.

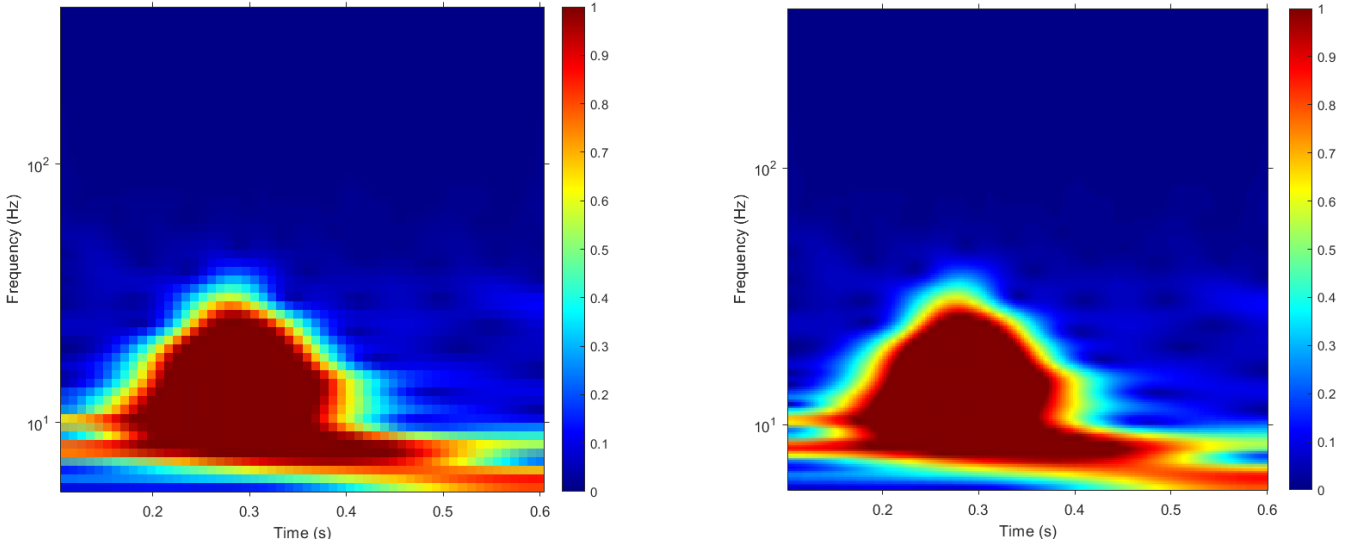


Figure 4.7: Scalogram representations of a randomly selected electrocardiogram. The scalogram on the left was resized to 56x56, whereas the one on the right was resized to 224x224. The colormap is composed of cold and hot colors, varying from blue at the weakest intensity to red at the strongest intensity.

For some matching approaches presented in the following two sections, the number of templates per subject needed to be reduced, thus, concatenation of templates was performed. For the *Set 1*, for training and testing, concatenation resulted in one new template per subjects, formed by the respective 20 initial templates, cardiac cycles or scalograms vectors, followed by one another. For *Set 2*, and only for testing purposes, concatenation resulted in three new templates per subject, each of them formed by 20 initial templates, followed by one another in similarity order.

Thereby, the template concatenation process resulted in 63 (1 x 63 subjects) and 189 (3 x 63 subjects) new templates, for the *Set 1* and *Set 2*, respectively.

4.2.4 Dimensionality Reduction

To ease the interpretability of this process it is worthwhile to mention that the size of the templates represents the number of features to deal with. Moreover, it is also important to refer that, the training and testing sets, with all the subjects, can be represented as a matrix in which the rows represent subject templates and columns represent features (the values of the templates).

Thus, considering the 63 subjects and the different number of features (or sizes of the templates), it is straightforward that the training and testing sets have dimension 63 x 188,160 and 63 x 3,010,560 for scalograms of sizes 56 and 224, respectively, and dimension 63 x 12,000 for cardiac cycles. Therefore, since the dimension of each template, i.e., the number of attributes, is considerably high, performing template matching would be computationally expensive regardless the approach used. In order to alleviate this problem, the independent component analysis (ICA) was applied, using the FastICA algorithm implemented in MATLAB, to reduce the dimension of the templates (which is equivalent to reduce the number of features, as each value in the template represents a different feature) [3].

The methodology used to determine the ICA representations consists of the following steps:

- Definition of the training and the testing sets, $\mathbf{X}_{\text{train}}$ and \mathbf{X}_{test} , respectively. In the present work, the training set corresponds to the templates obtained from the ECG signals of the first acquisition session, whereas the templates obtained from the second acquisition represent the testing set.
- Estimation of the ICs based on the training set and consequent definition of the matrix of the ICA coefficients, $\mathbf{A}_{\text{train}}$, which, according to Eq. 2.7, allows to obtain $\mathbf{X}_{\text{train}}$ depending on the estimated ICs, $\hat{\mathbf{s}}$.

4. BIOMETRIC DATA AND SYSTEMS

- Definition of the ICA coefficients matrix, \mathbf{A}_{test} , referring to the testing set \mathbf{X}_{test} , which corresponds to the projection of each templates of the \mathbf{X}_{test} in the ICA space generated by the estimated ICs, $\hat{\mathbf{s}}$. \mathbf{A}_{test} can be obtained through the following relation:

$$\mathbf{X}_{\text{test}} = \mathbf{A}_{\text{test}} \cdot \hat{\mathbf{s}} \Rightarrow \mathbf{A}_{\text{test}} = \mathbf{X}_{\text{test}} \cdot \hat{\mathbf{s}}^T \cdot (\hat{\mathbf{s}} \cdot \hat{\mathbf{s}}^T)^{-1} \quad (4.2)$$

As mentioned above, the application of the ICA aims to reduce the number of features. Considering the dimensions of the training and testing sets mentioned above, which are extremely high, by applying the ICA, the dimensionality is reduced to 63^2 , which will significantly minimize the computational cost.

The dimensionality reduction (DR) was only applied for some of the template matching approaches in the following two sections, for cardiac cycles and scalograms templates, in order to draw conclusions on the advantages of reducing the dimensionality of the templates in each scenario.

4.3 Identification Algorithm

The identification system was tested using cardiac cycles and scalograms as inputs. For the cardiac cycles, several classifiers were implemented in MATLAB to predict the identity of the subjects according to their ECG data, in two different configurations: *Configuration 20/20* and *Configuration 60/60*. In the former configuration, classifiers were trained with the *Set 1* from the training templates and tested with *Set 1* from the testing templates. In the *Configuration 60/60*, *Set 2* of the training and testing templates were used to train and test the classifiers, respectively. For these classifiers, templates concatenation and DR were not applied. For the scalograms, two distinct methodologies were executed: 1) a neural network assessed in *Configuration 20/20* and *Configuration 60/60*, in which templates concatenation and DR were not applied, and 2) a distance-based algorithm with concatenated and dimensionally reduced scalograms as input, assessed in *Configuration 1/1* and *Configuration 1/3*, in which, for each subject, one concatenated training template is compared with one testing template or compared with three testing templates, respectively.

4.3.1 Identification based on Cardiac Cycles

In the present work, several classifiers were tested in order to compare the performances of the identification of subjects based on their cardiac cycles. LDA, kNN, DT, and SVM were tested as classifiers, and the models were trained with the cardiac cycles obtained from the first acquisition, whereas the ECG from the second acquisition were used to test them. All the models were fed with normalized and not normalized templates. Classifiers were compared based on the following weighted evaluation metrics: accuracy, weighted precision and recall, and F1-Score.

4.3.1.1 LDA

The classification rule for LDA is very intuitive. The major computational effort is the training phase, i.e., the computation of the discriminant functions and their parameters. Once the training phase is completed, new data can be classified simply by solving the appropriate discriminant function for each class, and applying the classification rule. The classifier was trained with the training templates and then, it predicted the subjects' identity from the testing templates. Intrinsically, LDA has no parameters to be optimized.

4.3.1.2 kNN

The performance of KNN is optimized by two hyperparameters. First, it is crucial to find an appropriate k , which is not a trivial problem. There are many ways of choosing the number of neighbors to use (the k value), but a simple one is to test different k 's and choose the one with the best performance. For the *Configuration*

20/20, k was set from 1 to 20, whereas for *Configuration 60/60*, the algorithm was tested with k between 1 and 60. The second hyperparameter that influences the performance is the type of distance metric. In the present study, the Manhattan distance was the distance implemented, since it is the one recommended to be used in high-dimensionality problems.

The Manhattan distance, also called city-block or taxicab distance, between two vectors \mathbf{p} and \mathbf{q} in an n -dimensional real vector space with fixed Cartesian coordinate system is the sum of the lengths of the projections of the line segment between the points onto the coordinate axes [87]. It can be calculated according to the following equation:

$$d(\mathbf{p}, \mathbf{q}) = \|\mathbf{p} - \mathbf{q}\| = \sum_{i=1}^n |p_i - q_i| , \quad (4.3)$$

where (\mathbf{p}, \mathbf{q}) are vectors $\mathbf{p} = (p_1, p_2, \dots, p_n)$ and $\mathbf{q} = (q_1, q_2, \dots, q_n)$.

Fig. 5.1 on Chapter 5 shows the values of k that optimize the performance of the kNN model for normalized and not-normalized cardiac cycles in both configurations.

4.3.1.3 DT

Decision Trees can efficiently deal with large, complicated datasets without imposing a complicated structure. The training dataset was used to build a decision tree model and the testing dataset was classified. The DT complexity has crucial effect on its accuracy and it is explicitly controlled by the stopping criteria used and the pruning method employed. Usually, the tree complexity is measured by one of the following measures: the total number of nodes, total number of leaves, tree depth, and number of features used.

In the present work, the classifier was tested with the default parameters from Matlab, for both the normalized and not normalized cardiac cycles. The *MaxNumSplits* parameter, which is the maximal number of decision splits (or branch nodes) was set to $N-1$, being N the training sample size, the *MinLeafSize*, which is the minimum number of observation in the leaf nodes, was set to 1, whereas the *MinParentSize*, representing the minimum number of branch node observations, was set to 10.

4.3.1.4 SVM

The main hyperparameter of the SVM is the kernel. It maps the observations into some feature space. There are multiple standard kernels for these transformations, e.g., the linear kernel, the polynomial kernel, and the radial basis function kernel. The latter is the most used and most successful kernel, due to the flexibility of separating observations with this method. Besides the kernel, the cost parameter (C) and the gamma (γ) are also hyperparameters that should be tuned. According to Wainer et al. [88], for the RBF, the C and γ should be tuned in the ranges $[2^{-5}; 2^{15}]$ and $[2^{-15}; 2^3]$, respectively.

In the present work, three kernels were tested, namely linear, RBF and polynomial, and both C and γ were set between $[2^{-15}; 2^{15}]$. The combinations that optimize the performance of the system are presented in section 5.1.1.2.

4.3.2 Identification based on Scalograms

The scalograms were given as input for convolution neural networks and for a distance-based algorithm, differing in the configuration of the signals. The CNN was performed in *Configuration 20/20* and *Configuration 60/60*, being trained with the signals from the first acquisition session and tested with the signals from the second session. For the distance-based algorithm, the inputs were concatenated and dimensionally-reduced scalograms in *Configuration 1/1* and *Configuration 1/3*.

4. BIOMETRIC DATA AND SYSTEMS

4.3.2.1 Neural Networks

A simple 15-layer CNN was implemented in MATLAB to automatically learn the hidden patterns from the scalogram matrices, without feature engineering. It is composed of an input layer, three convolutional layers, three Batch normalization layers, three ReLU layers, two max-pooling layers, one fully connected layer, one softmax layer, and one classification layer. The first layer takes a 56 x 56 x 3 or 224 x 224 x 3 images as input. The second layer is a convolutional layer with 3, 8, and 3 as the filter size, number of filters, and number of padding size extracted features, respectively. In the third layer, a Batch normalization layer is used to speed up networking training and reduce the sensitivity to network initialization. This type of layers is used between convolutional and ReLU layers. As so, the fourth is a ReLU layer, which is a non-linear activation function. The fifth layer is a max-pooling layer with a pool size of [2,2]. This makes it possible to increase the number of filters in deeper convolutional layers without increasing the required amount of computation per layer. In this sixth layer, a 3-16-3 convolutional layer is applied. The seventh, eighth and ninth layers are Batch normalization, ReLU and max-pooling ([2,2]) layers, respectively. The tenth was a 3-32-3 convolutional layer. The eleventh is a Batch normalization layer followed by a ReLU layer again. The thirteenth is a fully connected layer, which combines all the features learned by the previous layers across the image to identify the larger patterns. This last fully connected layer, in this case, combines the features to classify the images. The fourteenth is a softmax layer, which consists of an activation function that normalizes the output of the fully connected layer. The output of this consists of positive numbers whose sum is one, which are used as classification probabilities by the fifteenth and last layer, i.e., the classification layer. This uses the probabilities returned by the softmax activation functions for each input to assign the input to one of the mutually exclusive classes and compute the loss.

4.3.2.2 Distance-based Identification Algorithm

The first step of the proposed template matching algorithm was to evaluate the differences between the training and testing templates, through a distance metric. The distance metric used was the Manhattan distance, which can be mathematically calculated according to Eq. 4.3. In this case, the distance between the training and testing templates were calculated using the following formula:

$$d_{ij} = |\mathbf{X}_{\text{train}}(i) - \mathbf{X}_{\text{test}}(j)|, \quad (4.4)$$

where $\mathbf{X}_{\text{train}}(i)$ and $\mathbf{X}_{\text{test}}(j)$ represent the raw vectors i and j of the matrices $\mathbf{X}_{\text{train}}$ and \mathbf{X}_{test} , respectively. By computing the distances between all the training and testing templates, a distance matrix with size 63^2 is generated.

In the present distance-based algorithm for identification, the templates used as inputs were the scalograms vectors concatenated and with their dimensionality reduced. The identification was performed in two different ways: 1) Comparing one template from the training with one template from the testing - *Configuration 1/1*; and 2) Comparing one template from the training with three templates from the testing - *Configuration 1/3*. For *Configuration 1/1*, a subject is correctly identified if, from all the distances between all the training templates and the testing template of the subject to be identified, the smallest distance is the one corresponding to the training template of that subject. For *Configuration 1/3*, the subject is correctly identified if the distances between at least two of his/her three testing templates and his/her training template are the lowest when compared to all the distances obtained from the other subjects' training templates.

The system is evaluated based on the accuracy, which represents the quotient between the number of subjects correctly identified ($N_{\text{Sub_correct}}$) and the number of subjects present on the database ($N_{\text{Sub_total}}$), and it is calculated according to the following equation:

$$A_{\text{identification}} = \frac{N_{\text{Sub_correct}}}{N_{\text{Sub_total}}} \cdot 100\% \quad (4.5)$$

4.4 Authentication Algorithm

The authentication system was tested using templates from cardiac cycles and scalograms as inputs. For both types of inputs, the authentication was performed through a distance-based template matching algorithm, implemented in MATLAB, similar to the one presented for the identification task. Then, a leave-one-out cross-validation method was performed for imposters testing. The performance of the system was assessed according to two evaluation metrics: accuracy and impostor score.

Authentication was performed in two configurations - *Configuration 1/1* and *Configuration 1/3* - for both inputs, meaning that the cardiac cycles and scalograms templates were concatenated. The former were tested with and without dimensionality reduced, whereas the latter was only tested when the DR was applied due to their high dimension.

4.4.1 Distance-based Authentication Algorithm

The first step of the proposed template matching algorithm was to evaluate the differences between the training and testing templates, through a distance metric. The distance metric used was the Manhattan distance, calculated according to Eq. 4.4. For the *Configuration 1/1*, a subject is correctly authenticated if the distance between his/her training and testing templates given by Eq. 4.4 do not exceed a threshold defined for that subject. For *Configuration 1/3*, the subject is authenticated if the distances between his/her training template and at least two of the three testing templates are lower than the threshold of that subject.

The threshold was defined individually for each subject, using the distance between the testing template(s) of the subject and the training templates of all the subjects. The threshold for each subject can be calculated according to the following equation:

$$T_i = \mu_i - \sigma_i, \quad (4.6)$$

where

$$\mu_i = \frac{\sum_{k=1}^{N_{signals}} \sum_{j=1}^{N_{sub}} d_k(i, j)}{N_{signals} \cdot N_{sub}}, \sigma_i = \sqrt{\frac{\sum_{k=1}^{N_{signals}} \sum_{j=1}^{N_{sub}} [d_k(i, j) - \mu_i]}{(N_{signals} \cdot N_{sub} - 1)}}, \quad (4.7)$$

with $N_{signals} = 1$ for *Configuration 1/1*, $N_{signals} = 3$ for *Configuration 1/3* and $N_{sub} = 63$.

To evaluate the performance of the authentication algorithm, the accuracy, which represents the quotient between the number of subjects correctly authenticated ($N_{Sub_correct}$) and the number of subjects present in the database (N_{Sub_total}), was calculated according to the following equation:

$$A_{authentication} = \frac{N_{Sub_correct}}{N_{Sub_total}} \cdot 100\% \quad (4.8)$$

4.4.2 Leave-one-out Cross-Validation

Besides evaluating the performance of the system by calculating the accuracy, it is also important to validate the capacity of the system to reject potential imposters. Thus, a leave-one-out cross-validation (LOOCV) was performed, which is a cross-validation approach that uses each subject as a “test” set, as it is the most used method to validate biometric authentication models [11, 37, 38, 46, 89, 90].

The first step to perform a LOOCV would be to build a training set with $n-1$ subjects, with n being the number of subjects present in the database (in this case, $n = 63$). Then, the Manhattan distances between the testing template of the subjects that was left out from the training set and all the training templates of the remainder subjects are computed. These distances are used to calculate the threshold for that subject, according to the

4. BIOMETRIC DATA AND SYSTEMS

following equation:

$$T_i = \mu_i - \sigma_i, \quad (4.9)$$

with μ_i and σ_i calculated through Eq. 4.7 and with $N_{signals} = 1$ or $N_{signals} = 3$ (for the Configuration 1/1 and Configuration 1/3, respectively) and $N_{sub} = 62$.

The process is repeated n times, changing the testing subject in each iteration, as represented in the scheme of Fig. 4.8.

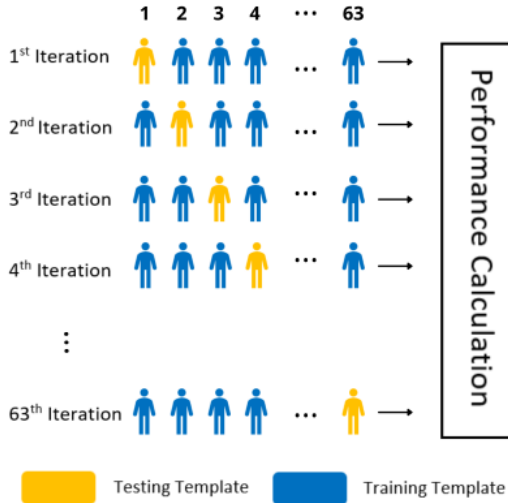


Figure 4.8: Representation of the training and testing templates in each iteration for the leave-one-out cross-validation method.

For Configuration 1/1, in each iteration, imposters are authenticated if the distances between the testing template of the subject left out and any of the training templates are below the threshold calculated for that tested subject. For Configuration 1/3, a subject is authenticated as an imposter if the distances between at least two of the testing templates of the subject considered “test” in that iteration and the training templates from any of the remainder subjects are below the threshold calculated for that tested subject.

The imposter rate is calculated through the mean of the number of imposters per subject, as present in the Eq.4.10:

$$I = \frac{\sum_{j=1}^{63} N_{Imp}(j)}{63} \cdot 100\%, \quad (4.10)$$

with $N_{Imp}(j)$ being the number of imposters when subject j is left out from the training set.

Chapter 5

Identification Results

This section presents the results obtained for the proposed identification systems. In the present study, for the identification and authentication systems, the biometrics of the electrocardiogram correspond to 1) the cardiac cycles, 2) the scalograms generated from cardiac cycles.

For the templates based on cardiac cycles, various classifiers were tested - kNNs, LDA, DTs, and SVMs - in *Configuration 20/20* and *Configuration 60/60*. In the former, the classifiers were trained with 20 templates per subject from the training set (from ECGs from the first data collection session) and tested with 20 templates from the test set (from ECGs from the second data collection session), whereas in the latter, 60 training templates were used to train the classifiers and 60 testing templates were used to test them. Concatenation was not applied to the signals for the identification process based on cardiac cycles. KNN and SVM were optimized and then, the performance of the four classifiers was compared with five evaluation metrics: accuracy, precision, recall, and F1-Score.

When using the biometric templates based on scalograms, two methods were proposed. The first method was to use a deep learning classifier - a 15-layer Neural Network - to conduct the identification in *Configuration 20/20* and *Configuration 60/60*. The second method used a distance-based algorithm, i.e., a 1-Nearest Neighbors (1-NN). In this, scalograms obtained from the templates of the first acquisition session were compared to the scalograms obtained from the signals of the second acquisition session in *Configuration 1/1* and *Configuration 1/3*, meaning that the templates were previously concatenated.

The different methodologies proposed are intended to draw conclusions on:

1. whether it is relevant or not to face an extra computational effort to generate the scalograms;
2. if normalization is a process that optimizes the performance of the system;
3. the differences between using more or fewer templates as inputs for the system;
4. which method is the most accurate and the most viable to be implemented in an identification system.

5.1 Identification based on Cardiac Cycles

For the cardiac cycles templates, different classifiers, namely kNN, LDA, DT, and SVM, were analyzed to identify the subjects on the database. The evaluation was held through two stages. The first stage is to optimize the classifiers, and the second is to compare the performance of each classifier when using not normalized or normalized templates.

5.1.1 Optimization of the Classifiers

The classifiers that were optimized were the kNN and SVM. LDA has no parameters to be optimized, whereas DT was tested using the default parameters from Matlab, mentioned in section 4.3.

5. IDENTIFICATION RESULTS

5.1.1.1 kNN Optimization

For kNN, there are two parameters that can be optimized - the distance metric and the k value. The distance metric used was not optimized and the chosen one was the Manhattan distance, since it is the most recommended to be used when there is high dimensionality in data [87]. The k was optimized by testing the system with different values. For *Configuration 20/20*, k was set between 1 and 20, and for *Configuration 60/60*, k was set between 1 and 60.

Fig. 5.1 shows the accuracy of the classifier according to the different values of k for *Configuration 20/20* on the left and *Configuration 60/60* on the right.

For *Configuration 20/20*, when using normalized cardiac cycles as input, the highest accuracy, 57.14%, was achieved when k was equal to 1. For the not normalized cardiac cycles, the accuracy of the kNN reached the maximum of 60.32%, with 3 and 11 neighbours. For *Configuration 60/60*, predicting the identification of subjects with the k parameter set to 1 allowed an IDR of 68.25% for normalized cycles. If normalization is not performed, the model identifies subjects more accurately with 13 neighbours, reaching an accuracy of 63.49%.

Thereby, the results of kNN in Table 5.1 correspond to a k value of 3 and 13 for *Configuration 20/20* and *Configuration 60/60*, respectively. In Table 5.2, k was set to 1 for both configurations.

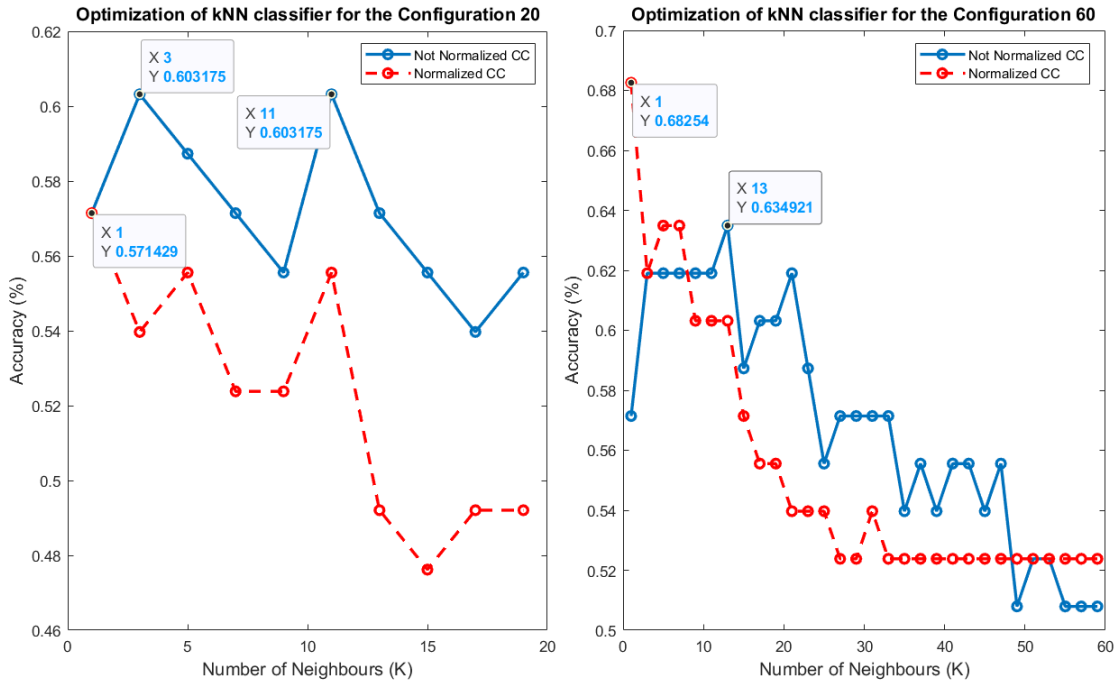


Figure 5.1: Optimization of the kNN Classifier for *Configuration 20/20* on the left and *Configuration 60/60* on the right, with not normalized and normalized cardiac cycles.

5.1.1.2 SVM Optimization

SVMs were also optimized by experimenting various kernel functions, values of C and γ . The kernel functions tested in the present study were the radial basis, linear and polynomial. The values of C and γ were set in the range $[2^{-15}; 2^{15}]$. To investigate the combinations of parameters that optimize the model, one heatmap was computed for each one of the kernels. Fig. 5.2, 5.3, 5.4 represent the optimizations for normalized cardiac cycles in *Configuration 20/20*, for the RBF, linear and polynomial kernels, respectively. The optimization process for the remainder configurations - normalized cardiac cycles in *Configuration 60/60* and not normalized cardiac cycles in both configurations - are presented in Appendix B).

Regarding the optimization of parameters C and γ for the RBF kernel, Fig. 5.2 shows that the highest accuracy

5.1 Identification based on Cardiac Cycles

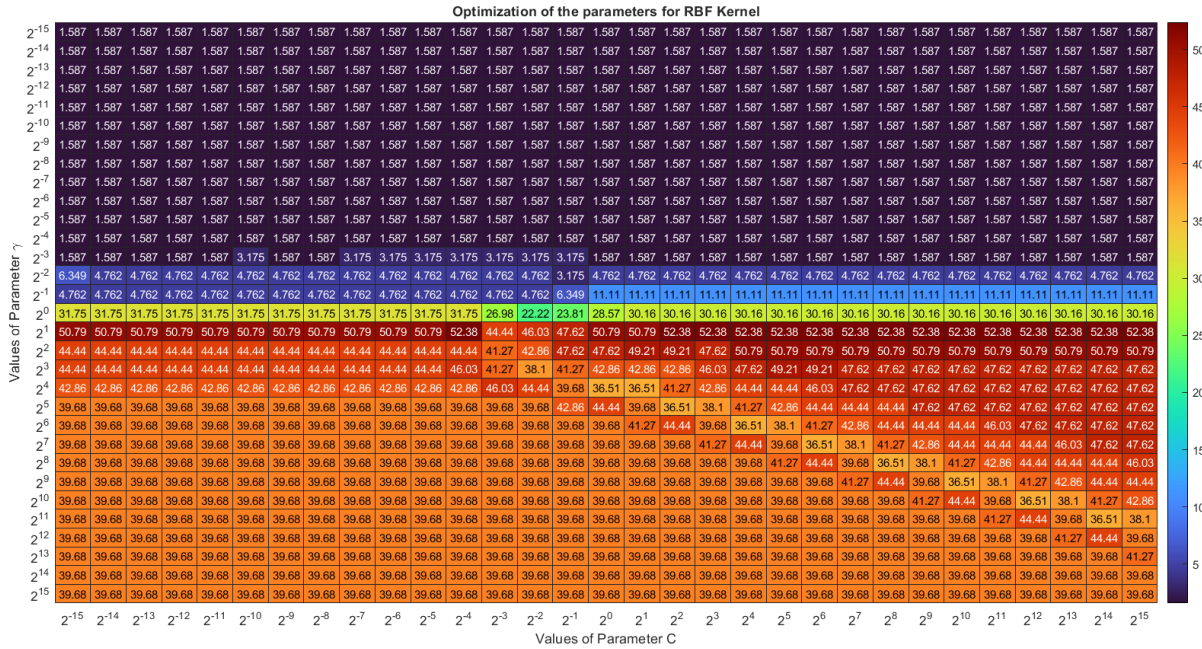


Figure 5.2: Optimization of the parameters for RBF kernel for normalized cardiac cycles in *Configuration 20/20*. The colors represent the accuracy of the system. Cold colors represent lower accuracies, whereas warm colors represent higher accuracies.

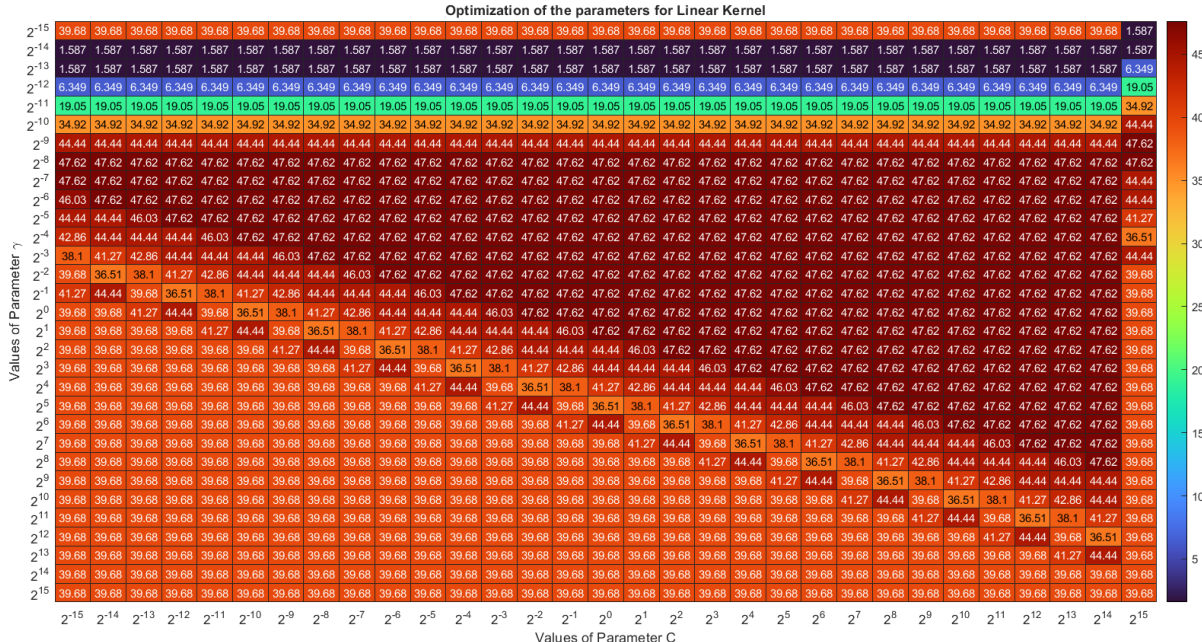


Figure 5.3: Optimization of the parameters for Linear Kernel for normalized cardiac cycles in *Configuration 20/20*. The colors represent the accuracy of the system. Cold colors represent lower accuracies, whereas warm colors represent higher accuracies.

achieved was 52.38%, when γ is set to 2^1 and C set to $\{2^{-4}, [2^2, 2^{15}]\}$. Concerning the optimization of the parameters for the linear Kernel represented in Fig. 5.3, the maximum accuracy achieved was 47.62% for many different parameter combinations. Fig. 5.4 shows that the optimization of the parameters for the polynomial kernel displayed a maximum accuracy of 47.62% in the following configurations: 1) $\gamma = 2^3$ and $C = [2^5, 2^{15}]$; 2) $\gamma = 2^5$ and $C = 2^9$; 3) $\gamma = 2^6$ and $C = 2^{11}$; 4) $\gamma = 2^7$ and $C = 2^{12}$; 5) $\gamma = 2^8$ and $C = 2^{14}$.

Thereby, for normalized cardiac cycles in *Configuration 20/20*, the parameters that optimize the performance of the SVM classifier at identifying subjects based on their ECG signals were: 1) RBF Kernel; 2) $\gamma = 2^1$ and 3) $C = \{2^{-4}, [2^2, 2^{15}]\}$, so the results on Table 5.1 concern the application of SVM with these parameters. For *Configuration 60/60*, the maximum accuracy, 58.73%, was achieved for many configurations with polynomial kernel and for the RBF kernel, with $\gamma = 2^2$ and $C = [2^3, 2^{15}]$. What concerns the not normalized cardiac cycles

5. IDENTIFICATION RESULTS

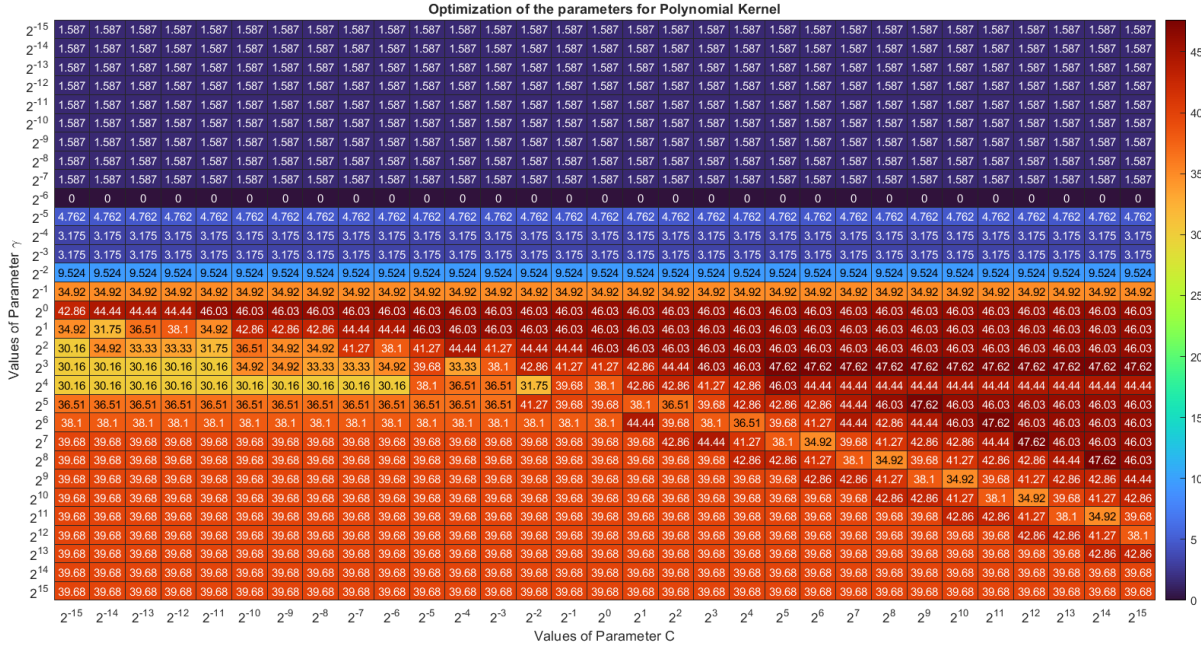


Figure 5.4: Optimization of the parameters for Polynomial Kernel for normalized cardiac cycles in *Configuration 20/20*. The colors represent the accuracy of the system. Cold colors represent lower accuracies, whereas warm colors represent higher accuracies.

in *Configuration 20/20*, the best accuracy was 60.32% and it was achieved with a RBF kernel and the parameters γ and C set to 2^{10} and 2^{-4} , respectively. For the not normalized cardiac cycles in *Configuration 60/60*, the best accuracy (61.90%) was reached when using a RBF kernel function, with parameter γ set to 2^{11} and parameter C set in the interval $[2^4, 2^{15}]$.

5.1.1.3 Discussion

Concerning the optimization of the kNN classifier, results showed that when the cardiac cycles are normalized, the algorithm performance is optimal for a shorter number of neighbors ($k = 1$), whereas for not normalized cardiac cycles, the optimal performance is achieved for a greater number of neighbors ($k=11$ and $k=13$ for *Configuration 20/20* and *Configuration 60/60*, respectively).

By performing the normalization, signals become scaled in the same range - between 0 and 1 - and so, not only signals from the same subject become more similar to each other, but also the signals from different subjects. Since the optimal performance for normalized signals is achieved when $k = 1$, this may indicate that normalization increases the similarities between the training and testing data of each subject.

When the normalization is not performed, signals overall are more distinct. Since the optimal performance is achieved for larger values of k , this may indicate that when using not normalized signals, the boundaries between classes are less clear, and consequently, the model needs to have a greater capacity of generalization (greater value of k) to accurately distinguish between subjects.

Regarding the optimization of the SVM classifier, the kernel function that optimizes the performance of the system is the RBF, since for all the configurations - whether normalization is performed or not, whether *Configuration 20/20* is used or *Configuration 60/60* - the highest accuracies are achieved when using RBF kernel. The polynomial function also achieved optimal performance for the normalized cardiac cycles in *Configuration 60/60*. Literature supports these results since most studies that resorted to the use of SVM for the classification process used the RBF kernel [30, 56, 82, 91], with the exception of [60, 44], where the linear kernel was used. Furthermore, Lin [37] investigated the best combination and the most appropriate kernel function, and results show that successful recognition rates are achieved when using a non-linear kernel - polynomial or RBF - whereas the linear kernel leads to worse accuracies.

The other two parameters - γ and C - in the optimal configuration of the SVM assume different values across

configurations and even along a single configuration, meaning that these two factors are less decisive to achieve a good accuracy.

5.1.2 Not Normalized vs Normalized Cardiac Cycles

The classifiers were evaluated according to several metrics - accuracy, precision, recall, and F1-Score. Table 5.1 and Table 5.2 present the results of the evaluation metrics for each of the classifiers, for not normalized and normalized cardiac cycles, respectively.

Table 5.1: Comparison of the performance of the identification task based on classifiers for not normalized cardiac cycles.

Not Normalized Cardiac Cycles					
Configuration	Classifier	Accuracy	Weighted Average		
			Precision	Recall	F1-Score
<i>Configuration 20/20</i>	LDA	74.60%	68.34%	67.70%	64.48%
	kNN	60.32%	53.08%	52.30%	49.56%
	DT	52.38%	42.04%	41.90%	38.18%
	SVM	60.32%	52.84%	54.84%	50.67%
<i>Configuration 60/60</i>	LDA	77.78%	71.88%	71.40%	68.23%
	kNN	63.49%	54.52%	51.72%	49.34%
	DT	52.38%	42.40%	40.21%	37.68%
	SVM	61.90%	57.81%	52.96%	50.08%

For not normalized cardiac cycles, results in Table 5.1 show that, except for DT, all the classifiers slightly increased their accuracy when tested in *Configuration 60/60*, that is, using 60 templates for each subject. The DT reached the same accuracy for both configurations.

For *Configuration 60/60* the classifier that performed best in terms of accuracy was the LDA, reaching 77.78%, followed by kNN with 63.49%, SVM with 61.90% and finally DT with 52.38%. For *Configuration 20/20*, the accuracies achieved were lower, as mentioned above, but LDA was also the one that predicted the identification of the subjects more accurately (74.60%), whereas DT was the less accurate (52.38%).

Despite accuracy being the most intuitive performance measure, since it is simply the ratio of correctly predicted subjects to the total subjects, the other metrics should also be considered to the evaluation of the classification system. The remaining metrics followed the accuracy pattern, being higher for the LDA classifier and lower for DT.

Thus, when using not normalized cardiac cycles as a biometric template, the classifier that performs best in identifying subjects is LDA in *Configuration 60/60*.

Table 5.2: Comparison of the performance of the identification task based on classifiers for normalized cardiac cycles.

Normalized Cardiac Cycles					
Configuration	Classifier	Accuracy	Weighted Average		
			Precision	Recall	F1-Score
<i>Configuration 20/20</i>	LDA	69.84%	64.19%	62.86%	58.49%
	kNN	57.14%	51.37%	50.63%	47.09%
	DT	34.92%	32.52%	29.68%	28.89%
	SVM	52.38%	49.70%	46.27%	44.27%
<i>Configuration 60/60</i>	LDA	79.37%	67.99%	69.13%	65.21%
	kNN	68.25%	52.55%	53.07%	49.54%
	DT	58.73%	40.12%	38.60%	36.27%
	SVM	58.73%	50.52%	49.76%	46.05%

In general, the comparison between the classifiers for normalized cardiac cycles is pretty similar to the comparison performed for the not normalized cycles. The four classifiers performed better in *Configuration 60/60*,

5. IDENTIFICATION RESULTS

since the accuracy and the other metrics were higher when using 60 signals for predicting the identification of the participants. Contrary to what happened for the not normalized cardiac cycles, DT were significantly more accurate when using more signals as inputs: 34.92% against 58.73%. The best classifier was also the LDA, with an accuracy of 79.37%, followed by the kNN with 68.25%, and both the SVM and DT with 58.73%. Although achieving the same accuracy, SVM outperformed DT, as it presents higher values in the remain metrics.

5.1.2.1 Discussion

For all the approaches experimented in the present study, the influence of the number of templates per subject on the accuracy of the classification task was evaluated. Results from Table 5.1 and Table 5.2 show that, whether normalization is performed or not, *Configuration 60/60* leads to higher accuracies than *Configuration 20/20*. More template segments capture better the variability of the subject's heartbeat, mainly due to the incorporation of noisier cardiac cycles in the training process. If the classifier is only trained with the most similar cardiac cycles, which happens in *Configuration 20/20*, it will probably fail more often at classifying noisier testing cycles.

In all configurations, the classifiers that achieved higher and lower accuracies were LDA and DT, respectively. LDA may have outperformed the machine learning classifiers due to the data used being linearly separable, i.e., the signals of a subject are very close to each other, and quite distinct from the signals of another subject. Thus, it was expected that the LDA would present a good performance, since the functioning of the LDA consists of finding the linear combination of features in which the within-class distance is minimized, and the between-class is maximized.

LDA is typically used in some real-life applications such as face recognition [92], medical diagnosis [93, 94, 93] and customer identification [95], which are topics related to the present study. However, to the best of our knowledge, most studies on ECG biometrics performing LDA, use it for dimensionality reduction or feature extraction rather than for classification. An exception is [34], in which the template matching was performed with an LDA distance classifier. The identification rates achieved were 96% and 95.3% for 100 subjects and 168 subjects, respectively. Our proposed algorithm underperform the algorithm from [34], due to the ECG data from the latter being achieved in a on-the-person approach with 12-leads, whereas our data was from a off-the-person acquisition set-up, making signals more susceptible to noise and interferences. Thereby, LDA has demonstrated the potential to be incorporated in ECG-based biometric systems.

On the contrary, DT achieved the lowest accuracies from all the classifiers tested. From current state-of-the-art, very few studies investigated the application of a DT for a biometric identification purpose. Dar et al. [96] proposed an algorithm in which feature extraction involved the fusion of DWT of the cardiac cycle and heart rate variability-based features and the classification is performed by using Random Forests. The system was tested with a publicly available database like ECG-ID from Physionet¹⁵, previously created for biometric purposes, and an accuracy of 83.88% was achieved. The discrepancy between this result and the accuracy obtained by our system may be due to two main reasons. Firstly, the ECG-ID database from Physionet¹⁵ consists of data collected using an on-the-person acquisition approach. This configuration makes the ECG less vulnerable to interference and consequently, signals will have better quality leading to a more accurate identification of the subjects. Secondly, even though there is more than one ECG recording per subject, most of them correspond to acquisitions that took place on the same day and even the same acquisition session. It is expected that ECG recordings from the same acquisition session will be very similar for each subject and, therefore, their considered training and testing recordings will be easily identified as belonging to the same subject, leading to high accuracies of the system. Besides this, the low accuracies obtained when using DT for classification in the present work may also be due to the fact that DT are prone to overfitting, meaning that they can be over-complex and, consequently, not being able to generalize well from the training data. This is problematic, specially if the test and training data are very different, which may happen when acquired in two different acquisitions separated by 3 months. These drawbacks may be the reason why almost none of the previous studies presented in Chapter 3 used DT to perform

the biometric identification of subjects.

This study also intends to investigate whether the normalization is advantageous or not, for the performance of the system. To the best of our knowledge, most of the studies, due to the inherent heartbeat waveform variability, performed normalization in order to obtain amplitude and time invariant characteristics applicable for biometric purposes [68]. Considering the best configuration, which is the one that uses more templates per subject (*Configuration 60/60*), our results proved that by normalizing templates, the accuracy increases for all classifiers, except for SVM. However, most studies using this classifier performed normalization of the signals. From current state-of-the-art, only one study performed a comparison between normalizing and not normalizing cardiac cycles for identification purposes with CYBHi. Bento et al. [1] proposed a temporal convolutional neural network as a classifier, and reached an accuracy of 54.98% when using normalized cardiac cycles, and 11.60% when the normalization was not performed. Therefore, normalization proved to be an essential step for the pre-processing of a biometric identification system.

5.2 Identification based on Scalograms

The scalogram-based templates were tested as inputs for an identification algorithm following two methodologies. Identification based on Neural Networks was tested in *Configuration 20/20* and *Configuration 60/60*, whereas the distance-based algorithm used concatenated scalograms in *Configuration 1/1* and *Configuration 1/3*.

5.2.1 Identification based on Neural Networks

The performance of the proposed 15-layer neural network was evaluated based on the accuracy, and the results are presented on Table 5.3.

Table 5.3: Comparison of the performance of the identification algorithm based on 15-layers NN between not normalized and normalized scalograms of *Size 56* and *Size 224*.

Size of Scalograms	Not Normalized Scalograms		Normalized Scalograms	
	Accuracy		Configuration	
Size 56	65.08%		63.49%	Configuration 20/20
	68.25%		68.25%	Configuration 60/60
Size 224	61.90%		63.49%	Configuration 20/20
	69.84%		68.25%	Configuration 60/60

According to the results in Table 5.3, the NN classifier is more accurate at identifying subjects if the number of inputs per subject is greater.

For *Size 56*, in *Configuration 20/20*, the accuracy achieved is higher for not normalized scalograms with 65.08%, when compared to normalized scalograms, with 63.49%. In *Configuration 60/60*, the accuracy was 68.25% whether the normalization was performed or not.

For *Size 224*, in *Configuration 20/20*, the system showed to be more accurate with normalized scalograms: 63.49% against 61.90%, obtained for not normalized. For *Configuration 60/60* the results were the opposite, with not normalized resulting in greater accuracy than normalized scalograms: 69.84% and 68.25%, respectively.

Finally, the highest accuracy was achieved using not normalized scalograms *Size 224* in *Configuration 60/60*, whereas the lowest was reached also for not normalized scalograms in *Size 224*, but for *Configuration 20/20* instead.

¹⁵<https://physionet.org/content/ecgiddb/1.0.0/> (Accessed on 29/12/2020).

5. IDENTIFICATION RESULTS

5.2.1.1 Discussion

Results from the Neural Networks when using scalograms are in agreement with the previously reported results obtained for the cardiac cycles in what concerns the number of templates per user, since *Configuration 60/60* allows the system to identify the subjects more accurately due to the inclusion of noisier signals when training the classifier.

According to our literature review, Byeon et al. [15] also proposed an intelligent deep model based on scalograms of electrocardiogram signals for biometrics. The database used was CU-ECG, directly built for the biometrics at Chosun University (CU) in Korea, in which only the lead-I was measured, in an on-the-person approach. Even though, each subject has sixty different recordings, all of them were acquired in the same acquisition session, meaning that this study did not evaluate the stability of ECG over time. The authors used scalograms sized 224x224, like in our proposed approach, and by applying a simple CNN classifier, reached an accuracy of 87.5% at the identification task. Our method reached a much lower accuracy, 69.84% for not normalized scalograms sized 224x224, but this result may be justified by the conditions in which our data was acquired. Firstly, it was an off-the-person approach, much more susceptible to noises as mentioned above, and secondly, the data considered as training and testing templates were acquired in two different day sessions, separated by 3 months. Under these conditions, current state-of-the-art do not present any study using NN for identification purposes with scalograms.

The accuracies achieved with and without normalization are very similar and, therefore, results demonstrated that normalization is not an essential procedure when using a CNN based on scalograms of ECG signals for biometric identification. Concerning the size of the scalograms, it did not prove to be a decisive factor with influence on the accuracy of the system for most of the configurations, meaning that despite the number of pixels of the scalogram, the classifier can distinguish subjects almost equally. Moreover, since size 224x224 is four times greater than size 56x56, the computational time of the former is also four times greater. Thereby, considering the accuracy and computational time of the system, using scalograms *Size 56* is the best approach.

5.2.2 Identification based on Distance Metrics

Identification was also tested through a distance-based method, in which the scalograms were concatenated and their dimensionality was reduced by the ICA. The algorithm was tested in *Configuration 1/1* and *Configuration 1/3*, for not normalized and normalized scalograms, in both sizes.

5.2.2.1 Not Normalized vs Normalized Scalograms

The evaluation of the algorithm lies in drawing conclusions on: 1) the size of the scalograms; 2) the configuration of the inputs and 3) the normalization of the scalograms. Table 5.4 presents the results obtained through the considered distance-based algorithm.

Table 5.4: Comparison of the performance of the identification algorithm based on distance metrics between not normalized and normalized scalograms *Size 56* and *Size 224*.

Size of Scalograms	Not Normalized Scalograms	Normalized Scalograms	Configuration
	Accuracy		
Size 56	50.79%	47.62%	Configuration 1/1
	58.73%	52.38%	Configuration 1/3
Size 224	47.62%	53.97%	Configuration 1/1
	44.44%	46.03%	Configuration 1/3

Results in Table 5.4 show that for *Size 56*, not normalized scalograms lead to higher accuracies when compared to normalized, for both configurations. For not normalized scalograms, the *Configuration 1/3* reached a higher accuracy, 58.73%, when compared to the other configuration, 50.79%. For *Size 224*, the exact opposite happens.

Normalized scalograms *Size 224* and *Configuration 1/1* optimize the performance of the system, with an accuracy of 53.97%.

The best performance of the system is 58.73% when using not normalized scalograms *Size 56* in a *Configuration 1/3*, whereas the worse performance is 44.44%, reached when the inputs are not normalized scalograms in *Size 224* and for *Configuration 1/3*.

5.2.2.2 ICA Dimensionality for Not Normalized Scalograms

As mentioned above, for the distance-based identification algorithm, the dimensionality of the scalograms was reduced using ICA. Thereby, the DR was tested in order to find the number of ICs that optimize the performance of the model. Since the best results concerned the use of not normalized scalograms for *Size 56* and normalized scalograms for *Size 224*, this evaluation was held for these configurations, respectively. Fig.5.5 shows the accuracies as a function of the number of IC, for *Size 56* on the left and *Size 224* on the right.

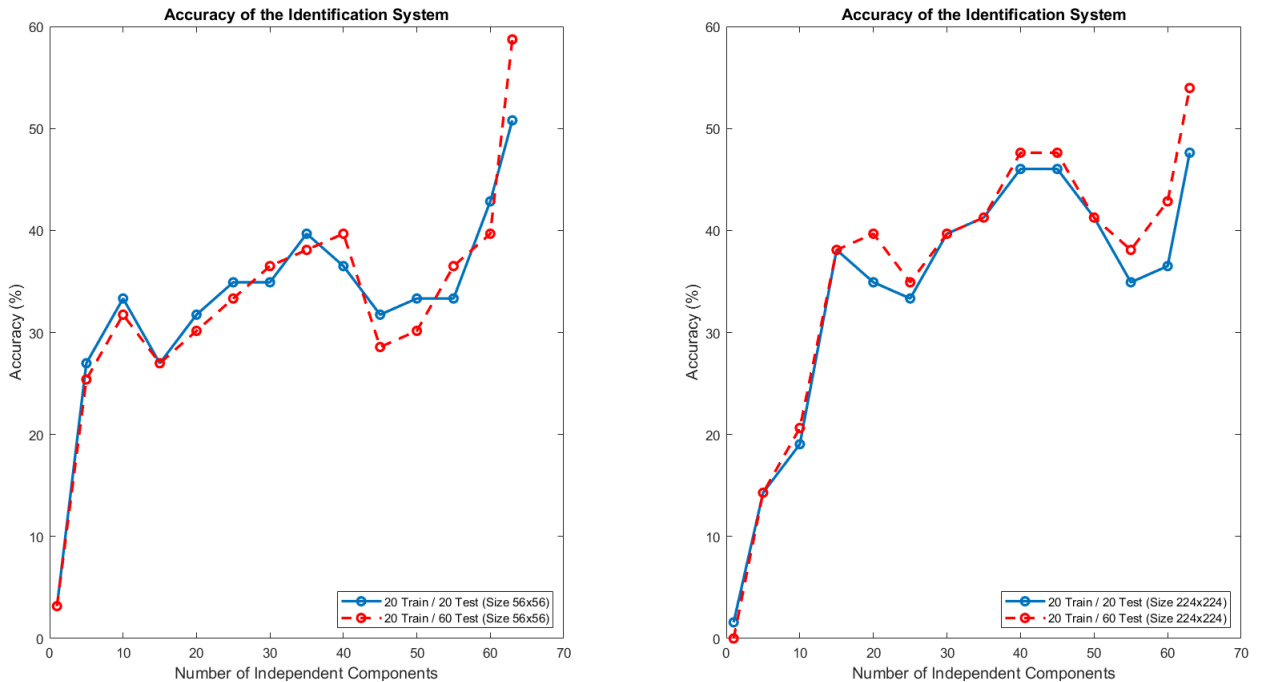


Figure 5.5: Representation of the accuracy obtained by the biometric identification algorithm based on distance metrics, when using different number of IC for not normalized scalograms in *Size 56* (on the left) and normalized scalograms in *Size 224* (on the right).

According to Fig. 5.5, for both sizes and both configurations the highest accuracies are achieved when the number of ICs is equal to the number of subjects on the database, i.e. 63. Despite the overall decrease in accuracy, when decreasing the ICs from 63 until reaching 10 ICs, the behaviour is slightly irregular, with some increases and decreases in the accuracy. However, with less than 10 features, the accuracy decreases exponentially.

5.2.2.3 Discussion

Concerning the evolution of the accuracy of the system when decreasing the number of ICs, Fig. 5.5 showed that it results in a decrease in the identification accuracy of the system. When applying the ICA, each IC is one feature that will be used to compare the templates of the subjects. When the number of ICs is equal to the number of subjects, there will be 63 features to be compared and used to discriminate between the 63 subjects on the database. In case of accuracy had not dropped immediately when the number of independent components was reduced, we could conclude that some of the features are redundant and unnecessary for class distinction. However, as this did not happen, the 63 features are, in fact, indispensable for distinguishing between subjects.

When the number of pixels is reduced, some information is lost. When performing normalization, information on the ECG voltage is also lost, making the scalograms more similar to each other. Thus, results proved that, if

5. IDENTIFICATION RESULTS

some information is lost by reducing the number of pixels of the scalograms (*Size 56*), the system needs the templates to be as different as possible from each other in order to accurately distinguish them. Hence, it was verified that normalization is advantageous when more pixels are considered.

Since the system has difficulties at matching scalograms *Size 224*, it was expected that the system will struggle when trying to classify noisier segments, which happened in *Configuration 1/3*. For *Size 56*, the opposite happened, since there are fewer pixels and, consequently, noisier signals will help to distinguish subjects.

The best performance, 58.73%, was achieved when using not normalized scalograms in *Size 56*. However, this result is lower than the one obtained for the corresponding configuration in the identification based on neural networks (not normalized scalograms in *Size 56* and *Configuration 60/60*), which was 68.25%. Thus, for scalograms, even though neural networks are computationally more time consuming, it is a more promising approach than the distance-based algorithm with concatenated signals.

Chapter 6

Authentication Results

This section presents the results obtained for the proposed authentication system. The biometrics of the ECG used were 1) the cardiac cycles and 2) the scalograms. Both were tested in two configurations: *Configuration 1/1* and *Configuration 1/3*.

Authentication was performed using a distance-based template matching algorithm, which compares the data from the testing sets - resulted from the second data collection session - and the training sets - resulted from the first data collection session. Then, a Leave-one-out cross validation was performed for impostor testing.

From the different configurations tested, conclusions are intended to be drawn on several aspects:

1. The advantage and disadvantage of applying ICA to the templates.
2. The benefits of normalizing the templates.
3. The differences between using more or less templates as inputs for the system.
4. The dissimilarities of using cardiac cycles or scalograms as biometric templates.

6.1 Authentication based on Cardiac Cycles

When using cardiac cycles as inputs, not normalized and normalized signals were tested with and without reducing their dimensionality in order to draw conclusions on the advantages of that procedure.

The distance-based template matching algorithm consists of comparing the testing templates (templates generated from the signals of the second acquisition session) with the training templates (templates generated from the signals of the first acquisition session) through a distance metric. The first step was to compute the Manhattan distance between the two templates. Fig. 6.1 shows the distance matrix between training and testing templates based on not normalized cardiac cycles with DR in *Configuration 1/1*.

In the distance matrix representation, cold colors (blue) correspond to lower distances whereas warm colors (red) correspond to higher distances. Fig. 6.1 shows a diagonal line, from the left to the right, in which the colors from all the entrances are blue. This means that the distances between the testing and training templates of each subject are, in general, small. This pattern can be an indicator that this algorithm would be a promising approach to authenticate subjects, since low distances (blue colors) are expected to be below the threshold set for each subject, which is what happens in the case of authentication.

Moreover, even though all the diagonal entrances are blue, there are several subjects whose diagonal entrances correspond to a lighter shade of blue, namely subjects number 9, 17, 21, 40, 53, and 56. From all the subjects, these are the ones most likely not be authenticated. The distance matrix also shows some subjects, namely 33, 36, and 60, that present higher distances (warm colors - various shades of red) in the entrances that correspond to the distances between their training templates and most of the testing templates from the remaining subjects. These shades of red indicate that the training templates of these subjects are the most different templates from all the

6. AUTHENTICATION RESULTS

testing templates on the database. Regarding the testing templates of these three participants, the colors associated to the distance of their testing and all the training templates are also warm colors, but in shades of yellow instead, meaning that their testing templates are also some of the most distinct signals. Since the two templates were acquired in two sessions separated by three months, this analysis can be an indicator that these subjects have a peculiar heartbeat.

To determine the accuracy of the system, the threshold of each subject is calculated by the mean and standard deviation of each column, according to Eq. 4.6. If the distance on the diagonal entrance is below the threshold for the correspondent column, the subject is authenticated. The number of authenticated subjects over the total number of subjects corresponds to the accuracy.

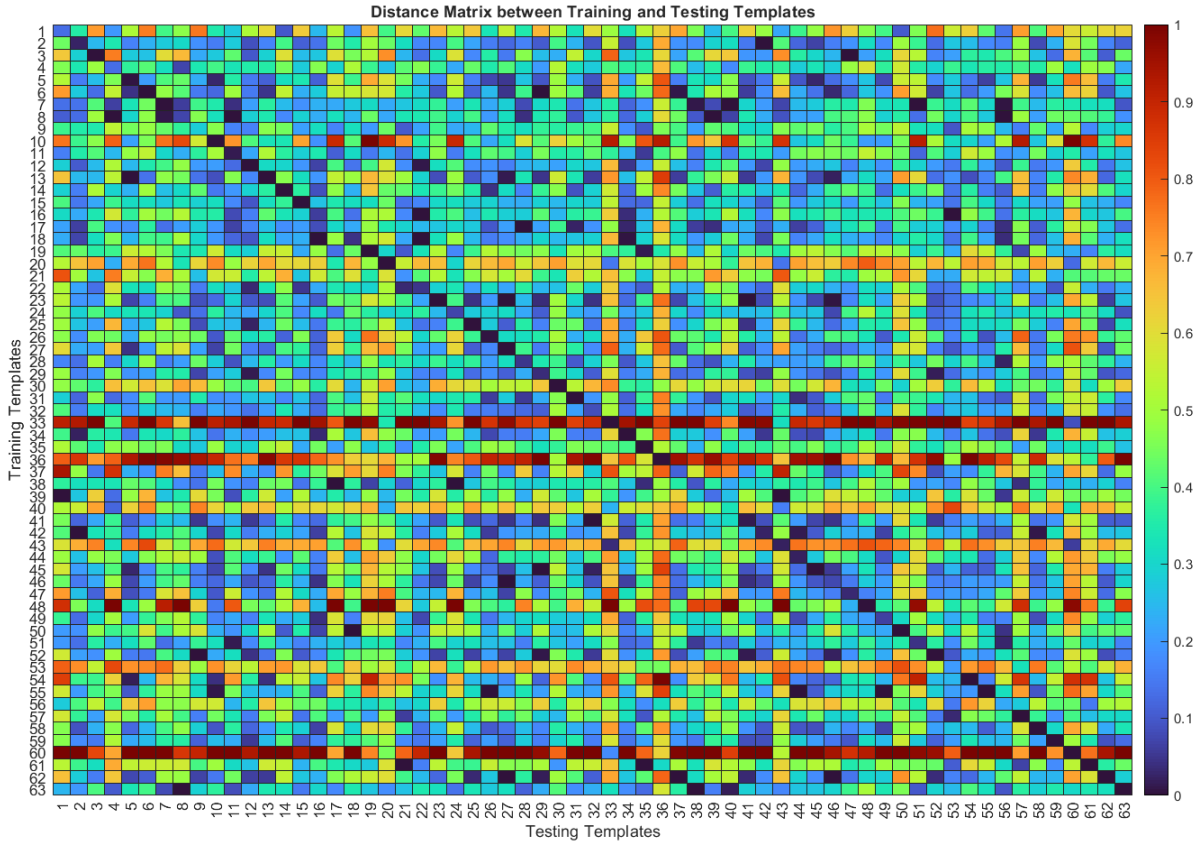


Figure 6.1: Distance Matrix between training and testing templates based on not normalized cardiac cycles with DR in *Configuration 1/1*.

Besides the accuracy, this template matching is also evaluated by performing a LOOCV, to assess the capacity of the system to reject potential imposters. Fig. 6.2 shows the authenticated imposters of each subject in *Configuration 1/1*, on the left, and *Configuration 1/3*, on the right, for the not normalized cardiac cycles with DR.

The diagonal lines are black because each entry corresponds to a single subject's training and testing templates, and a subject cannot be an imposter of him/herself. For *Configuration 1/1*, the heatmap is represented in two colors - dark blue corresponding to a non-impostor and light blue to an impostor. Thus, the imposters of each subject are represented in light blue in the vertical line corresponding to that specific subject. The figure on the left shows that there are some participants that are imposters of the vast majority of the other subjects on the database, since their corresponding horizontal lines have many light blue entrances. Participants 16, 17, 18, 24, 27, 43, and 45 are examples of this. The vertical lines allow us to verify the number of authenticated imposters of each participant. Subjects 5, 22, 27, 48, and 62 were the ones that presented more imposters. The impostor score for *Configuration 1/1* is the mean of the number of imposters per subject, that is, the mean of the number of light blues per column.

The figure on the right, which concerns the *Configuration 1/3*, is represented in four colors, since each subject has 3 testing templates to be authenticated: 1) dark blue corresponds to 0 templates authenticated as imposters; 2) light blue corresponds to 1; 3) yellow represents 2 and finally 4) red for 3 templates. In this configuration, a

6.1 Authentication based on Cardiac Cycles

subject is an impostor of another subject he/she is authenticated as an impostor for at least two of the three testing templates of the subject that is being considered, which means that only yellow and red entrances correspond to imposters. Subjects 52 and 53 do not present any impostor, since only one of their three templates present imposters, and at least two templates are needed to authenticate one subject as impostor. Subjects 15, 16, 18, 42, and 58 are some of the subjects that have fewer imposters, more specifically, no more than 5. The subjects that have more imposters authenticated (more than 10) are subjects 12, 21, 36, 45, and 60. Regarding the horizontal lines on the heatmap, subjects 1, 10, 30, 33, 36, 48, 53, 56, and 60 are imposters of no more than 2 subjects, and in particular, 36 and 48 are not registered as impostor of any of the subjects. There are also some subjects that are imposters of more than 17 subjects, such as the participants 7, 17, 23, and 63. The impostor score for *Configuration 1/3* is the mean of the sum of yellow and red entrances per column.

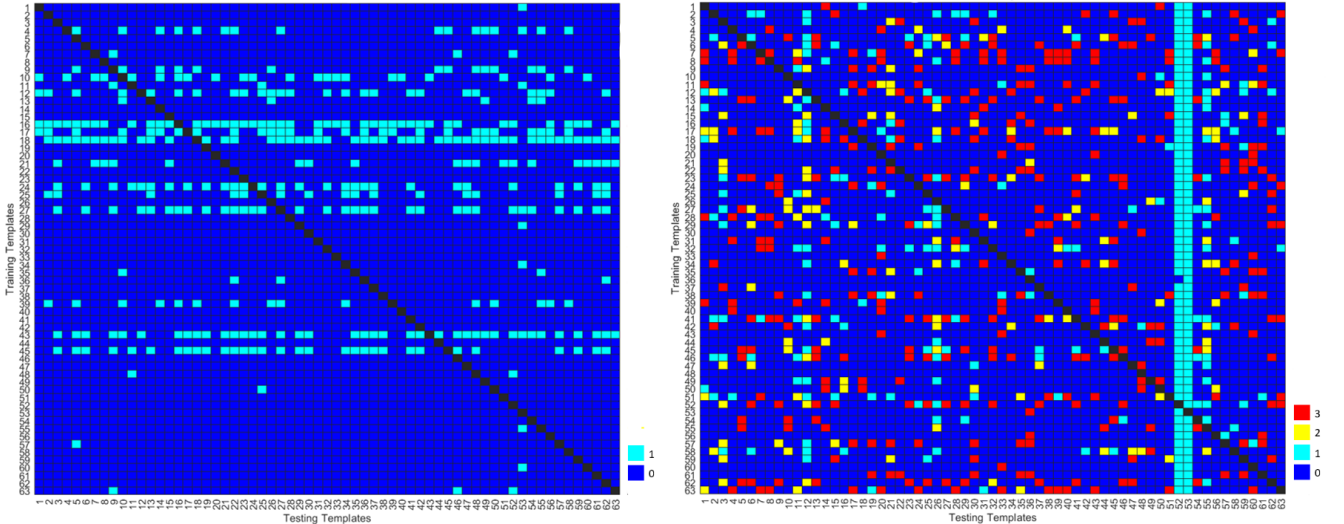


Figure 6.2: Number of authenticated imposters when using scalograms from not normalized cardiac cycles (*Configuration 1/1* and *Configuration 1/3*, on the left and right, respectively). The colors represent the number of templates of each subject that are authenticated as imposters. For *Configuration 1/1*, there is only one template per subject that can be authenticated as an impostor, while for *Configuration 1/3* there is a maximum of 3 templates. Color Legend: ■ 0 ■ 1 ■ 2 ■ 3.

Table 6.1 and Table 6.2 present the accuracies and impostor scores obtained when using cardiac cycles with and without DR, respectively.

Despite the DR, obtained results show that accuracy is higher, and quite similar, for the not normalized cardiac cycles in both configurations (around 90%). Therefore, we can conclude, that normalization significantly degrades the performance in terms of authentication accuracy. It can also be observed that, when dimensionality was reduced, the accuracies of the system for the normalized cardiac cycles, in both configurations, were substantially higher than when DR is not applied (an increase of 22%).

Table 6.1: Comparison of the accuracy of the authentication algorithm between not normalized and normalized segments with and without DR.

	Not Normalized Cardiac Cycles		Normalized Cardiac Cycles	
Configuration	Accuracy			
	Without DR	With DR	Without DR	With DR
Configuration 1/1	90.48%	88.89%	57.14%	79.37%
Configuration 1/3	90.48%	87.30%	55.56%	77.78%

6. AUTHENTICATION RESULTS

Table 6.2: Comparison of the impostor score of the authentication algorithm between not normalized and normalized segments with and without DR.

	Not Normalized Cardiac Cycles		Normalized Cardiac Cycles	
Configuration	Impostor Score			
	Without DR	With DR	Without DR	With DR
Configuration 1/1	13.21%	12.93%	7.71%	13.80%
Configuration 1/3	13.06%	12.95%	7.56%	13.57%

Regarding the results without ICA, not normalized inputs led to higher values of impostor score, with 13.21% for *Configuration 1/1* and 13.06% for *Configuration 1/3*, whereas for the normalized cycles, the system achieved lower impostor scores: 7.71% and 7.56% for *Configuration 1/1* and *Configuration 1/3*, respectively.

Thus, normalization led to lower values of accuracy and impostor scores, which are contradictory results, since the system struggled to authenticate the right subject (low accuracy) but succeeded to reject potential imposters (low impostor score).

On the other hand, with ICA, the capacity of the system to reject imposters slightly increases when using not normalized cardiac cycles as inputs. *Configuration 1/1* resulted in an impostor score of 12.93% and 13.80% for not normalized and normalized cycles, whereas *Configuration 1/3* resulted in 12.95% and 13.57%, respectively.

Therefore, we can conclude that, when applying ICA, the best performance in terms of both accuracy and impostor score was achieved with not normalized cardiac cycles in *Configuration 1/1*.

6.1.1 Discussion

For the authentication with cardiac cycles without DR, results showed that both accuracies and impostor scores are very similar for *Configuration 1/1* and *Configuration 1/3*, meaning that the number of cardiac cycles used to authenticate a subject has almost no influence on the performance of the system. When the DR was applied, results were relatively better (higher accuracy and lower impostor score) when the template matching is performed with only 20 cycles - *Configuration 1/1*. Thus, by using fewer testing cardiac cycles, it would take less time to acquire the ECG at the time of authentication, making the system easier to use, which, consequently, could be an advantage for it to become socially accepted.

Without ICA, the accuracies and impostor scores obtained were both remarkably higher for not normalized cardiac cycles. Thus, normalization proved to be an essential procedure to efficiently reject potential imposters, but it prejudices the capacity of the system to correctly authenticate the right subjects. When DR was applied, not normalized cardiac cycles led to higher accuracies but also to lower impostor scores, which was not verified without ICA. In this case, the system is able to authenticate subjects with an accuracy of 88.89% and to reject imposters with a rate of 87.07%. Results proved that the normalization approximates the templates, and consequently, the template matching algorithm will struggle to distinguish subjects based on a distance measure. Comparing the different configurations tested in the proposed study and taking into account the accuracies, impostor scores, and computational time, the best approach is to authenticate subjects resorting to 20 not normalized cardiac cycles without ICA. Despite leading to the highest identification rate (90.48%) and to an admissible impostor score (13.21%), the computational time to compare testing templates increases due to the higher dimensionality of the templates (although ICA takes a long time to be performed, the transformation of testing templates accordingly is promptly computed).

To the best of our knowledge, any studies using CYBHi proposed a distance-based template matching algorithm for authentication purposes. However, some studies, whose conditions of acquisition, feature selection, or classification methods allow us to compare results, were considered.

Arteaga-Falconi et al. [5] did an off-the-person experimental acquisition using a lead-I ECG sensor with

two electrodes fitted onto a mobile phone's case. The ECG acquisition was conducted in two sessions, in two different days and at different times of the day, for 2 minutes long, just like the database used in the present work (CYBHi [2]). The authentication algorithm proposed was a hierarchical validation scheme that evaluates each feature individually and if the differences between the training and testing features are below the accepted range of tolerance, the authentication of that feature is validated. They reached an accuracy of 81.82% using fiducial features based on cardiac cycles. Although the database used is not the same as the one used in this work, the acquisition conditions were quite similar, as was the feature extraction process. The template matching algorithm is quite different from ours, however, it has some similarities such as the use of a threshold to assess the possible authentication. Although it is impossible to compare performance due to the use of difference databases, our approach achieved higher accuracy than the accuracy reported by this study.

Samarin et al. [3], despite not using CYBHi, created a particular dataset, with an off-the-person sensor, performing two data acquisition sessions with 4 months in between. The methodology proposed by Samarin was quite similar to ours, including the signal segmentation and outlier removal procedures, and the features extracted - the cardiac cycles - were also normalized and dimensionally reduced, but using PCA rather than ICA. The template matching was performed using logistic regression, Manhattan distance-based kNN and SVM, resulting in EER of 13.92%, 8.82%, and 5.74%, respectively. These results seem quite promising, since the lower the EER, the higher the accuracy of the system.

As the databases used where different, we cannot do a direct comparison to any of these two studies ([3, 5]). Therefore, future work should investigate this using the same database, so that conclusions on the performance of different approaches can be drawn accurately.

Bento et al. [1] proposed an authentication algorithm based on cardiac cycles using temporal convolutional neural networks, reaching an EER of 10.25% when normalization is performed, whereas for not normalized cardiac cycles an EER of 23.56% was achieved. They conclude that normalizing each individual led to much better generalization across sessions. In this case, the database was the same, but the classification process was quite different. Moreover, the evaluation metrics used were not the same and so, conclusions cannot be drawn on which one performed better. However, both seem promising approaches for the authentication purpose, since a low equal error rate and a high accuracy were achieved by [1] and in the present work, respectively. With regard to normalization, [1] presented opposite results from ours because, while in our case, the results were better without normalization, although the difference is almost insignificant, for Bento's approach, normalization is completely indispensable for a viable system.

6.2 Authentication based on Scalograms

Opposite to what happened for the cardiac cycles, scalograms were only used with their dimensionality reduced by applying ICA, due to their enormous size. As for the identification system, scalograms were tested in two sizes: *Size 56* and *Size 224*.

Table 6.3 shows the accuracy of the system for the various configurations tested in this study, whereas Table 6.4 shows the corresponding impostor scores.

Table 6.3: Comparison of the accuracy of the authentication algorithm between not normalized and normalized scalograms *Size 56* and *Size 224*.

	Not Normalized Scalograms	Normalized Scalograms	
Size of Scalograms	Accuracy		Configuration
Size 56	92.06%	92.06%	Configuration 1/1
	92.06%	98.42%	Configuration 1/3
Size 224	93.65%	93.65%	Configuration 1/1
	93.65%	93.65%	Configuration 1/3

6. AUTHENTICATION RESULTS

For scalograms computed from not normalized cardiac cycles, the results showed no differences in accuracy between using *Configuration 1/1* and *Configuration 1/3*, for both sizes. However, the accuracy was higher when using scalograms with more pixels as inputs to the system: 92.06% for *Size 56* and 93.65% for *Size 224*. When using the normalized scalograms with *Size 56*, the system reached accuracies of 92.06% for *Configuration 1/1* and 98.42% for *Configuration 1/3*. *Size 224* did not cause differences among configurations, achieving an accuracy of 93.65%. The best performance was achieved when using *Configuration 1/3* for normalized scalograms with *Size 56*.

Table 6.4: Comparison of the Impostor Score of the authentication algorithm between not normalized and normalized scalograms *Size 56* and *Size 224*.

	Not Normalized Scalograms	Normalized Scalograms	
Size of Scalograms	Impostor Score		Configuration
Size 56	16.21%	14.34%	Configuration 1/1
	16.21%	14.34%	Configuration 1/3
Size 224	15.16%	14.59%	Configuration 1/1
	14.97%	14.52%	Configuration 1/3

For *Size 56*, the impostor scores achieved using *Configuration 1/1* and *Configuration 1/3* were exactly the same and were higher for not normalized scalograms than for normalized: 16.21% and 14.34%, respectively. For *Size 224*, the impostor scores were higher for both configurations using not normalized scalograms. Specifically, for *Configuration 1/1*, the impostor score was 15.16% for not normalized and 14.59% for normalized scalograms, whereas for *Configuration 1/3*, the impostor score was 14.97% for not normalized and 14.52% for the normalized templates.

Combining the accuracy and impostor score as evaluation metrics, the best performance of the distance-based authentication system is achieved for normalized scalograms resized to 56x56 in *Configuration 1/3*.

6.2.1 ICA Dimensionality for Normalized Scalograms

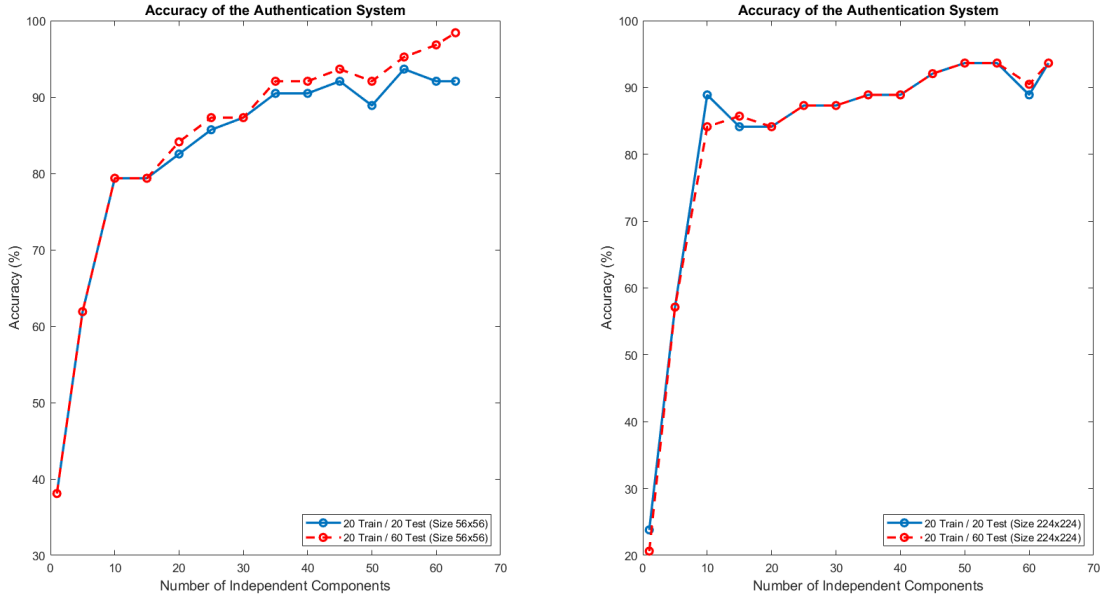


Figure 6.3: Representation of the accuracy obtained by the biometric authentication system when using different number of ICs for normalized scalograms.

The accuracy of the system was evaluated when decreasing the number of independent components. This analysis was only performed for the normalized scalograms since it is the configuration that optimizes the perfor-

mance of the algorithm.

Fig. 6.3 presents the accuracies achieved when using different numbers of independent components for normalized scalograms with *Size 56* on the left and *Size 224* on the right. For both sizes, results show that the highest accuracy is reached when the number of independent components is equal to the number of subjects on the database, i.e., 63. However, even though the accuracy decreases when the number of ICs decreases, the decrease is quite slow until the number of ICs reaches 10. When using 10 ICs, accuracies of around 80% and 85% were reached for *Size 56* and *Size 224*, respectively. From that point on, the performance of the algorithm decreases significantly and it is no longer viable.

6.2.2 Discussion

This study evaluated the evolution of the accuracy when decreasing the number of components in order to find how many ICs were significant and carried important information. For both sizes (*Size 56* and *Size 224*), the optimal performance corresponds to the use of the same number of ICs and subjects, in this case, 63. Bouveresse et al. [97] proved that when too many ICs are extracted, they will tend to contain a significant contribution related to noise. However, in this case, as for the identification algorithm, the 63 ICs considered contain useful information and are clearly needed to separate the signals from the 63 subjects. Results also show that, if fewer features are used, the performance will decrease, failing in distinguishing between all subjects. However, with 10 ICs, the system proved to still be viable since the accuracies reached were around 80%-85%.

According to El-Abed et al. [98], the evaluation metrics for a biometric system must include, besides the accuracy, the average authentication/identification time since a biometric system must be sufficiently efficient in a way that the user must be able to accomplish the task easily and in a timely manner. Considering the computational time of applying the ICA to reduce dimensionality, and knowing that the fewer ICs, the less time it takes to compute, the system should find a balance between accuracy and computational cost in order to build an efficient biometric system.

Regarding the different configurations tested, the optimal configuration, concerning the accuracy and imposter score, was to use 60 scalograms *Size 56* computed from normalized cardiac cycles to perform the template matching. With this configuration, the system is able to accurately authenticate genuine users with an authentication rate of 98.42% and to reject users with a rate of 85.66%. The computational time of this configuration is also much smaller as the size of the scalograms is 4 times smaller than *Size 224*. To the best of our knowledge, no studies used scalograms to perform the authentication, rather than identification. However, scalograms proved to be quite a promising approach for the authentication task.

Chapter 7

Conclusion

Research on ECG signals has advanced a long way from its clinical roots to novel application domains in areas so diverse as biometric recognition. Unlike conventional biometrics, which are neither secrets nor robust enough against falsification, ECG is inherited to an individual which is highly secure and impossible to be forged. Most importantly, ECG has an inherent real-time feature of vitality signs which ensures that it cannot be acquired unless the person to be authenticated is present at the authentication desk. Therefore, it is robust enough against the falsified credentials to be enrolled in the system. This dissertation has evaluated the feasibility of ECG as a biometric for individual identification and authentication tasks.

Several methodologies and apparatus are described for human biometric identification and authentication based on ECG signals collected at the fingers and hand palms. The database used in this work was the CYBHi database, created by Silva et al. [2] for biometrics purposes, in which the measurement apparatus only required slight contact with the subject hand without the need of pregelled electrodes, providing a signal acquisition, setup similar to the ones already used by other, largely accepted. The benefits from the use of such database are:

1. Its an off-the-person acquisition setup with consequent lower intrusiveness, allowing to reduce the acquisition time, as it ensures a high user acceptability and simple setup. Moreover, this solution can be embedded into ordinary objects, and wearable technologies can be developed for ECG acquisition, opening doors for the most varied real-world applications.
2. ECG data was acquired during two distinct moments, separated by three months apart, which makes this dataset particularly useful for benchmarking the performance of identification and authentication systems, taking into account potential variations in the heartbeat waveform over time.

Although the benefits of this database, it also brings some extra challenges. First of all, signals collected at the hand and fingers, specially using dry electrodes, have a lower signal-to-noise ratio, which raises several challenges namely in terms of filtering, segmentation, and outlier detection. Besides this, the three-month separated acquisitions lead to worse performances, when compared to within-session tasks, due to the variability of ECG over time. However, the across-session modality used with this type of databases is the most relevant modality, as biometric systems must function for an indefinite amount of time and throughout several years.

One of the great assets of this study is the fact that it tests several approaches and methodologies in the different phases of the biometric system, in order to compare and evaluate them, concluding about the advantages and disadvantages of each one and, consequently, find the optimal solution according to the results obtained.

Concerning the templates generation procedure, two types of templates were considered. The first was the cardiac cycles, which is the most commonly used template for ECG-based biometric research. The other template was the scalograms of the cardiac cycles, a time-frequency representation of the cardiac cycles. Since ECG signals, especially when collected at the fingers, are sensitive to noise, studies have been conducted by transforming signals into the frequency domain, which proved to be efficient for analyzing noisy signals. The scalograms templates were tested with two sizes - 56x56 and 224x224 - in order to evaluate the amount of information that

the system needs to successfully recognize individuals. Results for all the methodologies showed a better performance for *Size 56*, meaning that signals sized 224x224 may contain so much detailed information from each subject that it is difficult to find a signal that matches so many characteristics. Moreover, the scalograms generation is a computationally time-consuming process and the smaller the size of the scalograms, the less time it takes for the process to compute. A limitation of this work is that it has only compared the methodologies based on the performance obtained, rather than also investigating the computational time of each.

Another aspect that was tested concerned the outlier removal procedure, and consisted of verifying the influence of the number of templates, per subject, on the accuracy of the system. From the outlier removal procedure resulted two sets of templates for each subject: 1) *Set 1*, with the 20 signals closer to each other, and 2) *Set 2*, with the 60 signals closer to each other. The results showed that this is not a linear issue, as for some configurations the performance is better when noisier signals are included, while for others it is better to just include cleaner signals.

For the identification process using the cardiac cycles of the individuals, the optimal performance was achieved when using the LDA classifier, with normalized inputs, reaching an accuracy of 79.37%. For the identification with scalograms sized 56x56, the optimal performance was achieved when using the neural network, reaching an accuracy of 68.25%. Thus, using cardiac cycles optimizes the performance of the identification system, both for accuracy and computational time, as generating the scalograms is a time-consuming process. Although the achieved results with this database show good performance rates, there is a considerable margin for improvement, since the identification rates achieved when using databases with one single multi-lead on-the-person acquisition setups are much higher.

For the authentication process using cardiac cycles, the accuracy and impostor score achieved were 90.47% and 13.21%, respectively, when normalization and DR are not computed. For the scalograms, sized 56x56, the accuracy was 98.42%, whereas the impostor score was 14.34%. Although the scalograms present more promising results, future work should investigate the computational time of each process to allow a better conclusion about the most accurate method, taking into account all the important characteristics of a biometric system.

These off-the-person approaches to acquire ECG signals can be implemented in some wearable identification/authentication devices, which are promising for future applications due to their convenience. Currently, however, their signals are still weak and unstable. Therefore, the increase of the number of leads in this identification devices can be a solution because other lead signals may contain useful information, as multi-lead systems can display information about the status of the heart from different angles. Thus, identification and authentication using multi-lead signals acquired off-the-person should be further researched.

Further experiments should also be carried out to evaluate the system with a large database, comprising users of all age, abnormal ECG data, and long span of time interval between ECG recordings, in order to simulate the reality of the functioning of a biometric system when installed in some technological application.

Bibliography

- [1] Nuno Filipe Abalada do Val Bento. “ECG Biometrics using Deep Neural Networks”. *Dissertation Master of Science in Biomedical Engineering* (2019). URL: <http://hdl.handle.net/10362/75491>.
- [2] Hugo Plácido da Silva et al. “Check Your Biosignals Here: A new dataset for off-the-person ECG biometrics”. *Computer Methods and Programs in Biomedicine* 113 (2014), pp. 503–514. DOI: 10.1016/j.cmpb.2013.11.017.
- [3] Nikita Samarin and Donald Sannella. “A key to your heart: Biometric authentication based on ECG signals”. *arXiv* (2019). eprint: 1906.09181.
- [4] Joao Ribeiro Pinto, Jaime S. Cardoso, and Andre Lourenco. “Evolution, current challenges, and future possibilities in ECG Biometrics”. *IEEE Access* 6 (2018), pp. 34746–34776. DOI: 10.1109/ACCESS.2018.2849870.
- [5] Juan Sebastian Arteaga-Falconi, Hussein Al Osman, and Abdulmotaleb El Saddik. “ECG Authentication for Mobile Devices”. *IEEE Transactions on Instrumentation and Measurement* 65.3 (2016), pp. 591–600. DOI: 10.1109/TIM.2015.2503863.
- [6] Leif Sornmo and Pablo Laguna. *Bioelectrical Signal Processing in Cardiac and Neurological Applications*. Academic Press, (2013). ISBN: 9780124375529.
- [7] Fahim Sufi, Ibrahim Khalil, and Jiankun Hu. “ECG-Based Authentication”. *Handbook of Information and Communication Security*. Springer Berlin Heidelberg, (2010), pp. 309–331. DOI: 10.1007/978-3-642-04117-4_17.
- [8] L. Biel et al. “ECG analysis: A new approach in human identification”. *IEEE Transactions on Instrumentation and Measurement* 50.3 (2001), pp. 808–812. DOI: 10.1109/19.930458.
- [9] Steven A. Israel et al. “ECG to identify individuals”. *Pattern Recognition* 38.1 (2005), pp. 133–142. DOI: 10.1016/j.patcog.2004.05.014.
- [10] Masaki Kyoso and Akihiko Uchiyama. “Development of an ECG identification system”. *Proceedings of the 23rd Annual International Conference of the IEEE* 4 (2001), pp. 3721–3723.
- [11] Carlos Carreiras et al. “Evaluating template uniqueness in ECG biometrics”. *Lecture Notes in Electrical Engineering* 370 (2015), pp. 111–123. DOI: 10.1007/978-3-319-26453-0_7.
- [12] Hugo Plácido Da Silva et al. “Finger ECG signal for user authentication: Usability and performance”. *IEEE 6th International Conference on Biometrics: Theory, Applications and Systems, BTAS 2013*. IEEE Computer Society, (2013). ISBN: 9781479905270. DOI: 10.1109/BTAS.2013.6712689.
- [13] Simon Eberz et al. “Broken Hearted: How To Attack ECG Biometrics”. *Network and Distributed System Security Symposium (NDSS)* (2017). DOI: 10.14722/ndss.2017.23408.
- [14] Jae Neung Lee and Keun Chang Kwak. “Personal Identification Using a Robust Eigen ECG Network Based on Time-Frequency Representations of ECG Signals”. *IEEE Access* 7 (2019), pp. 48392–48404. DOI: 10.1109/ACCESS.2019.2904095.

- [15] Yeong Hyeon Byeon, Sung Bum Pan, and Keun Chang Kwak. “Intelligent deep models based on scalograms of electrocardiogram signals for biometrics”. *Sensors (Switzerland)* 19.4 (2019). DOI: 10.3390/s19040935.
- [16] Sinam Ajitkumar Singh and Swanirbhar Majumder. “a Novel Approach Osa Detection Using Single-Lead Ecg Scalogram Based on Deep Neural Network”. *Journal of Mechanics in Medicine and Biology* 19.4 (2019), pp. 1–18. DOI: 10.1142/S021951941950026X.
- [17] Andreas Starzacher and Bernhard Rinner. “Evaluating KNN, LDA and QDA classification for embedded online feature fusion”. *Proceedings of the 2008 International Conference on Intelligent Sensors, Sensor Networks and Information Processing* (2008), pp. 85–90. DOI: 10.1109/ISSNIP.2008.4761967.
- [18] Shantanu V. Deshmukh and Omid Dehzangi. “ECG-Based Driver Distraction Identification Using Wavelet Packet Transform and Discriminative Kernel-Based Features”. *2017 IEEE International Conference on Smart Computing, SMARTCOMP 2017* (2017), pp. 1–7. DOI: 10.1109/SMARTCOMP.2017.7947003.
- [19] Vili Podgorelec and Milan Zorman. “Encyclopedia of Complexity and Systems Science”. *Encyclopedia of Complexity and Systems Science* (2020), pp. 1–28. DOI: 10.1007/978-3-642-27737-5.
- [20] Selcan Kaplan Berkaya et al. “A survey on ECG analysis”. *Biomedical Signal Processing and Control* 43 (2018), pp. 216–235. DOI: 10.1016/j.bspc.2018.03.003. URL: <https://doi.org/10.1016/j.bspc.2018.03.003>.
- [21] Nahid Ghofrani and Reza Bostani. “Reliable features for an ECG-based biometric system”. *2010 17th Iranian Conference of Biomedical Engineering, ICBME 2010 - Proceedings* November (2010), pp. 3–4. DOI: 10.1109/ICBME.2010.5704918.
- [22] Konstantinos N. Plataniotis, Dimitrios Hatzinakos, and Jimmy K.M. Lee. “ECG biometric recognition without fiducial detection”. *Biometrics Symposium, BCC 2006* (2006), pp. 6–11. DOI: 10.1109/BCC.2006.4341628.
- [23] Gerd Wübbeler et al. “Verification of humans using the electrocardiogram”. *Pattern Recognition Letters* 28.10 (2007), pp. 1172–1175. DOI: 10.1016/j.patrec.2007.01.014.
- [24] Gary Garcia Molina et al. “Morphological synthesis of ECG signals for person authentication”. *European Signal Processing Conference Eusipco* (2007), pp. 738–742.
- [25] Ramaswamy Palaniappan and Shankar M. Krishnan. “Identifying individuals using ECG beats”. *2004 International Conference on Signal Processing and Communications, SPCOM* (2004), pp. 569–572. DOI: 10.1109/spcom.2004.1458524.
- [26] Zhang Zhaomin and Wei Daming. “A new ECG identification method using bayes’ theorem”. *IEEE Region 10 Annual International Conference, Proceedings/TENCON* (2007), pp. 1–4. DOI: 10.1109/TENCON.2006.344146.
- [27] Somsanouk Pathoumvanh, Surapan Airphaiboon, and Kazuhiko Hamamoto. “Robustness study of ECG biometric identification in heart rate variability conditions”. *IEEJ Transactions on Electrical and Electronic Engineering* 9.3 (2014), pp. 294–301. DOI: 10.1002/tee.21970.
- [28] N. Venkatesh and Srinivasan Jayaraman. “Human electrocardiogram for biometrics using DTW and FLDA”. *Proceedings - International Conference on Pattern Recognition* (2010), pp. 3838–3841. DOI: 10.1109/ICPR.2010.935.
- [29] Shih Chin Fang and Hsiao Lung Chan. “Human identification by quantifying similarity and dissimilarity in electrocardiogram phase space”. *Pattern Recognition* 42.9 (2009), pp. 1824–1831. DOI: 10.1016/j.patcog.2008.11.020.

BIBLIOGRAPHY

- [30] Can Ye, Miguel Tavares Coimbra, and B. V.K.Vijaya Kumar. “Investigation of human identification using two-lead Electrocardiogram (ECG) signals”. *IEEE 4th International Conference on Biometrics: Theory, Applications and Systems, BTAS 2010* (2010), pp. 1–8. DOI: 10.1109/BTAS.2010.5634478.
- [31] Ruggero Donida Labati et al. “Adaptive ECG biometric recognition: A study on re-enrollment methods for QRS signals”. *IEEE Workshop on Computational Intelligence in Biometrics and Identity Management, CIBIM 2015*-Janua.January (2015), pp. 30–37. DOI: 10.1109/CIBIM.2014.7015440.
- [32] Xiang Zhou et al. “A method of ECG template extraction for biometrics applications”. *2014 36th Annual International Conference of the IEEE Engineering in Medicine and Biology Society, EMBC 2014* (2014), pp. 602–605. DOI: 10.1109/EMBC.2014.6943663.
- [33] Adrian D.C. Chan et al. “Wavelet distance measure for person identification using electrocardiograms”. *IEEE Transactions on Instrumentation and Measurement* 57.2 (2008), pp. 248–253. DOI: 10.1109/TIM.2007.909996.
- [34] T. W. D. Shen, W. J. Tompkins, and Y. H. Hu. “Implementation of a one-lead ECG human identification system on a normal population”. *Journal of Engineering and Computer Innovations* 2.1 (2011), pp. 12–21. URL: <http://www.academicjournals.org/JECI/PDF/2011pdf/Tsu%20wang%20et%20al%20pdf.pdf>.
- [35] André Cigarro Matos, André Lourenço, and José Nascimento. “Embedded System for Individual Recognition Based on ECG Biometrics”. *Procedia Technology* 17 (2014), pp. 265–272. DOI: 10.1016/j.protcy.2014.10.236.
- [36] Noureddine Belgacem. “ECG Based Human Authentication using Wavelets and Random Forests”. *International Journal on Cryptography and Information Security* 2.2 (2012), pp. 1–11. DOI: 10.5121/ijcis.2012.2201.
- [37] Shyan Lung Lin et al. “Individual identification based on chaotic electrocardiogram signals during muscular exercise”. *IET Biometrics* 3.4 (2014), pp. 257–266. DOI: 10.1049/iet-bmt.2013.0014.
- [38] David Pereira Coutinho, Ana L.N. Fred, and Mário A.T. Figueiredo. “ECG-based continuous authentication system using adaptive string matching”. *BIOSIGNALS 2011 - Proceedings of the International Conference on Bio-Inspired Systems and Signal Processing* January (2011), pp. 354–359. DOI: 10.5220/0003292003540359.
- [39] David Pereira Coutinho, Ana L.N. Fred, and Mário A.T. Figueiredo. “One-lead ECG-based personal identification using Ziv-Merhav cross parsing”. *Proceedings - International Conference on Pattern Recognition* (2010), pp. 3858–3861. DOI: 10.1109/ICPR.2010.940.
- [40] Qingxue Zhang, Dian Zhou, and Xuan Zeng. “PulsePrint: Single-arm-ECG biometric human identification using deep learning”. *2017 IEEE 8th Annual Ubiquitous Computing, Electronics and Mobile Communication Conference, UEMCON 2017* 2018-Janua (2017), pp. 452–456. DOI: 10.1109/UEMCON.2017.8249111.
- [41] Ana Priscila Alves and Carlos Carreiras. “CardioWheel : ECG Biometrics on the Steering Wheel”. 2 (2015), pp. 267–270. DOI: 10.1007/978-3-319-23461-8.
- [42] Juan S. Arteaga-Falconi, Hussein Al Osman, and Abdulmotaleb El Saddik. “ECG and fingerprint bimodal authentication”. *Sustainable Cities and Society* 40.November (2018), pp. 274–283. DOI: 10.1016/j.scs.2017.12.023.
- [43] Afonso Eduardo, Helena Aidos, and Ana Fred. “ECG-based Biometrics using a Deep Autoencoder for Feature Learning An Empirical Study on Transferability”. *Proceedings of the 6th International Conference on Pattern Recognition Applications and Methods* (2017). DOI: 10.5220/0006195404630470.

- [44] Majid Komeili et al. “On evaluating human recognition using electrocardiogram signals: From rest to exercise”. *Canadian Conference on Electrical and Computer Engineering 2016-Octob* (2016), pp. 16–19. DOI: 10.1109/CCECE.2016.7726726.
- [45] Kyeong Seop Kim et al. “A robust human identification by normalized time-domain features of electrocardiogram”. *Annual International Conference of the IEEE Engineering in Medicine and Biology - Proceedings* 7 VOLS (2005), pp. 1114–1117. DOI: 10.1109/ieemb.2005.1616615.
- [46] Foteini Agrafioti and Dimitrios Hatzinakos. “ECG based recognition using second order statistics”. *Proceedings of the 6th Annual Communication Networks and Services Research Conference, CNSR 2008* (2008), pp. 82–87. DOI: 10.1109/CNSR.2008.38.
- [47] Ikenna C Odinaka. *Identifying Humans by the Shape of Their Heartbeats and Materials by Their X-Ray Scattering Profiles*. Tech. rep. URL: https://openscholarship.wustl.edu/eng%7B%5C_%7Dtds/8.
- [48] Mouhcine Guennoun et al. “Continuous authentication by electrocardiogram data”. *TIC-STH'09: 2009 IEEE Toronto International Conference - Science and Technology for Humanity*. (2009), pp. 40–42. ISBN: 9781424438785. DOI: 10.1109/TIC-STH.2009.5444466.
- [49] Yogendra Narain Singh and Phalguni Gupta. “ECG to individual identification”. *BTAS 2008 - IEEE 2nd International Conference on Biometrics: Theory, Applications and Systems*. (2008), pp. 1–8. ISBN: 9781424427307. DOI: 10.1109/BTAS.2008.4699343.
- [50] Yogendra Narain Singh and Phalguni Gupta. “Correlation-based classification of heartbeats for individual identification”. *Soft Computing* 15.3 (Nov. 2011), pp. 449–460. DOI: 10.1007/s00500-009-0525-y. URL: <https://link.springer.com/article/10.1007/s00500-009-0525-y>.
- [51] Y. Gahi et al. “Biometric identification system based on electrocardiogram data”. *Proceedings of New Technologies, Mobility and Security Conference and Workshops, NTMS 2008* (2008), pp. 1–4. DOI: 10.1109/NTMS.2008.ECP.29.
- [52] S. Zahra Fatemian and Dimitrios Hatzinakos. “A new ECG feature extractor for biometric recognition”. *DSP 2009: 16th International Conference on Digital Signal Processing, Proceedings* (2009), pp. 1–6. DOI: 10.1109/ICDSP.2009.5201143.
- [53] J. M. Irvine et al. “A new biometric: human identification from circulatory function”. *Joint Statistical Meetings of the American Statistical Association, San Francisco March 2017* (2003), pp. 1957–1963. URL: <https://www.tib.eu/en/search/id/BLCP%7B%5C%7D3ACN065893460/A-New-Biometric-Human-Identification-from-Circulatory/>.
- [54] Steven A. Israel and John M. Irvine. “A sequential procedure for individual identity verification using ECG”. *Eurasip Journal on Advances in Signal Processing* 3 (2009), pp. 1–13. DOI: 10.1155/2009/243215.
- [55] Ikenna Odinaka et al. “ECG biometric recognition: A comparative analysis”. *IEEE Transactions on Information Forensics and Security* 7.6 (2012), pp. 1812–1824. DOI: 10.1109/TIFS.2012.2215324.
- [56] Maryamsadat Hejazi et al. “ECG biometric authentication based on non-fiducial approach using kernel methods”. *Digital Signal Processing: A Review Journal* 52 (2016), pp. 72–86. DOI: 10.1016/j.dsp.2016.02.008. URL: <http://dx.doi.org/10.1016/j.dsp.2016.02.008>.
- [57] Semih Ergin et al. “ECG based biometric authentication using ensemble of features”. *Iberian Conference on Information Systems and Technologies, CISTI*. IEEE Computer Society, (2014), pp. 1–6. ISBN: 9789899843431. DOI: 10.1109/CISTI.2014.6877089.
- [58] Muhammad Najam Dar et al. “ECG biometric identification for general population using multiresolution analysis of DWT based features”. *2015 2nd International Conference on Information Security and Cyber Forensics, InfoSec 2015* ((2015)), pp. 5–10. DOI: 10.1109/InfoSec.2015.7435498.

BIBLIOGRAPHY

- [59] Dhouha Rezgui and Zied Lachiri. “ECG biometric recognition using SVM-based approach”. *IEEJ Transactions on Electrical and Electronic Engineering* 11 (2016), S94–S100. DOI: 10.1002/tee.22241.
- [60] Ming Li and Shrikanth Narayanan. “Robust ECG biometrics by fusing temporal and cepstral information”. *Proceedings - International Conference on Pattern Recognition* (2010), pp. 1326–1329. DOI: 10.1109/ICPR.2010.330.
- [61] Hugo Silva et al. “ECG biometrics: Principles and applications”. *BIOSIGNALS 2013 - Proceedings of the International Conference on Bio-Inspired Systems and Signal Processing* (2013), pp. 215–220. DOI: 10.5220/0004243202150220.
- [62] Andre Lourenço, Hugo Silva, and Ana Fred. “ECG-based biometrics: A real time classification approach”. *IEEE International Workshop on Machine Learning for Signal Processing, MLSP*. (2012), pp. 1–6. ISBN: 9781467310260. DOI: 10.1109/MLSP.2012.6349735.
- [63] Foteini Agrafioti, Francis M. Bui, and Dimitrios Hatzinakos. “Secure telemedicine: Biometrics for remote and continuous patient verification”. *Journal of Computer Networks and Communications* (2012), pp. 1–11. DOI: 10.1155/2012/924791.
- [64] Yongjin Wang et al. “Analysis of Human Electrocardiogram for Biometric Recognition”. *EURASIP Journal on Advances in Signal Processing* 2008 (2008). DOI: 10.1155/2008/148658.
- [65] Antonio Fratini et al. *Individual identification via electrocardiogram analysis*. (2015). DOI: 10.1186/s12938-015-0072-y.
- [66] Ognian Boumbarov, Yuliyan Velchev, and Strahil Sokolov. “ECG personal identification in subspaces using radial basis neural networks”. *Proceedings of the 5th IEEE International Workshop on Intelligent Data Acquisition and Advanced Computing Systems: Technology and Applications, IDAACS’2009* September (2009), pp. 446–451. DOI: 10.1109/IDAACS.2009.5342942.
- [67] Sairul I. Safie, John J. Soraghan, and Lykourgos Petropoulakis. “Electrocardiogram (ECG) biometric authentication using pulse active ratio (PAR)”. *IEEE Transactions on Information Forensics and Security* 6.4 (2011), pp. 1315–1322. DOI: 10.1109/TIFS.2011.2162408.
- [68] André Lourenço, Hugo Silva, and Ana Fred. “Unveiling the biometric potential of finger-based ECG signals”. *Computational Intelligence and Neuroscience* 2011 (2011), pp. 1–8. DOI: 10.1155/2011/720971.
- [69] Rafik Matta et al. “Real-time continuous identification system using ECG signals”. *Canadian Conference on Electrical and Computer Engineering*. (2011), pp. 001313–001316. ISBN: 9781424497898. DOI: 10.1109/CCECE.2011.6030676.
- [70] Masaki Kyoso. “A Technique for Avoiding False Acceptance in ECG identification”. *IEEE EMBS Asian-Pacific Conference on Biomedical Engineering, 2003* (2003), pp. 190–191.
- [71] Ikenna Odinaka et al. “ECG biometrics: A robust short-time frequency analysis”. *2010 IEEE International Workshop on Information Forensics and Security, WIFS 2010* (2010), pp. 1–6. DOI: 10.1109/WIFS.2010.5711466.
- [72] Andre Cigarro Matos, Andre Lourenco, and Jose Nascimento. “Biometric recognition system using low bandwidth ECG signals”. *2013 IEEE 15th International Conference on e-Health Networking, Applications and Services, Healthcom 2013* Healthcom (2013), pp. 518–522. DOI: 10.1109/HealthCom.2013.6720731.
- [73] David Pereira Coutinho et al. “Novel fiducial and non-fiducial approaches to electrocardiogram-based biometric systems”. *IET Biometrics* 2.2 (2013), pp. 64–75. DOI: 10.1049/iet-bmt.2012.0055.

- [74] Sukkharak Saechia, Jeerasuda Koseeyaporn, and Paramote Wardkein. “Human identification system based ECG signal”. *IEEE Region 10 Annual International Conference, Proceedings/TENCON* (2005), pp. 2–5. DOI: 10.1109/TENCON.2005.300986.
- [75] Junping Zhang, Yuan Cheng, and Changyou Chen. “Low resolution gait recognition with high frequency super resolution”. *Lecture Notes in Computer Science (including subseries Lecture Notes in Artificial Intelligence and Lecture Notes in Bioinformatics)*. Vol. 5351 LNAI. (2008), pp. 533–543. ISBN: 354089196X. DOI: 10.1007/978-3-540-89197-0_49.
- [76] Chuang Chien Chiu, Chou Min Chuang, and Chih Yu Hsu. “A novel personal identity verification approach using a discrete wavelet transform of the ECG signal”. *Proceedings - 2008 International Conference on Multimedia and Ubiquitous Engineering, MUE 2008* (2008), pp. 201–206. DOI: 10.1109/MUE.2008.67.
- [77] Janani C. Sriram et al. “Activity-aware ECG-based patient authentication for remote health monitoring”. *ICMI-MLMI'09 - Proceedings of the International Conference on Multimodal Interfaces and the Workshop on Machine Learning for Multimodal Interfaces* (2009), pp. 297–304. DOI: 10.1145/1647314.1647378.
- [78] Fahim Sufi, Ibrahim Khalil, and Ibrahim Habib. “Polynomial distance measurement for ECG based biometric authentication”. *Security and Communication Networks* 3.4 (2010), pp. 303–319. DOI: 10.1002/sec.76.
- [79] Saeid Wahabi et al. “On evaluating ECG biometric systems: Session-dependence and body posture”. *IEEE Transactions on Information Forensics and Security* 9.11 (2014), pp. 2002–2013. DOI: 10.1109/TIFS.2014.2360430.
- [80] Wael Louis, Majid Komeili, and Dimitrios Hatzinakos. “Continuous authentication using One-Dimensional Multi-Resolution Local Binary Patterns (1DMRLBP) in ECG biometrics”. *IEEE Transactions on Information Forensics and Security* 11.12 (2016), pp. 2818–2832. DOI: 10.1109/TIFS.2016.2599270.
- [81] Foteini Agrafioti and Dimitrios Hatzinakos. “Fusion of ECG sources for human identification”. *2008 3rd International Symposium on Communications, Control, and Signal Processing, ISCCSP 2008* March (2008), pp. 1542–1547. DOI: 10.1109/ISCCSP.2008.4537472.
- [82] João Ribeiro Pinto et al. “Towards a continuous biometric system based on ECG signals acquired on the steering wheel”. *Sensors (Switzerland)* 17.10 (2017), pp. 1–14. DOI: 10.3390/s17102228.
- [83] Hugo Silva et al. “Study and evaluation of a single differential sensor design based on electro-textile electrodes for ECG biometrics applications”. *Proceedings of IEEE Sensors*. (2011), pp. 1764–1767. ISBN: 9781424492886. DOI: 10.1109/ICSENS.2011.6127028.
- [84] Gustavo Lenis et al. “Comparison of Baseline Wander Removal Techniques considering the Preservation of ST Changes in the Ischemic ECG: A Simulation Study”. *Computational and Mathematical Methods in Medicine* 2017 (2017), pp. 1–13. DOI: 10.1155/2017/9295029.
- [85] Dominique Makowski et al. “NeuroKit2: A Python toolbox for neurophysiological signal processing”. *Behavior Research Methods* (2021). DOI: 10.3758/s13428-020-01516-y.
- [86] John M. Irvine et al. “eigenPulse: Robust human identification from cardiovascular function”. *Pattern Recognition* 41.11 (2008), pp. 3427–3435. DOI: 10.1016/j.patcog.2008.04.015.
- [87] Deepak Sinwar and Rahul Kaushik. “Study of Euclidean and Manhattan Distance Metrics using Simple K-Means Clustering”. *International Journal for Research in Applied Science and Engineering Technology* V (2014), pp. 270–274.

BIBLIOGRAPHY

- [88] Jacques Wainer and Pablo Fonseca. “How to tune the RBF SVM hyperparameters? An empirical evaluation of 18 search algorithms”. *Artificial Intelligence Review* 54.6 (2021), pp. 4771–4797. DOI: 10.1007/s10462-021-10011-5. arXiv: 2008.11655. URL: <https://doi.org/10.1007/s10462-021-10011-5>.
- [89] Carlos Carreiras et al. “ECG signals for biometric applications: Are we there yet?” *ICINCO 2014 - Proceedings of the 11th International Conference on Informatics in Control, Automation and Robotics* 2 (2014), pp. 765–772. DOI: 10.5220/0005160507650772.
- [90] Carla Oliveira and Ana Fred. “ECG-based authentication : Bayesian vs. nearest neighbour classifiers”. *BIOSIGNALS 2009 - Proceedings of the 2nd International Conference on Bio-Inspired Systems and Signal Processing* (2009), pp. 163–168. DOI: 10.5220/0001549901630168.
- [91] Joana S. Paiva, Duarte Dias, and João P.S. Cunha. *Beat-ID: Towards a computationally low-cost single heartbeat biometric identity check system based on electrocardiogram wave morphology*. Vol. 12. 7. (2017), pp. 1–32. ISBN: 1111111111. DOI: 10.1371/journal.pone.0180942.
- [92] Juwei Lu, Kostantinos N. Plataniotis, and Anastasios N. Venetsanopoulos. “Face recognition using LDA-based algorithms”. *IEEE Transactions on Neural Networks* 14.1 (2003), pp. 195–200. DOI: 10.1109/TNN.2002.806647.
- [93] Duygu Çalışır and Esin Doğantekin. “An automatic diabetes diagnosis system based on LDA-Wavelet Support Vector Machine Classifier”. *Expert Systems with Applications* 38.7 (2011), pp. 8311–8315. DOI: 10.1016/j.eswa.2011.01.017.
- [94] Donna Giri et al. “Automated diagnosis of Coronary Artery Disease affected patients using LDA, PCA, ICA and Discrete Wavelet Transform”. *Knowledge-Based Systems* 37 (2013), pp. 274–282. DOI: 10.1016/j.knosys.2012.08.011.
- [95] Ian Sutherland and Kiattipoom Kiatkawsin. “Determinants of guest experience in Airbnb: A topic modeling approach using LDA”. *Sustainability (Switzerland)* 12.8 (2020). DOI: 10.3390/SU12083402.
- [96] Muhammad Najam Dar et al. “ECG based biometric identification for population with normal and cardiac anomalies using hybrid HRV and DWT features”. *2015 5th International Conference on IT Convergence and Security, ICITCS 2015 - Proceedings* (2015), pp. 1–5. DOI: 10.1109/ICITCS.2015.7292977.
- [97] D. Jouan-Rimbaud Bouvieresse et al. “Two novel methods for the determination of the number of components in independent components analysis models”. *Chemometrics and Intelligent Laboratory Systems* 112 (2012), pp. 24–32. DOI: 10.1016/j.chemolab.2011.12.005.
- [98] Mohamad El-abed et al. “Evaluation of Biometric Systems To cite this version : Evaluation of Biometric Systems Evaluation of Biometric Systems”. *IEEE International Conference on Hand-Based Biometrics (ICHB)* (2014), pp. 149–169.
- [99] André Lourenço et al. “Real time electrocardiogram segmentation for finger based ECG biometrics”. *BIOSIGNALS 2012 - Proceedings of the International Conference on Bio-Inspired Systems and Signal Processing* (2012), pp. 49–54. DOI: 10.5220/0003777300490054.
- [100] Yogendra Narain Singh and S K Singh. “Evaluation of Electrocardiogram for Biometric Authentication”. *Journal of Information Security* 03.01 (2012), pp. 39–48. DOI: 10.4236/jis.2012.31005.
- [101] Ruggero Donida Labati, Roberto Sassi, and Fabio Scotti. “ECG biometric recognition: Permanence analysis of QRS signals for 24 hours continuous authentication”. *Proceedings of the 2013 IEEE International Workshop on Information Forensics and Security, WIFS 2013* (2013), pp. 31–36. DOI: 10.1109/WIFS.2013.6707790.
- [102] Hugo Silva and Carlos Carreiras. “Outlier Detection in Non-intrusive”. *International Conference Image Analysis and Recognition* 7950 (2013), pp. 43–52.

- [103] Jin Wang et al. “Human identification from ECG signals via sparse representation of local segments”. *IEEE Signal Processing Letters* 20.10 (2013), pp. 937–940. DOI: 10.1109/LSP.2013.2267593.
- [104] Muhammad Najam Dar et al. “ECG biometric identification for general population using multiresolution analysis of DWT based features”. *2015 2nd International Conference on Information Security and Cyber Forensics, InfoSec 2015*. Institute of Electrical and Electronics Engineers Inc., (2015), pp. 5–10. ISBN: 9781467369886. DOI: 10.1109/InfoSec.2015.7435498.
- [105] Se Young Chun. “Single pulse ECG-based small scale user authentication using guided filtering”. *2016 International Conference on Biometrics, ICB 2016* (2016). DOI: 10.1109/ICB.2016.7550065.
- [106] Carmen Camara et al. “Real-time electrocardiogram streams for continuous authentication”. *Applied Soft Computing Journal* 68.August (2018), pp. 784–794. DOI: 10.1016/j.asoc.2017.07.032.
- [107] Anita Pal and Yogendra Narain Singh. *ECG biometric recognition*. Vol. 834. Springer Singapore, (2018), pp. 61–73. ISBN: 9789811300226. DOI: 10.1007/978-981-13-0023-3_7. URL: <http://dx.doi.org/10.1007/978-981-13-0023-3%7B%5C%7D7>.
- [108] Ho J. Kim and Joon S. Lim. “Study on a Biometric Authentication Model based on ECG using a Fuzzy Neural Network”. *IOP Conference Series: Materials Science and Engineering* 317.1 (2018). DOI: 10.1088/1757-899X/317/1/012030.
- [109] Carlos Carreiras et al. “A unifying approach to ECG biometric recognition using the wavelet transform”. *Lecture Notes in Computer Science (including subseries Lecture Notes in Artificial Intelligence and Lecture Notes in Bioinformatics)* 7950 LNCS (2013), pp. 53–62. DOI: 10.1007/978-3-642-39094-4_7.
- [110] Marta S. Santos et al. “Eigen heartbeats for user identification”. *BIO SIGNALS 2013 - Proceedings of the International Conference on Bio-Inspired Systems and Signal Processing* (2013), pp. 351–355. DOI: 10.5220/0004249503510355.
- [111] Karan Singh, Akshit Singhvi, and Vinod Pathangay. “Dry contact fingertip ECG-based authentication system using time, frequency domain features and support vector machine”. *Proceedings of the Annual International Conference of the IEEE Engineering in Medicine and Biology Society, EMBS 2015-Novem* (2015), pp. 526–529. DOI: 10.1109/EMBC.2015.7318415.

Appendix A

Related work

Table A.1: Related Work on ECG-based biometrics - Part I (adapted from [4]). Legend: NS - Number of Subjects; OP - Off-the-Person; DR - Dimensionality Reduction; MA - Multiple Acquisitions; SA - Single Acquisition.

Author	Year	Dataset	NS	Session	OP	Features/DR	Decision	Results
Biel et al. [8]	2001	Private	20	MA	No	Fiducial Features/ PCA	SIMCA	IDR 100%
Kyoso et al. [10]	2001	Private	9	SA	No	QRS duration and QT time	Mahalanobis distance + LDA	IDR 94.2%
Israel et al. [9]	2005	Private	49	MA	No	RQ, RS, RP, RL, RP', RT, RS', RT', P and T widths, ST, PQ, PT, LQ, ST' / LDA	Contingency matrix majority voting	IDR: 97%
Saechia et al. [74]	2005	-	-	-	No	Fourier Transform of PQRST (whole), P, QRS, and T	Neural Networks	FRR: Whole 17.1% Apart 2.85%
Plataniotis et al. [22]	2006	PTB	14	SA	No	Autocorrelation coefficients / DCT	Norm. Euclidean dist. + Gaussian LLR	IDR 100% FAR 0.02%
Zhang et al. [26]	2006	Private (leads I, II, V1, and V2)	502	SA	No	Amplitudes, durations, intervals, levels and areas / PCA	Bayes- minimum- error-rate	IDR L.I 85.3% L.II 92.0% L.V1 95.2% L.V2 97.4%
Molina et al. [24]	2007	Private	10	SA	Yes	R-R segments	DTW path + kNN	EER 2%
Agrafioti et al. [81]	2008	PTB + MIT NSR	27	SA	No	Normalized autocorrelation / DCT or LDA	Correlation + kNN	IDR: DCT 96.3% LDA 100%

Table A.2: Related Work on ECG-based biometrics - Part II (adapted from [4]). Legend: NS - Number of Subjects; OP - Off-the-Person; DR - Dimensionality Reduction; MA - Multiple Acquisitions; SA - Single Acquisition.

Author	Year	Dataset	NS	Session	OP	Features/DR	Decision	Results
Chan et al. [33]	2008	Private	50	MA	Yes	Signal-averaged ECG	PRD, CC, WDIST + kNN	IDR: PRD 70% CC 80% WD 89%
Irvine et al. [86]	2008	Private	39	MA	No	Covariance matrix eigenvectors / PCA	kNN	IDR 100%
Fang et al. [29]	2009	Private (one or three leads)	100	-	No	Avg. beat phase space portrait	Correlation; Mutual nearest pt. dist. + kNN	IDR: 1 lead 93% 3 leads 99%
Guennoun et al. [48]	2009	Private	16	MA	No	Fiducial amplitude and time feat. / Physiological-state-indepen. feature select.	Mahalanobis dist. + Thresh. and Voting	FRR 0.01% FAR 0%
Coutinho et al. [39]	2010	Private	19	MA	Yes	Uniformly quantized avg. beats	Ziv-Merhav relative entropy + kNN	IDR 99.5%
Li et al. [60]	2010	MIT NSR	18	SA	No	Hermite poly. expansion; Cepstral features / HLDA	SVM + GMM-UBM fusion	IDR 98.3% EER 0.5%
Odinaka et al. [71]	2010	Private	269	MA	No	Log-STFT spectrogram / Bin selection	Gaussian models LLR	IDR 99% EER 0.37%
Ye et al. [30]	2010	MIT Arrh. MIT NSR1 MIT LT MIT NSR2	47 18 65 18	SA	No No No No	Daubechies DWT / ICA	RBF SVM	IDR 99.6% IDR 99.3% IDR 98.1% IDR 97.5%
Coutinho et al. [38]	2011	Private	19	SA	No	User-tuned Lloyd-Max quantized avg. beat	Ziv-Merhav cross parsing similarity + kNN	EER 0.36%
Lourenço et al. [83]	2011	Private	16	SA	Yes	Avg. normalized beat	Euclidean dist. + kNN	IDR 94.3% EER 13%
Safie et al. [67]	2011	PTB (healthy or w/ arrhythmias)	112	MA	No	Pulse Active Ratio	Euclidean dist. + kNN	EER: Heal. 9.98% Arrh. 19.2%
Shen et al. [34]	2011	Private	168	SA	Yes	Amplitudes, durations, slopes, angles, and QRS area / LDA	Correlation + kNN	IDR 98%
Sufi et al. [78]	2011	MIT Arrh.	-	SA	No	Cardioid graph centroid, extremas, area and perimeter	Straight line and percentage dist. + kNN	MIDR 1% FAR 0.5% FRR 0.5%
Agrafioti et al. [63]	2012	Private	42	SA	No	Autocorrelation coeff. / LDA	Euclidean dist. + kNN	EER 3.96%
Lourenço et al. [99]	2012	Private	32	SA	Yes	Segmented heartbeats	kNN	EER 9.39%

A. RELATED WORK

Table A.3: Related Work on ECG-based biometrics - Part III (adapted from [4]). Legend: NS - Number of Subjects; OP - Off-the-Person; DR - Dimensionality Reduction; MA - Multiple Acquisitions; SA - Single Acquisition.

Author	Year	Dataset	NS	Session	OP	Features/DR	Decision	Results
Singh et al. [100]	2012	MIT Arrh. + ST-T + MIT NSR + PTB + Private	80	SA	No	Interval, angle and amplitude fid. features	Euclidean dist. + kNN	EER 10.8%
Coutinho et al. [73]	2013	PTB	51	SA	No	Fid. latency and amplitude from mean waveform subsampling	Euclidean dist. + kNN	IDR 99.9%
		Private	26					EER 0.01% IDR 99.6% EER 0.70%
Labati et al. [101]	2013	E-HOL. 24h	185	MA	No	QRS Segment set templates	Cross-corr. similarity mat. + kNN	EER 5.36%
Silva et al. [102]	2013	Private	63	MA	Yes	Mean and median ensemble beats	Euclidean and cosine dist. + kNN and SVM	EER kNN 0.99% SVM 9.10%
Wang et al. [103]	2013	PTB	100	SA	No	Max-pooling representation elements	kNN	IDR 99.5%
Pathoumvanh et al. [27]	2014	Private (normal + increased HRV)	10	MA	No	CWT / FLDA	Euclidean dist. + kNN	IDR: Norm 97% HRV 80%
Labati et al. [31]	2014	E-HOL 24h	185	MA	No	QRS segments	Cross-corr. simil. kNN	EER 5.36%
Lin et al. [37]	2014	Private	26	SA	Yes	Corr. dimension Lyapunov exp.	SVM	IDR 81.7%
Matos et al. [35]	2014	Private	10	MS	Yes	STFT window features / Kullback-Leibler	LLR + kNN	IDR 100% EER 14%
Dar et al. [96]	2015	MIT Arrh.	47	SA	No	Haar Transform / GBFS	kNN	IDR 93.1%
		MIT NSR	18	SA	No			IDR 99.4%
		ECG-ID	90	MA	No			IDR 83.2%
Dar et al. [104]	2015	MIT Arrh.	47	SA	No	Haar Transform and HRV / GBFS	Random Forest	IDR 95.9% FAR 4.1%
		MIT NSR	18	SA	No			IDR 100% EER 0%
		ECG-ID	90	MA	No			IDR 83.9% FAR 16.1%
Carreiras et al. [11]	2016	Private	618	MA	No	Segmented heartbeats	kNN	EER 9.01% MIDR 15.6%
Chun et al. [105]	2016	ECG-ID	89	MA	No	Guided filtering avg. beat / PCA	DTW or Euclidean dist. + kNN	EER: DTW 5.2% Eucl. 2.4%
Hejazi et al. [56]	2016	Private	52	SA	Yes	Autocorrelation coeff. / KPCA	SVM	IDR 76.3% FAR 3.5% FRR 4.83%
Pinto et al. [82]	2017	Private	6	SA	Yes	DCT coefficients	SVM	IDR 94.9% EER 2.66%
Camara et al. [106]	2017	MIT NSR	10	MA	No	Walsh-Hadamard features, outliers rejected	kNN	IDR 94.8%
Komeili et al. [44]	2017	UofTDB (different sessions or postures)	82	MA	Yes	CWT, STFT, AC, max., set., dev., kurtosis and skewness / MSFS	SVM	EER Sess. 6.9% Post. 3.7%

Table A.4: Related Work on ECG-based biometrics - Part IV (adapted from [4]. Legend: NS - Number of Subjects; OP - Off-the-Person; DR - Dimensionality Reduction; MA - Multiple Acquisitions; SA - Single Acquisition.

Author	Year	Dataset	NS	Session	OP	Features/DR	Decision	Results
Paiva et al. [91]	2017	PTB	10	SA	No	Fiducial distances ST, RT and QT	SVM	IDR 97.5% FAR 5.71% FRR 3.44%
Lee et al. [14]	2018	Private	55	-	No	R-R segments, including two or three heartbeats (hb.)	Cosine, euclidean, manhattan dists., and CC	IDR: 2 hb. 89.9% 3hb. 93.3%
Pal et al. [107]	2018	PTB	10	SA	No	Interval, amplitude, angle and area fiducial features / KPCA	Euclidean distance	IDR 97.1%
Kim et al. [108]	2018	-	73	SA	No	Haar Wavelet Transform	Fuzzy membership ANN	FRR 1.68% FAR 5.84%

Table A.5: Techniques and performances comparison for previous studies using CYBHi database. Legend: DR - Dimensionality Reduction.

Authors	Year	Features / DR	Decision	Identification Performance	Authentication Performance
Lourenço et al. [68]	2011	QRS Detection + Time and Amplitude normalization	kNN (Euclidean dist.)	IDR 94.3%	EER 13.0%
Lourenço et al. [99]	2012	R-peaks Detection	kNN (Euclidean dist.) SVM	Eid 17.65% (1sec) Eid 5.61% (5sec) Eid 28.07% (1sec) Eid 8.87% (5sec)	EER 9.39% (1sec) EER 2.75% (5sec) FRR 51.55% (1sec) FRR 13.91% (5sec)
Carreiras et al. [109]	2013	Wavelet Transform + Segmentation Algorithm + Outlier Removal	kNN based on RDWT (rbio5.5 and db3 wavelets)	EID rbio5.5: 36.6% db3: 38.8%	EER rbio5.5: 13.9% db3: 14.1%
Santos et al. [110]	2013	QRS Detection / PCA	kNN (Euclidean dist.)	Error Probability <5%	-
Silva et al. [102]	2013	QRS Detection + Outlier Detection	kNN (Euclidean dist. Cosine dist.)	-	EER Euc. dist.: 12.4% Cosine dist.: 12.4%
Silva et al. [12]	2013	QRS Detection + Segmentation Algorithm + Outlier Removal	kNN based on: Euc. dist. Cosine dist. SVM	-	EER Euc. dist.: 5.2% Cosine dist.: 4.5% SVM 9.1%
Singh et al. [111]	2015	Time features: PQRS fragment localized around each R-peaks Frequency features: FFT coefficentes	SVM (libSVM)	-	EER 3.4%
Bento et al. [1]	2018	Segmentation + Peak Detection + Segment Elimination	Recurrent NN Convolutional NN	55.58% (CYBHi) 58.91% (CYBHi) 99.79% (Fantasia) 96.88% (ECG-ID)	10.57% (CYBHi) 10.01% (CYBHi)

Appendix B

Optimizations of SVM

B.0.1 SVM Optimization for Normalized Cardiac Cycles in Configuration 60/60

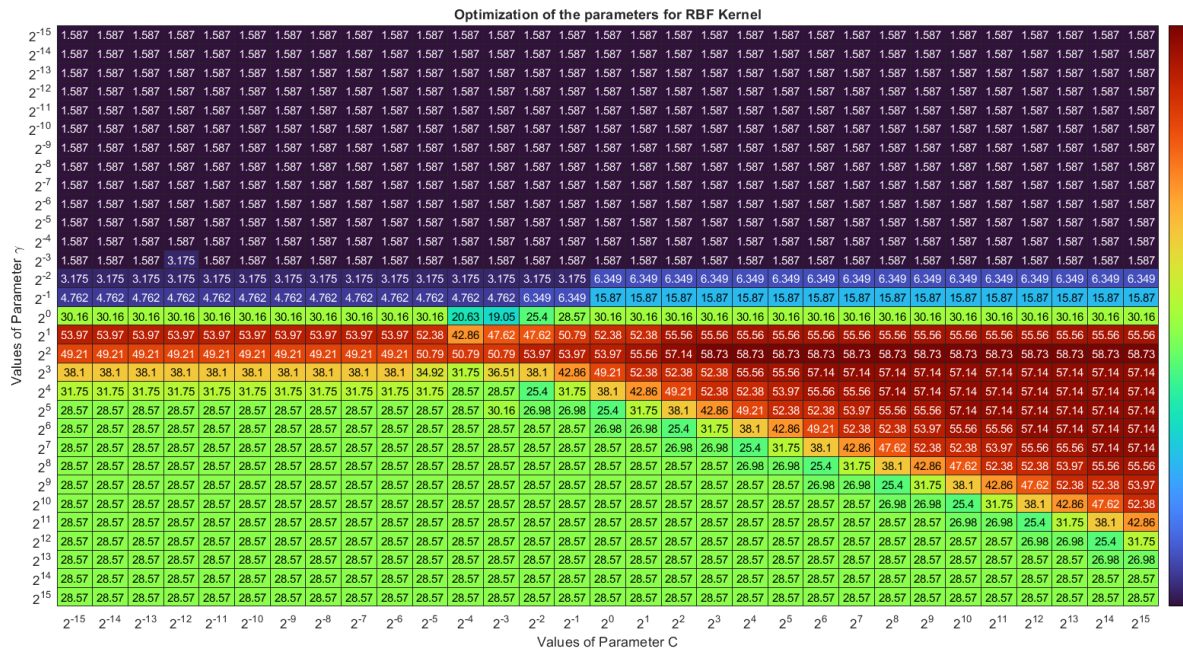


Figure B.1.1: Optimization of the parameters for RBF Kernel for normalized cardiac cycles in Configuration 60/60. The colors represent the accuracy of the system. Cold colors represent lower accuracies, whereas warm colors represent higher accuracies.

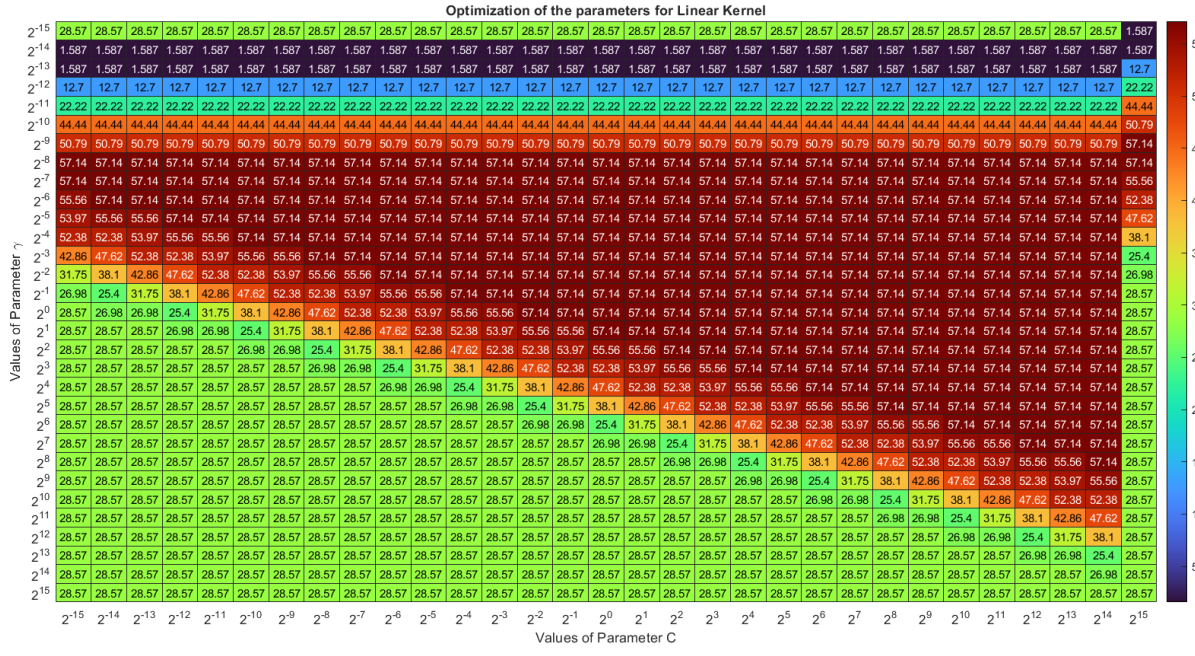


Figure B.1.2: Optimization of the parameters for Linear Kernel for normalized cardiac cycles in Configuration 60/60. The colors represent the accuracy of the system. Cold colors represent lower accuracies, whereas warm colors represent higher accuracies.

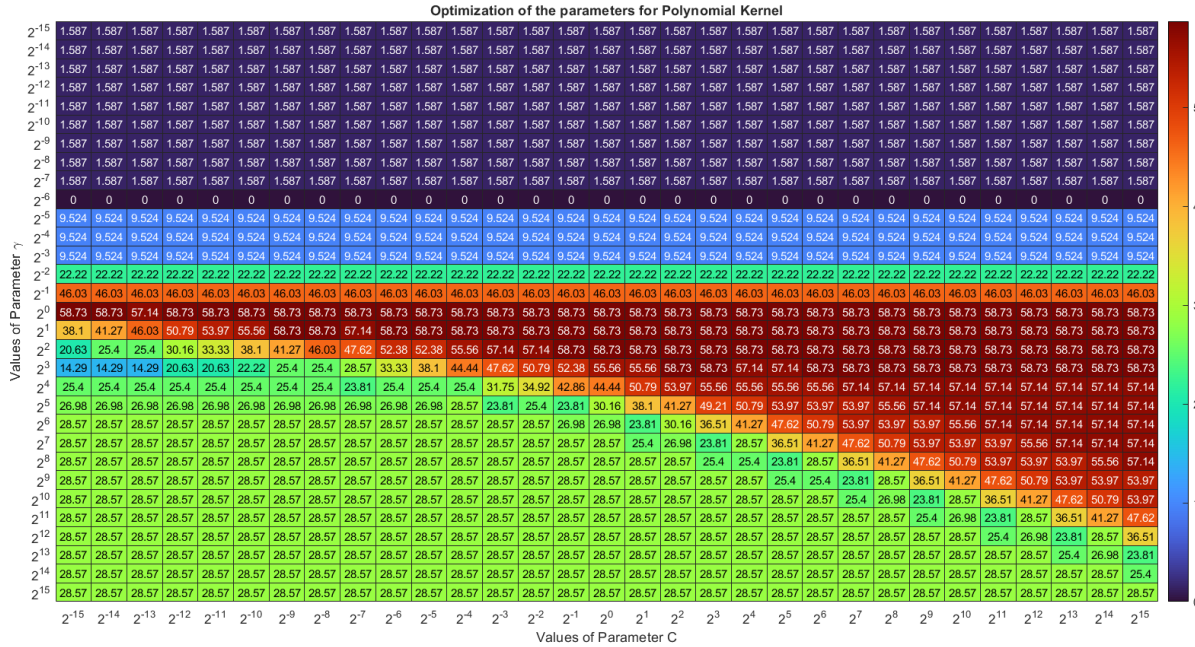


Figure B.1.3: Optimization of the parameters for Polynomial Kernel for normalized cardiac cycles in Configuration 60/60. The colors represent the accuracy of the system. Cold colors represent lower accuracies, whereas warm colors represent higher accuracies.

B. OPTIMIZATIONS OF SVM

B.0.2 SVM Optimization for Not Normalized Cardiac Cycles in Configuration 20/20

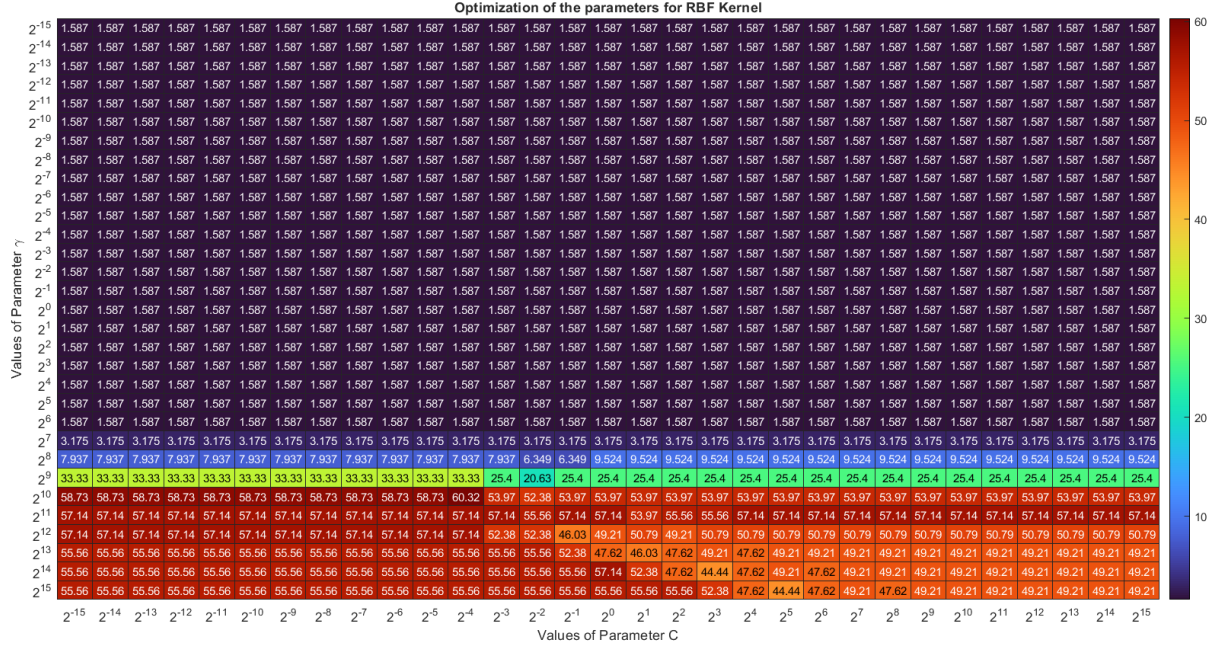


Figure B.2.1: Optimization of the parameters for RBF Kernel for not normalized cardiac cycles in Configuration 20/20. The colors represent the accuracy of the system. Cold colors represent lower accuracies, whereas warm colors represent higher accuracies.

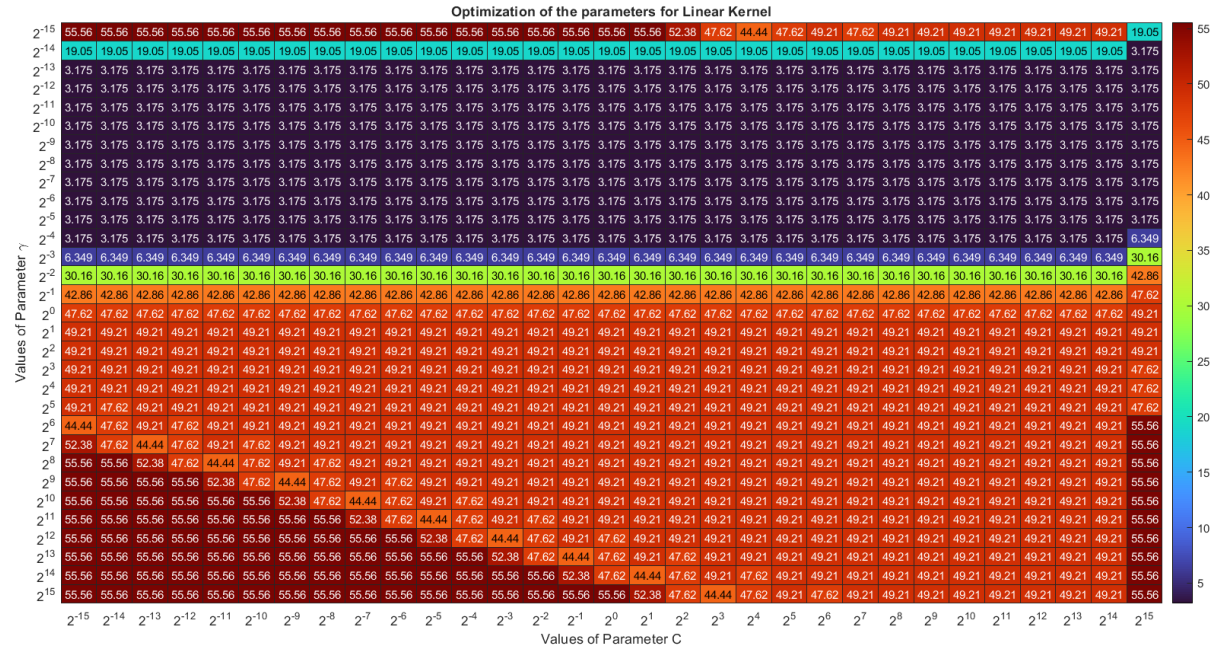


Figure B.2.2: Optimization of the parameters for Linear Kernel for not normalized cardiac cycles in Configuration 20/20. The colors represent the accuracy of the system. Cold colors represent lower accuracies, whereas warm colors represent higher accuracies.

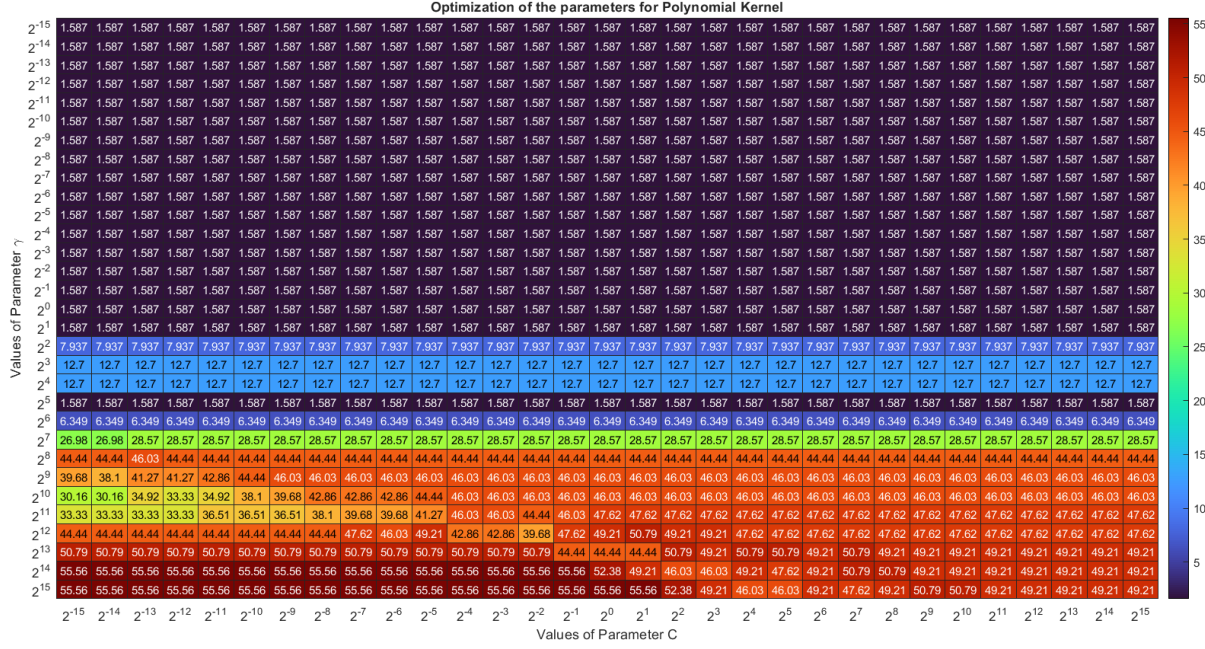


Figure B.2.3: Optimization of the parameters for Polynomial Kernel for not normalized cardiac cycles in *Configuration 20/20*. The colors represent the accuracy of the system. Cold colors represent lower accuracies, whereas warm colors represent higher accuracies.

B.0.3 SVM Optimization for Not Normalized Cardiac Cycles in Configuration 60/60

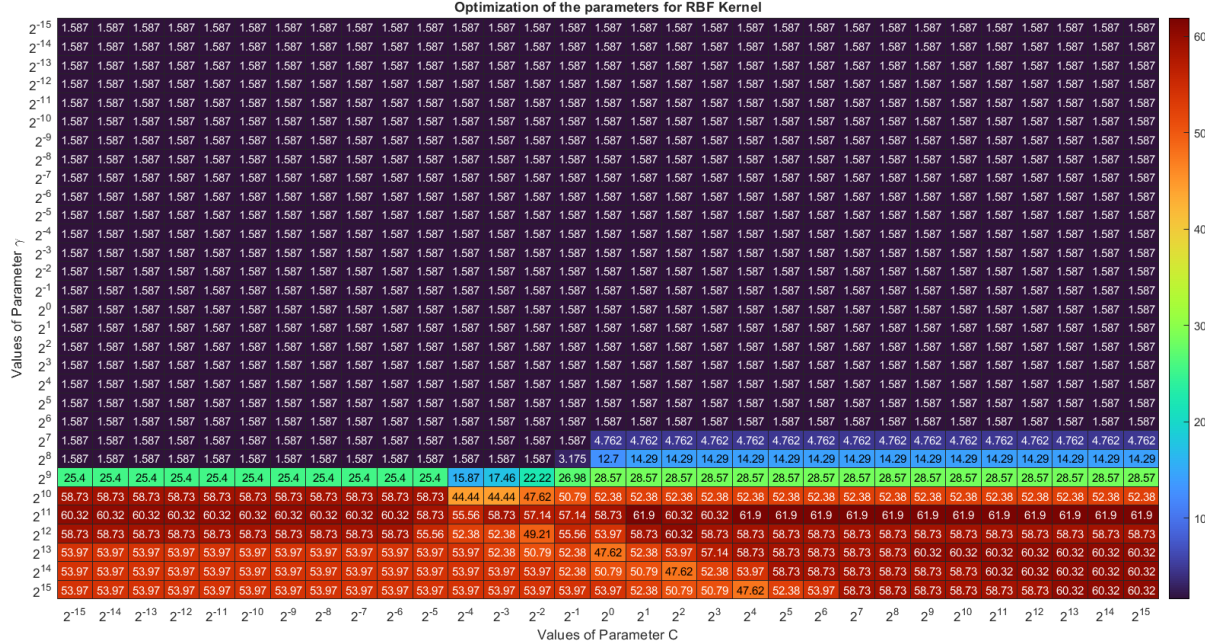


Figure B.3.1: Optimization of the parameters for RBF Kernel for not normalized cardiac cycles in *Configuration 60/60*. The colors represent the accuracy of the system. Cold colors represent lower accuracies, whereas warm colors represent higher accuracies.

B. OPTIMIZATIONS OF SVM

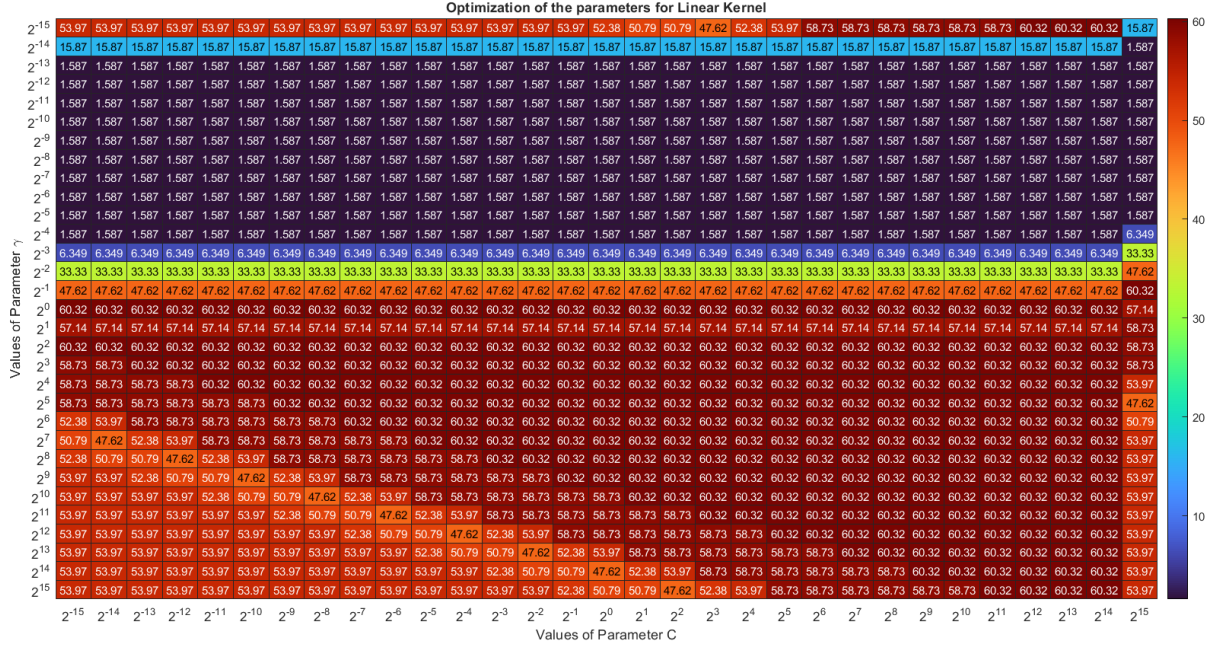


Figure B.3.2: Optimization of the parameters for Linear Kernel for not normalized cardiac cycles in *Configuration 60/60*. The colors represent the accuracy of the system. Cold colors represent lower accuracies, whereas warm colors represent higher accuracies.

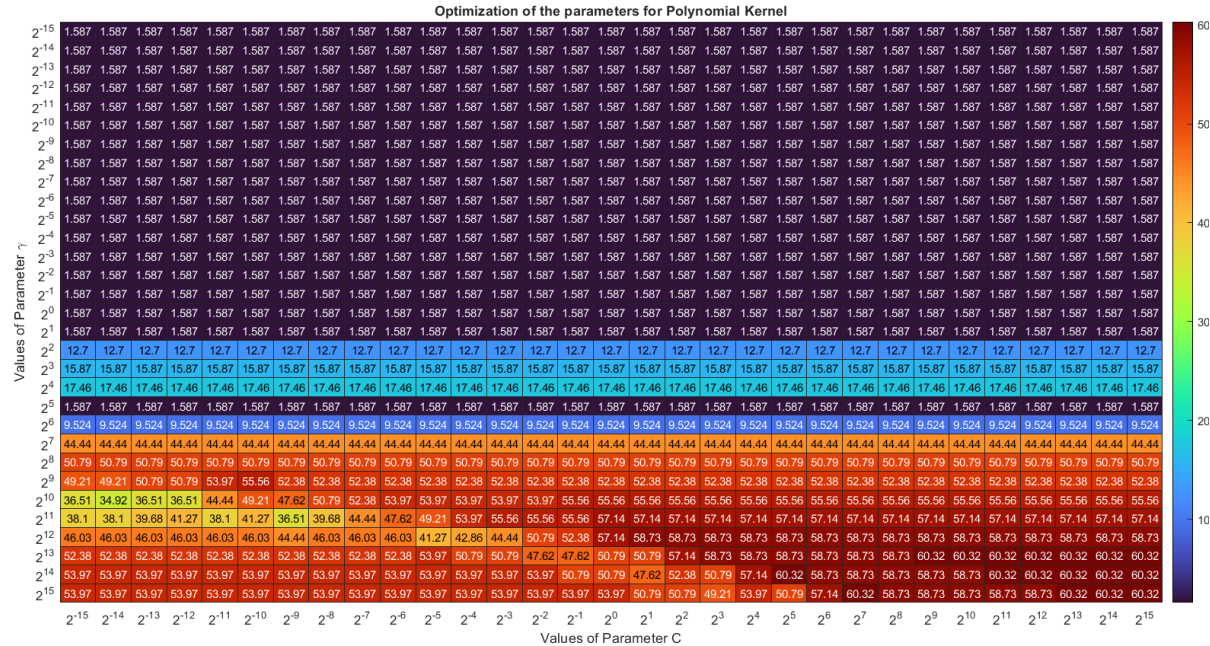


Figure B.3.3: Optimization of the parameters for Polynomial Kernel for not normalized cardiac cycles in *Configuration 60/60*. The colors represent the accuracy of the system. Cold colors represent lower accuracies, whereas warm colors represent higher accuracies.